Masters Theses (All Theses, All Years)   Electronic Theses and Dissertations

2017-05-26

The Incorporation of Decellularized Cardiac ECM into Fibrin Microthreads

Kaitlyn A. Marengo
Worcester Polytechnic Institute

Follow this and additional works at: https://digitalcommons.wpi.edu/etd-theses

The Incorporation of Decellularized Cardiac ECM into Fibrin Microthreads

Kaitlyn Amié-Elizabeth Marengo

A thesis to be submitted to the faculty of Worcester Polytechnic Institute in partial fulfillment of the requirements for the Degree of Master of Science

Submitted by:
Kaitlyn A Marengo
Department of Biomedical Engineering

Approved by:

Glenn R Gaudette, PhD
Associate Professor
Department of Biomedical
Engineering

Raymond L Page, PhD
Professor of Practice
Department of Biomedical
Engineering

George D Pins, PhD
Associate Professor
Department of Biomedical
Engineering

May 31, 2017

Abstract

Stem cell therapies have shown promising capabilities in regaining the functionality of scar tissue following a myocardial infarction. Biological sutures composed of fibrin have been shown to more effectively deliver human mesenchymal stem cells (hMSCs) to the heart when compared to traditional cell delivery mechanisms. While the biological sutures do show promise, improvements can be made. To enhance the fibrin sutures, we propose to incorporate native cardiac extracellular matrix (ECM) into the fibrin microthreads to produce a more *in vivo*-like environment. This project investigated the effects that ECM incorporation has on fibrin microthread structure, mechanics, stem cell seeding, and pro-angiogenic potential. Single microthreads composed of fibrin or fibrin and ECM were subjected to uniaxial tensile testing. It was found that the microthreads consisting of both fibrin and ECM had significantly high elastic moduli than fibrin only microthreads. Cell seeding potential was evaluated by performing a 24-hour hMSC seeding experiment using sutures of the varying microthread types. A CyQuant cell proliferation assay was used to determine the number of cells seeded onto each suture type. The results determined that there was no statistical difference between the numbers of cells seeded on the types of sutures. To examine the pro-angiogenic potential the microthreads had, a 24-hour endothelial progenitor outgrowth cell (EPOC) outgrowth assay was used. Fibrin and 15% ECM-fibrin microthreads were placed within the scratch of an EPOC culture and evaluated every 6 hours for 24 hours. We found that the 15% ECM microthreads had significantly increased the EPOC outgrowth, approximately 16% more distance travelled than fibrin microthreads and 18% more than no microthreads. Our combined results suggest that ECM does not affect hMSC attachment to biological sutures but does increase the pro-angiogenic potential of the microthreads due to their increase in guiding EPOC outgrowth.

Acknowledgements

First, I would like to thank my advisor Glenn Gaudette for his constant feedback, support, insight and guidance throughout the course of this project as well as my time here at WPI as both an undergraduate student and a graduate student. I would also like to thank my committee members Raymond Page and George Pins for their help in guiding me through this project. I would like to express my sincerest gratitude to all the members of the Gaudette Lab. Katrina Hansen, Joshua Gershlak, and Emily Robbins, you have all been so supportive and I am so grateful for all the times you helped or assisted me with an experiment or taught me a new lab technique. I am also so grateful for you helping me through writing my thesis as well as editing and helping me practice for my final presentation. Many thanks to the Biomedical Engineering Department at WPI for the use of their resources as well as the guidance through my graduate studies. Finally, I would like to extend a special thank you to my parents, brothers, family, and boyfriend Adam for their love and support throughout the past two years. I don't think I could have made it this far without any of them.

Table of Contents

Table of Figures

List of Tables

Chapter 1: Introduction

This project investigates the incorporation of native decellularized rat cardiac extracellular matrix (ECM) into fibrin microthreads and the effect that ECM incorporation has on the attachment of human mesenchymal stem cells (hMSCs) onto sutures for use in delivery to the infarcted heart. This project also investigates the effect that ECM incorporation will have on endothelial progenitor cell outgrowth. Previous work in the Gaudette lab shows that fibrin sutures can act as a delivery mechanism for hMSCs to infarcted myocardium [1]. This chapter serves as a review of the cardiac anatomy, the effects of infarction on healthy cardiac tissue, a summary of the current treatments of myocardial infarctions (MI), and an introduction of the extracellular matrix and its potential applications.

Chapter 2. Background

2.1 Myocardial Function and Myocardial Infarction

The heart is a pump that circulates oxygenated and nutrient rich blood throughout the whole body. In the heart, there are four chambers: the right atrium, the right ventricle, the left atrium and the left ventricle. These four chambers are made of cardiac muscle, also known as myocardium. The inner surface of the myocardium is known as the endocardium while the outer surface is the epicardium [2]. The flow of blood begins when deoxygenated blood is received by the right atrium from the superior vena cava. The right atrium contracts and pumps blood into the right ventricle which then sends the deoxygenated to the lungs through the pulmonary artery where it becomes oxygenated. The newly oxygenated blood then enters the left atrium through the pulmonary vein. The blood is then pumped into the left ventricle and forced out into the aorta where is it circulated throughout the whole body [3]. After circulating through the body, the blood enters the superior vena cava and the process repeats. The left ventricle acts as the final pump to bring the blood to the entire body leading to it having thick muscle and

exhibiting the highest internal chamber pressure. The contraction of the heart is controlled through gap junctions that propagate action potentials across the myocardium [4, 5].

The myocardium is fed nutrients and oxygenated blood through coronary circulation. If a portion of the coronary circulation becomes blocked, the contractile muscle cells of the heart, or cardiomyocytes, are starved of oxygen and nutrients. This causes metabolic and physiological changes to occur within the heart [6, 7]. A non-continuous flow of oxygen and glucose to the myocardium causes adenosine triphosphate (ATP) production to switch from the aerobic pathway to the anaerobic pathway. Less ATP is produced causing the contractions of the heart to be weaker. The ATP production continues to slow as creatine phosphate reserves become used up. If myocardial ischemia continues, hydrogen ions, an anaerobic respiration byproduct, accumulates causing the intracellular pH to decrease [6].

The pH imbalance causes osmotic flooding of cardiomyocytes and edema, thus causing permanent damage to the myocardium. Following these changes, a natural inflammatory response will occur. Monocytes, neutrophils, and macrophages will migrate to clear the area of the damaged tissue and cells. Fibroblasts will also infiltrate the area and deposit fibrous collagen. These events create and further expand the infarct [8].

Cardiovascular disease (CVD) is currently the leading cause of global deaths, accounting for 17.3 million deaths per year, a number that is expected to grow to 23.6 million by 2030 [9]. One of the most prevalent forms of CVD is myocardial infarction (MI). Every year in the United States, approximately 720,000 people suffer from and MI. Of these, early 515,000 cases are first time MIs and 205,000 are recurring MIs in people who have already experienced one or more MIs [10]. When a MI occurs, approximately one billion cardiomyocytes can be affected, which decreases the workload of the heart [11]. This nonfunctioning scar tissue that forms from the MI inhibits the heart's ability to contract. This can lead to the development of heart disease. In 2010, over one million patients were diagnosed with heart failure, or the inability to sufficiently pump blood throughout the body, following a MI. Heart failure

can alter a patients' ability to perform daily activities and tasks that require even minimal physical exertion [12].

2.2 Clinical Treatments

The regenerative capability of the heart is extremely limited and following an MI, the heart cannot repair itself. Thus, in order to repair the heart following an MI, medical intervention is required. Ultimately, the only way to cure irreparable heart failure developed from an untreated MI is a total organ replacement. However, transplantation inherently has many drawbacks. The odds of a heart being available for transplant is 3.5 in every 1000 deaths, or approximately 2000 hearts available each year. This poses a problem as the number of patients on the heart transplant waitlist is above or equal to 3,000 on any given day. Even for those lucky enough to receive a transplant, the risk of organ rejection post-operation is high. While the first year survival rate of heart transplants is 88%, the main cause of death is infection due to the rejection of the donor heart. The percentage of patients developing acute rejection increases from 23% in the first year after operation to 45% in the fifth year after operation [13]. Because of the limited ability of organs available for transplant and the risk of rejection, clinical therapies have been developed to treat heart failure and even potentially regenerate the necrotic tissue developed from a MI.

If a MI is left untreated, scar tissue formation will occur and can change the dimensions of the left ventricle and can cause ventricular wall thinning [14]. As infarct size increases, the ejection fraction, or amount of blood contained within the left ventricle that is ejected with each heartbeat, decreases [14]. In order to maintain normal cardiac output and stroke volume, the contractile pattern and length of the uninjured myocardium changes, often called compensatory responses, and increases the risk of ventricular aneurysm and rupture [14].

Current treatments for MI are aimed at treating the symptoms and effects of the infarction, but do not heal the infarct zone itself. These treatments include coronary bypass and ventricular remodeling.

Coronary bypass is a revascularization procedure that is used to restore blood flow to the myocardium [15]. Coronary artery bypass grafting (CABG) uses a blood vessel to redirect the blood flow around the infarction site and restore blood flow to the ischemic area. This treatment however does no regenerate cardiomyocytes or restore function of the collagenous scar tissue [15].

Ventricular remodeling is used to reshape the heart by either a direct linear closure or an endoventricular patch plasty [16]. For a direct linear closure, a surgeon will reshape the heart by removing the infarcted region and suturing the heart back together. Depending on the infarct size, there may be an insufficient amount of healthy tissue to close the hole created by removing the infarcted region. Because of this, when closing, the surgeon may need to use a synthetic patch to close any remaining gaps in the ventricular wall [17]. This procedure restores the original dimensions of the heart and restores the internal pressure of the ventricle [17].

In the event that the infarcted region is too large to be safely removed, an endoventricular patch plasty is the preferred method for ventricular remodeling. The patch, which is anchored to the ventricular wall, can either be synthetic or autologous tissue. A surgeon will place the patch over the infarcted site and suture it in place. During this procedure, the infarcted region could be removed and the patch could be used to close the hole left behind [17].

The patches used in both of these methods, restore the volume of the ventricle and prevent shrinking of the heart [17, 18]. The synthetic materials commonly used for the patches, polyethylene terephthalate (PET, or commercially known as Dacron) ad polytetrafluoroethylene (PTFE) are inert and possess mechanical properties that are much stronger than native cardiac tissue [19]. The difference in mechanical properties causes fibrotic tissue to develop in the regions where native heart tissue meets the implant, and so, even with this procedure, scar tissue formation can reoccur and develop into large regions of fibrosis [19].

2.3 Cellular Therapies for Tissue Regeneration

Cellular therapies have been developed to regenerate function of tissue that has been damaged by injury or disease. Specifically, in cardiac regeneration, cell therapies are aimed at restoring the original function of the myocardium as opposed to removing the infarct as done in previously mentioned treatments. Cell types that have been used to restore myocardium during cellular therapies include bone marrow stem cells, skeletal myoblasts, embryonic stem cells, cardiac stem cells and fetal cardiomyocytes [20-23]. Most of the cell types however, present drawback that make them less than appealing for use in cellular therapies. Skeletal myoblasts, for instance, lack the capability to electrically couple with myocardium tissue and have been shown to cause fibrillation. Embryonic stem cells present the potential for tumor formation, cardiac stem cells have controversial existence, and fetal cardiomyocytes lack the ability to be obtained in sufficient numbers [20-23]. With the issues regarding these cell types, bone marrow stem cells, specifically human mesenchymal stem cells (hMSCs), are left as the most promising cell type for cardiac repair [24-26].

2.3.1 Mesenchymal Stem Cells for Cardiac Repair

Derived from adult bone marrow, hMSCs are adherent, multipotent cells that have the ability to differentiate into bone, cartilage and fat [28]. hMSCs have many characteristics that make them appealing for use in regenerative medicine including, ease of isolation, high expansion potential *in vitro*, and genetic stability [27-29]. In cardiac regeneration, hMSCs can induce angiogenesis, or the formation of new blood vessels, can be used allogenically without immune response, and can differentiate into a cardiomyocyte-like phenotype [24, 28, 30]. When delivered into the heart, hMSCs have been shown to improve the cardiac function by reducing the infarct size and increasing the ventricular pressure [31-36].

Intramyocardial (IM) cell injections have been used as a method for cell delivery to improve cardiac function following a MI. However, there are several limitations that are associated with IM injections such as low cellular engraftment and retention, poor cell localization, low cell survival and the

lack of a matrix for cell adhesion [12, 24-26, 37]. In order for cellular therapies to be successful in the regeneration of myocardium, the delivery method must be improved.

Several studies have investigated the engraftment of hMSCs following IM injections. A study performed by Hou et al. delivered radiolabeled peripheral blood mononuclear cells (PBMNCs) using an intramyocardial (IM) injection, an intracoronary (IC) injection or an interstitial retrograde coronary venous (IRV) method into a pig model. Six days following induced myocardial ischemia by balloon occlusion for forty-five minutes, 10 million 111 indium-oxine-labeled human PBMNCs were delivered via IC, IM, or IRV injections. One hour after cell deliver, animals were euthanized and organs were harvested for assessment of cell distribution using gamma ray emission counting. The results of this study concluded that the majority of cells delivered were not retained by the heart. Cell retention for the IM injection was 11 ± 3%, IC injection was 2.6 ± 0.3%, and IRV injection was 3.2 ± 1%. It was found that many of the cells intended for delivery of the heart became entrapped in other organs including the lungs, liver, and spleen [38].

In a similar study performed by Guyette et al, IM injections were used to deliver 100,000 quantum dot loaded hMSCs into an infarcted rat heart. Following one hour post injection, animals were euthanized and the hearts were harvested. The hearts were then fixed and cryosectioned to quantify the amount of engrafted hMSCs. The results showed an 11.8 ± 6.2% engraftment rate of cells when delivered via IM injection [39].

These two studies showed that when injecting a liquid cellular suspension into contracting heart muscle, a resulting high percentage of cell leakage out of the heart occurs. This is partially due to the heart's contraction and the puncture hole created by the needle during injection [12, 37]. This liquid suspension, either of phosphate buffered saline or media, does not provide a proper matrix to aid in cell attachment and thus successful delivery [25, 26, 40]. Because of this, there is a need for an effective delivery mechanism to deliver hMSCs into a heart to regenerate infarcted tissue following an MI.

2.4 Fibrin

2.4.1 Fibrin Scaffolds for Tissue Engineering

Fibrin is a biopolymer that is naturally occurring in the body that has been used as a biomaterial for tissue regeneration. Fibrin is created in the body following a series of coagulation reactions that are triggered by platelet adhesion following an injury. This platelet adhesion initiates the production of thrombin, a protease which has the ability to cleave fibrinogen. Fibrinogen is a blood protein that when cleaved by thrombin, forms fibrin. When these two come together to form fibrin, the fibrin becomes insoluble and stops bleeding at a wound site and further promotes healing [41].

The provisional matrix formed by fibrin in the body aids in the wound healing proves by providing a scaffold for cell adhesion, migration and infiltration [41]. Cell adhesion is promoted onto fibrin due to the fact that fibrin contains the protein sequence arginine-glycine-aspartic acid (RGD), a known ligand that promotes cell adhesion. Other benefits of fibrin include the advantage of being able to be produced from autologous fibrinogen and thrombin, its natural growth factors that it contains, as well as its Food and Drug Administration (FDA) approval for use as clinical glues and sealants [42-44].

Fibrin is a versatile biopolymer and can be used in various forms in tissue engineering applications. Fibrin hydrogels are a popular form for tissue engineering and can be used for applications including adipose, cardiovascular, ocular, muscle, liver, skin, cartilage, neural, and bone tissues [45]. In order to be successfully used for these applications, fibrin hydrogels can be combined with different polymers (polyurethanes, polycaprolactones, polycaprolacton-based polyurethanes, b-tricalciumphosphates, etc.) to create customizable mechanical, surface, and degradation properties [45]. As stated previously, fibrin had been FDA approved to be used as a glue or sealant. Fibrin glues can be used for a wide range of applications including bone, cartilage, cornea, heart, blood vessel, tendon, and ligament regeneration [45]. As a glue, it is used to seal or adhere tissues, reduce blood loss during surgical procedures, accelerate healing, as well as protect against infection [46]. Fibrin glues have also been shown to be used as scaffold

matrix for the delivery of cells to a tissue to promote regeneration [47-49]. In any form, a fibrin scaffold can be coated with extracellular matrix proteins, such as fibronectin, vitronectin, laminin, and collagen, to enhance biological activity and cellular adhesion [50].

2.4.2 Fibrin Microthreads

With the known advantageous uses of fibrin for tissue engineering, a fibrin extrusion process was developed at WPI [51]. Fibrinogen and thrombin are co-extruded to form fibrin microthreads. These threads can then be bundled and formed together to form one large diameter thread. This thread can then be used to create fibrin biological sutures. These sutures have been sown to be an effective scaffold for the delivery of human mesenchymal stem cells (hMSCs) into the heart. In the study by Guyette et al mentioned previously, hMSCs were delivered using fibrin sutures. This delivery mechanism exhibited a cell engraftment rate of 63.6±10.6%, a significant increase when compared to the IM injection group at 11.8±6.2 % cell engraftment [39]. The fibrin suture delivery mechanism not only shows an increased engraftment rate of cells delivered into the heart, but also had a more localized delivery when compared to IM injections.

Despite this improved engraftment rate of cells, the initial density of cells seeded onto the sutures remains low. During seeding, 100,000 hMSCs are delivered to the fibrin sutures and allowed 24 hours for cell attachment. However, after the 24 hours, approximately only 10,000 hMSCs are seen to adhere to the sutures [52]. The number of cells adhered onto the sutures could be increased using different methods such as increasing the cell density delivered to the sutures for seeding, increasing the seeding time above 24 hours, or coating the sutures with adhesion proteins. If given the cell attachment percentage remains the same while seeding (10%), increasing the number of cells delivered to the suture would result in a higher number of cells still being wasted, or not adhering to the suture. This makes this approach unfavorable.

Increasing the culture time would allow hMSCs to proliferate on the suture, leading to a higher number of cells on the suture. Unfortunately, the problem with this approach is that hMSCs secrete fibrinolytic enzymes that would degrade the suture over a longer seeding period. This would create a weaker suture that would not have the mechanical strength needed to suture through the heart and deliver the hMSCs [53]. In a study by Coffin et al., 1 cm length fibrin biological sutures were seeded with 50,000 cells in aprotinin supplemented media for time period of 1, 2, 3, and 5 days. The action of aprotinin on kallikrein leads to the inhibition of fibrinolysis. Aprotinin was proposed to decrease the fibrin suture degradation due to its properties of inhibiting proteases such as trypsin. The study showed that at the longer seeding time points (2, 3, and 5 days), the number of cells seeded onto the sutures increased with time. Mechanical testing of fibrin sutures cultured in aprotinin supplemented media also showed a higher elastic modulus and ultimate tensile strength than sutures cultured without aprotinin [54].

The final method to potentially improve cell attachment onto fibrin sutures is coating the sutures with known adhesion proteins. By providing adhesion promoters into the fibrin or onto the fibrin suture surface, cellular attachment would increase. Materials used to increase cellular attachment and adhesion include extracellular matrix proteins such as collagen, fibronectin, laminin, and vitronectin [50]. In a study by Kowaleski et al., fibrin sutures that were coated in vitronectin showed an increase in cell adhesion, 19,604±1.8929 cells, when compared to uncoated sutures, 6,821±739 cells [52].

2.5 Extracellular Matrix

The tissues in the body are comprised of cells living within the extracellular matrix (ECM). The ECM provides not only structural and mechanical support for cells *in vivo*, but also play a very important role in function. As seen in Figure 1, the ECM comprises of a mixture of proteins, polysaccharides, glycoproteins, and growth factors that are in varying ratios depending on the tissue type, function, and overall health which impacts the protein composition as well as the mechanical properties of the tissue

[55]. The differing compositions give the ECM of a tissue a specific stiffness. This stiffness has been shown to affect cellular biochemical signaling [56].
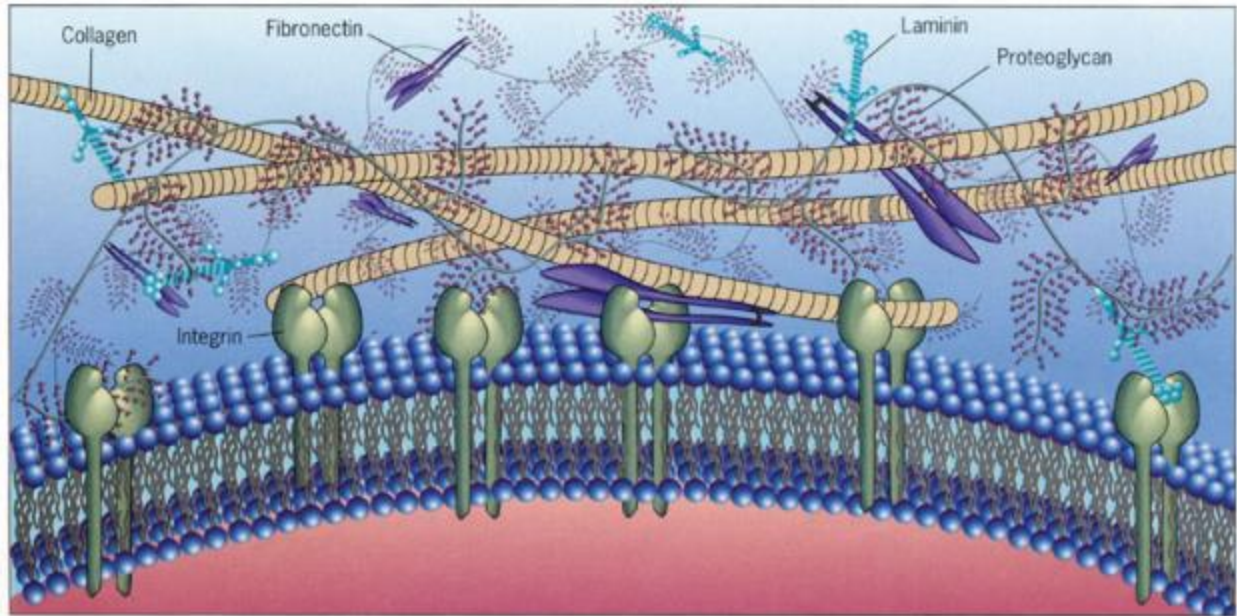
Figure 1 Diagram of the Extracellular Matrix [57]

2.5.1 Proteins of the Extracellular Matrix

Cellular adhesion onto the ECM is signaled by the proteins that are present. The most abundant proteins found within the ECM *in vivo* are collagens, laminins, and fibronectins. Depending on the tissue function, location, and structure, these proteins come in varying concentrations. Aside from these proteins, there are smaller protein fractions that are found for specific tissue types.

Collagen is the main structural protein found within the ECM and is found in different connective tissues in the body, making it the most abundant protein in the body. Between 25 and 35 percent of the total body protein is comprised of collagen and it makes up around three quarters of the dry weight of skin [58, 59]. Collagen is made of a bundle of three parallel, left-handed polyproline II-type helices formed together in a triple helix that typically has two identical $\alpha1$ chains and an additional different $\alpha2$ chain [59]. Collagen's amino acid sequence consists of repeating amino acid sequences of either glycine-proline-X or glycine-X-hydroxyproline where X is any other amino acid other than glycine, proline or hydroxyproline. This amino acid structure makes collagen easily identifiable as well as allows for the

19

variety of $\alpha 1$ and $\alpha 2$ chains which produce many different types of collagen [60]. Currently, there have been 28 different types of collagen that have been identified with the major collagen types being collagen I, II, III, IV, and V [61]. Of these types, collagen I is the most common collagen type and is the primary structural collagen in mammalian tissues. Collagen I provides mechanical support and stability of tissues [58]. Cell attachment to collagen is supported through specific binding sites and integrins [62].

Laminins are a group of proteins found in the ECM that comprise the basal membrane of the ECM. They are trimeric proteins, meaning it is formed by three chains: an α chain, a β chain, and a γ chain. The chain composition determines the name of the laminin [63]. With this nomenclature, there have been fifteen varieties of laminins identified. The three trimeric proteins that make up the laminin form a cross-like structure which allows for binding to cell membranes and other laminin chains to form a laminin sheet [64]. Laminin has been proven to be an important integrin for binding sites for cells and that lack of laminin production caused by genetic defects can be lethal [65].

Fibronectin, as stated previously, is another prominent protein found in the ECM. The structure of fibronectin is dimeric and consists of identical monomers that are linked by disulfide bonds [66]. Within the body, there are two main types of fibronectin, one a soluble protein and the other an insoluble protein. The soluble protein version is a major protein component in blood plasma which is produced by hepatocytes. The insoluble protein version is found in the ECM and is secreted mostly by fibroblasts. The main role of this insoluble fibronectin is aiding in cellular attachment, migration, growth, and differentiation [66]. Cell adhesion to fibronectin is done through the integrin $\alpha 5\beta 1$ binding the repeating amino acid sequence RGD [67].

2.5.2 Integrin Binding

The binding between cells and the extracellular matrix requires transmembrane cell adhesion proteins to link the matrix to the cytoskeleton of the cell. While some transmembrane proteoglycans have been shown to act as co-receptors for matrix components, the primary receptors for mammalian cells for

binding are the integrins. Integrins also play a role in cell-cell adhesion for blood cells [68]. Integrins are transmembrane obligate heterodimers, meaning they consist of two subunits: an α (alpha) and a β (beta). In mammals, there have been eighteen α subunits and eight β subunits that have been discovered [69]. In total, there have been twenty-four heterodimers that have been identified [70]. Integrins form across the cell membrane and act as the main contact between the cell cytoskeleton and the ECM. Specific integrins have been shown to bind to certain proteins as shown in Table 1 below.

Table 1 Integrin-Ligand Binding Specificity [71]

Integrin	Protein
$\alpha_1\beta_1$	Collagens, Laminins
$\alpha_2\beta_1$	Collagens, Laminins
$\alpha_3\beta_1$	Laminins
$\alpha_4\beta_1$	Fibronectin
$\alpha_5\beta_1$	Fibronectin
$\alpha_6\beta_1$	Laminins
$\alpha_7\beta_1$	Laminins
$\alpha_v\beta_1$	Vitronectin
$\alpha_v\beta_3$	Vitronectin, Fibronectin
$\alpha_v\beta_6$	Fibronectin
$\alpha_v\beta_8$	Fibronectin
$\alpha_6\beta_4$	Laminins

When integrins are expressed, they are in a bent structure. It has been postulated that integrins are always bent however evidence has indicated that this bent manner is only observed when the integrins are inactivated. Integrins are activated when the cytoskeleton protein talin primes the integrin by binding to the β subunit and causing a conformational change in the integrin structure to go from bent to fully extended [72]. Once the integrin is activated, binding between the ligands from the ECM and the integrin can occur.

2.5.3 Growth Factors

Growth factors are naturally occurring substances that are able to signal cellular processes such as growth, proliferation, migration, differentiation as well as a variety of other processes. Growth factors act as signaling molecules between cells as well as the matrix in which the cells are present. Common

21

growth factors include vascular endothelial growth factor (VEGF) and the family of fibroblast growth factors (FGFs). VEGF is a potent angiogenic factor that is essential to angiogenesis as well as plays an important role for the cardiovascular system. VEGF expression has been shown in cardiac myofibroblasts which play a major role in the repair of tissue following an infarction [73].

Fibroblast growth factors are a family of growth factors that play roles in a variety of tissues and contribute to cell proliferation, differentiation and survival. In cardiac tissue, FGF has been shown to be upregulated following a cardiac injury, such as an infarct, and contribute to tissue remodeling [74]. Following tissue decellularlization, these growth factors remain within the extracellular matrix along with the other proteins and ECM components. The growth factors present in the decellularized ECM attribute to the success ECM based scaffold applications [75].

2.5.3 Extracellular Matrix Based Scaffolds

The promising properties of ECM have encouraged the development of biological scaffold materials composed of ECM derived from varying tissues. These ECM scaffolds have been shown to facilitate remodeling of many tissues in preclinical animal studies and in human clinical applications. The ECM used in these scaffolds can be derived from various tissue types including skin [76], heart valves [77-83], nerves [84, 85], blood vessels [86-89], small intestinal submucosa [90-92], tendons [93], ligaments [94], and skeletal muscle [95]. These tissues are also derived from multiple species such as humans, pigs (porcine), cows (bovine), and even horses (equine).

The ECM is comprised of a convoluted mixture of molecules arranged in a specific three-dimensional (3-D) pattern that determines structural and biological properties of a tissue. As a scaffold, the ECM is biodegradable, unless processed in a way that forms unbreakable crosslinks between molecules. These two properties; the complex structure and *in vivo* biodegradability, have proven to show positive effects in the process of remodeling that determines clinical outcomes.

Right now, there are a number of commercially available ECM-based scaffold products that have been used in a clinical setting that prove the advantageous aspects of using ECM to repair diseased or damaged tissues. These products include porcine and bovine derived heart valves for human heart valve replacement, decellularized and crosslinked human dermis (Alloderm, Lifecell) and chemically crosslinked purified bovine type I collagen (Contigen, Bard, Inc.). Other products have been used for skin, cartilage, bone, and nerve tissue repair and regeneration.

2.5.4 Extracellular Matrix Based Treatments for Cardiac Repair

In addition to the commercially available ECM products, many experimental studies have been conducted to explore other areas of application for ECM based treatment. As mentioned previously, the ECM from many different organs can be used to regenerate tissues and cells *in vivo*. While the ECM from any organ is comprised of many of the same proteins and molecules, each organ has a unique composition or proteins and other molecules that provides a tissue specific microenvironment for the resident cells. In a study by Sullivan et al. the extracellular matrix of a rat heart was characterized in a healthy state as well as in an infarcted state at different time points. A healthy heart is composed of several proteins including collagen I, collagen VI, laminin and fibronectin. This composition creates a unique microenvironment that is able to guide cell proliferation and differentiation into a cardiac lineage [96].

Many studies have explored the effects that cardiac ECM has on cellular events. In a study by Singelyn et al., a decellularized cardiac ECM based hydrogel was created and evaluated in both *in vitro* and *in* vivo experiments. First, the cardiac ECM hydrogel was incubated with cardiomyocytes and evaluated for cell survival and attachment for up to 5 days. The results were compared to cardiomyocytes cultured on collagen coated dishes and collagen gels. It was found that the cells were able to survive on the ECM hydrogel for up to 5 days. The cardiac ECM hydrogel was also evaluated in a vascular cell migration assay. A Chemotaxis 96-well Cell Migration Assay Kit was used to evaluate the attraction of human coronary artery endothelial cells (HCAECs) and rat aortic smooth muscle cells (RAMSCs) toward

the cardiac ECM hydrogel. The results were compared to a migration assay of the cells toward collagen, fetal bovine serum and pepsin. The migration assay revealed that the RAMSC migration was significantly increased when migrating toward the cardiac ECM hydrogel. The migration of the HCAECs followed this same trend of an increased migration toward the cardiac ECM hydrogel. The results of this experiment showed that the matrix was able to promote migration of vascular cells [97].

Following the *in vitro* study, the researchers performed an *in vivo* study where they injected the cardiac ECM hydrogel into the left ventricular wall of rats. The hearts were evaluated at a short term 4-hour time point and a long term 11-day time point. Following immunohistochemical staining for endothelial cells and smooth muscle cells, the researchers saw significant infiltration of both cell types within the matrix region at 11 days. The 4-hour time point was revealed to be too early for the evaluation of cell infiltration into the matrix [97].

Another study performed by French et al., sought to explore the effects that cardiac ECM has on cardiac progenitor cell (CPC) function *in vitro*. Cells were isolated from adult male rats and were cultured in different matrices. The culture conditions consisted of coating tissue culture plates in either cardiac ECM or Collagen I (COL) isolated from rat tails. Following culture, the CPCs were analyzed for gene expression during cardiogenic differentiation using quantitative PCR transcription. The results of this experiment suggested that the cells seeded onto the cardiac ECM demonstrated an enhanced differentiation toward the cardiac lineage and a decreased maturation toward a fibroblastic lineage. Western blots were also performed on protein samples taken from CPC culture media under the ECM and COL conditions after 7 days. The data from the western showed that CPCs cultured on cardiac ECM had significantly higher levels of Gata-4 and Nkx2.5, known cardiomyocyte markers, when compared to the cells cultured on COL [98].

This study performed many other assays on the CPCs cultured on cardiac ECM and COL including assays for proliferation, survival and adhesion. These experiments revealed many findings. First, the

proliferation assay showed that after 48 hours of cell culture on the cardiac ECM, the CPC had a significant increase in proliferation when compared to those seeded on COL. The survival assay, which consisted of an Annexin V stain performed after 12 hours of CPC culture in serum starved media, showed a decrease in apoptosis for the CPCs cultured on cardiac ECM when compared to those cultured on COL. Finally, a microfluidic adhesion assay was performed under increasing levels of shear stress. The results of this experiment showed that CPCs cultured on cardiac ECM adhered more strongly as compared to those cultured on COL. This study shows that when CPCs are cultured on a 2-D culture plate coated with cardiac ECM, the cells have enhanced adhesion, maturation, proliferation and survival when compared to cells cultured on collage I alone [98].

Cardiac ECM based materials have been shown to be used as successful platforms to increase the differentiation of progenitor cells into a cardiac lineage, promote cardiac cell proliferation and guide endothelial cell migration. These factors prove cardiac ECM to be a useful tool in cardiac regeneration as well as a potential tool to improve our fibrin microthread based biological sutures.

Chapter 3: Hypothesis and Specific Aims

We hypothesize that incorporating decellularized cardiac extracellular matrix into fibrin microthreads will enhance the potential as a stem cell delivery platform when microthreads are used in the form of a suture and will promote endothelial progenitor cell outgrowth.

Specific Aim 1: Produce Fibrin-ECM microthreads, confirm ECM protein incorporation and examine the effect that ECM incorporation has on mechanical and structural performance of fibrin-ECM threads when compared to fibrin only microthreads.

Solubilized extracellular matrix derived from lyophilized decellularized rat hearts will be incorporated into fibrin microthreads during the microthread production process previously developed by Cornwell et al [51]. The ECM will be incorporated at concentrations of 0, 5, 10, 15, 20, and 30 µL of ECM per 1 mL of fibrinogen and thrombin. With increasing concentration of ECM, the crosslinking between fibrinogen and thrombin can be affected, leading to the structure and mechanical stability of the microthreads to change. Diameters of the ECM-fibrin microthreads will be measured to evaluate how microthread structure changes with increasing ECM incorporation. Microthread swelling capability will be determined by the ratio between wet thread diameter measurements and dry diameter measurements. Mechanical properties will be evaluated using single threads in a uniaxial tensile test. The elastic modulus, ultimate tensile strength, and strain at failure will be used to assess mechanical properties of the ECM-fibrin microthreads. The data acquired from the diameter measurements as well as mechanical testing will be compared to data obtained from control fibrin microthreads.

Specific Aim 2: Determine the effect of ECM protein incorporation on cell adhesion to fibrin-ECM sutures.

If the extracellular matrix is the structure that provides cues for cellular adhesion, migration and differentiation *in vivo*, the incorporation of native ECM proteins into fibrin microthreads will inhibit cells

to adhere to sutures at a higher density. To determine the effect on cell attachment, 100,000 hMSCs will be seeded onto sterile ECM-fibrin sutures for 24 hours. Following seeding, sutures will undergo a Cyquant DNA Assay to count the number of cells adhered to the sutures as well as Hoescht and Phalloidin staining for visual confirmation of cell seeding.

Specific Aim 3: Determine the effect of ECM protein incorporation on endothelial progenitor cell outgrowth.

Cell outgrowth of endothelial progenitor outgrowth cells (EPOCs) will be evaluated to show the effect that the ECM incorporated into the fibrin presents. EPOCs will be plated into a 6-well plate at 10,000 cells/cm^2 and allowed to reach full confluency. A standard scratch assay will then be performed by scratching the plate surface with a 200uL micropipette tip down the approximate center of each well. In wells 1 and 2, a 15% ECM microthread will be placed within the scratch and weighed down so that it does not move. This will be repeated for fibrin microthreads in wells 3 and 4. Wells 5 and 6 will serve as control wells and will be left blank. The outgrowth in each well will be evaluated every 6 hours for 24 hours by obtaining images at four designated locations in each well. Following the 24-hour outgrowth, the average distance travelled of the cells will be determined from the images. Finally, the microthreads will be removed from the 6-well plate and will be stained with DAPI to determine if any cell attachment onto the microthreads occurred.

Chapter 4: Aim #1: Produce ECM Microthreads, Confirm ECM Incorporation and Test for Mechanical Properties

4.1 Introduction

The purpose of this aim is to evaluate the effect that ECM has on the mechanical properties and structure of fibrin microthreads when incorporated at varying concentrations. Decellularized cardiac extracellular matrix will be solubilized into a homogeneous mixture and then incorporated into a fibrin microthread procedure previously developed by Cornwell et al [51]. Once ECM-fibrin microthreads are created in varying concentrations, they will be tested and evaluated for ECM incorporation confirmation through immunohistochemical staining for major cardiac ECM proteins and mechanical properties such as elastic modulus and ultimate tensile strength.

Our hypothesis is that the ECM solution will be successfully incorporated into fibrin microthreads when incorporated into fibrinogen and thrombin separately prior to solution mixing. Also, we hypothesize that by incorporating ECM into fibrin, the microthread diameters will decrease as ECM concentration within the microthreads increases. Lastly, we hypothesize that the microthread mechanical properties of elastic modulus and ultimate tensile strength will decrease with increasing ECM concentration.

4.2 Methods

4.2.1 Rat Heart Decellularization Process

All animal procedures were performed in accordance with the Institutional Animal Care and Use Committee at Worcester Polytechnic Institute and NIH Guide for the Care and Use of Laboratory Animals. Hearts were isolated from Sprague Dawley retired breeder adult rats following animal euthanasia with an intracardiac sodium pentobarbital injection. Hearts were stored in Dulbecco's phosphate buffered saline (DPBS) (Corning) and frozen at -30°C until ready to use. For decellularization, hearts were thawed and

www.manaraa.com

transferred to a petri dish containing fresh DPBS. A perfusion-based decellularization process was unnecessary as the structure of the heart would not be kept intact during further processing. This lead to the choosing of an immersion-based decellularization process. To prepare the hearts for decellularization, they were minced into small pieces approximately 3mm x 3mm x 3mm.

Minced heart tissue of approximately four hearts was then placed into one 50 mL conical tube containing 25 mL of 1% sodium dodecyl sulfate (SDS; Sigma) in deionized (DI) water. The conical tubes were rotated on a Scilogex MX-T6-S rotator until tissue samples appeared translucent, approximately 1 to 2 days with the 1% SDS solution being changed every 12 hours. Following SDS immersion, the heart tissue pieces were rotated in 25 ml 1% Triton-X 100 (Sigma) in DI water for 24 hours with the solution being changed once after 12 hours. The final step of the decellularization process was to clear the tissue in DI water for 24 hours, changing the DI water after 12 hours. This final step washed any remaining chemicals from the tissue sections.

Following the final step of decellularization, the DI water was removed from the conical tubes and the ECM pieces were re-suspended in approximately 10 mL of fresh DI water for storage. The conical tubes were then placed in a -80°C and stored until tissue lyophilization. The decellularization process of the cardiac tissue is illustrated in Figure 2 below. A detailed procedure of cardiac decellularization can be found in Appendix A.1.

*Figure 2 **Left:** Full hearts obtained from adult Sprague Dawley rats. **Middle:** Heart tissue minced into small pieces. **Right:** Decellularized cardiac tissue.*

4.2.2 Decellularized ECM Lyophilization

Decellularized heart tissue was lyophilized using an SP Scientific VirTis Benchtop Pro with Omnitronics lyophilizer (SP Scientific, Warminster, PA). Conical tubes containing frozen decellularized heart tissues in DI water were prepared for lyophilization. Briefly, the caps to the conical tubes were removed. Next, a KimWipe was placed over the opening of the conical tube and was secured tightly with tape. This is seen in Figure 3.
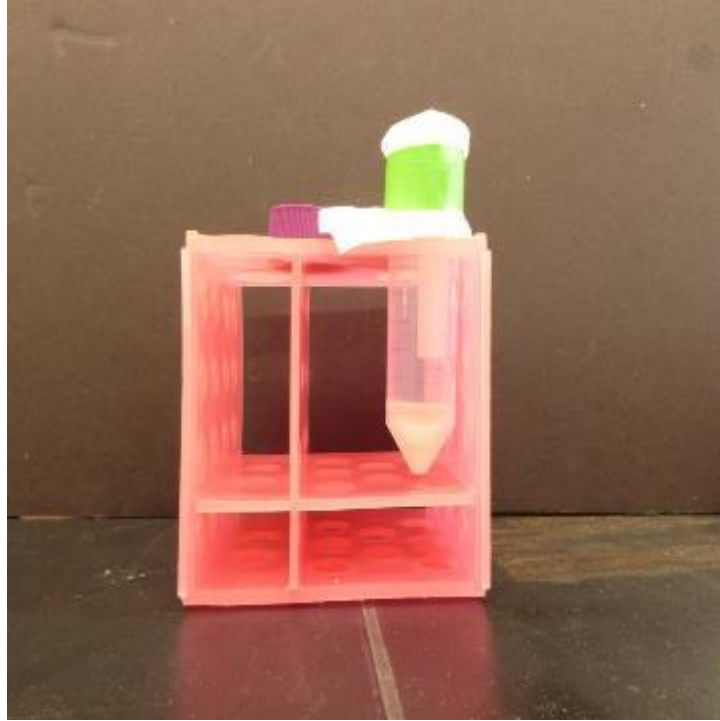
Figure 3 Decellularized ECM frozen in approximately 10mL of DI water prepared for lyophilization.

The KimWipe will allow for the lyophilizer to pressurize the tubes while ensuring that no ECM is lost within the conical tube. Finally, the conical tubes were kept on ice until they were placed in the lyophilizer to ensure no premature thawing occurred.

While the ECM samples were being prepared the VirTis lyophilizer was turned on and set to reach a temperature of -104.3°C and a pressure of about 14 millitorr (mTorr). When the machine was ready, the conical tubes were placed in a glass chamber and vacuum sealed onto the machine. Samples were lyophilized until all ice crystals had been visually removed. This process could take between 12 hours and 4 days, depending on the initial DI water volume within the conical tube. Lyophilized ECM samples were stored in a -80 °C freezer, to keep moisture out of the tissue, until ECM solubilization. Figure 4 below shows the decellularized ECM after it had been lyophilized. A detailed procedure of ECM lyophilization can be found in Appendix A.2.

Figure 4 Decellularized ECM has been lyophilized at -104.3°C and 14mTorr for approximately 48 hours

4.2.3 Lyophilized ECM Solubilization

Lyophilized ECM samples were obtained from a -80 °C freezer and placed on ice. ECM was ground into a powder using a mortar and pestle that had been stored at -80˚C to ensure that the lyophilized ECM did not thaw. Large-sized pieces of ECM needed additional cutting with iris scissors into smaller pieces for successful grinding.

Extracellular matrix solubilization was performed using a previously defined protocol [99]. Briefly, 10mg of porcine gastric pepsin (Sigma Aldrich) was dissolved in 10ml of 0.1M HCl. Then, 100mg of ground ECM was added to the solution and stirred using a magnetic stir plate. The original protocol called for 48 hours of stirring however, upon inspection our ECM had not fully solubilized at 48 hours and so the solution was stirred until nearly full solubilization could be seen. It was found that after 5 days, the ECM was fully or nearly fully solubilized. After solubilization, the ECM solution was neutralized to a pH of 7.4 with 1M NaOH and refrigerated for up to 1 week. The figure below, Figure 5, shows the ECM throughout

32

the process of solubilization. The final concentration of the solubilized ECM was 100mg/10mL or 10mg/mL. A detailed procedure of lyophilized ECM solubilization can be found in Appendix A.3.

*Figure 5 Solubilization process of decellularized ECM. **Left:** 100mg of the lyophilized ECM is measured and placed into a glass scintillation vial. **Middle:** A solution of 10mg of pepsin and 10ml of 0.1M HCl is added to the ECM. **Right:** The ECM is fully solubilized following 5 days of constant stirring.*

4.2.4 ECM-Fibrin Microthread Co-Extrusion

ECM-Fibrin microthreads were co-extruded using solutions of fibrinogen and thrombin supplemented with ECM by altering a previously developed protocol for fibrin microthread extrusion [51]. Briefly, thrombin isolated from bovine plasma (Sigma, St. Louis, MO T4648) at a concentration of 40 U/ml was frozen at -20˚C as a stock solution; and diluted to a concentration of 6 U/ml in 40mM $CaCl_2$ (200uL thrombin in 850uL of 10mM $CaCl_2$) for extrusion. Fibrinogen (Sigma, St. Louis, MO F4753) was dissolved in HEPES buffered saline solution (HBSS, 20mM HEPES, 0.9% NaCl) at a concentration of 70 mg/ml and stored at -20˚C. Fibrinogen and thrombin aliquots were placed in room temperature water and warmed to 37˚C. Separately, approximately 1mL of the solubilized ECM solution was isolated from the stock solution and placed in a 1.7mL microcentrifuge tube. The ECM solution was then filtered using decreasing

33

sized hypodermic needles. First the ECM solution was filtered through an 18-gauge needle to remove larger insolubilized pieces of ECM. The ECM solution was then filtered through both 20-gauge and 22-gauge needles in succession. Finally, the ECM solution was filtered through a 27-gauge needle to filter out any final ECM particles that could potentially clog the polyethylene tubing used during microthread extrusion. The filtered ECM was then placed in a separate 1.7mL microcentrifuge tube.

The fibrinogen and thrombin were then prepared with the incorporation of ECM at varying concentrations between 0 and 20 percent ECM (v/v). Briefly, for the 5% ECM microthreads, 950μL of thrombin and fibrinogen were individually transferred to separate 1.7mL microcentrifuge tubes. Next, 50μL of the filtered ECM solution was added into the tubes and mixed thoroughly. The thrombin and fibrinogen ECM solutions were then drawn up into separate 1mL syringes using 20-gauge needles. The needles were removed and the syringes were loaded and secured into a New Era 6-channel syringe pump (New Era Syringe Pumps, Farmingdale, NY). The thrombin and fibrinogen syringes were attached to the input ports on a FibriJet blending connector (Nordson Micromedics, Loveland, CO). Polyethylene (PE) tubing with an inner diameter of 0.38 mm (Scientific Commodities Inc, Lake Havasu City, AZ) threaded onto a 27-gauge needle was attached to the output port of the blending connector. The solutions were pumped at a rate of 0.23mL/min through the PE tubing into a room temperature bath of 10mM HEPES with 20mM $CaCl_2$ buffer at pH of 7.4 and the microthreads were extruded using a hand-drawn technique. Following extrusion, the microthreads were kept in the HEPES bath for 15 minutes to allow for formation. The ECM-fibrin microthreads were then removed from the bath and hung horizontally across a cardboard box to air dry overnight. Other ECM-fibrin concentrations for microthread formation are shown in Table 2. The procedure for ECM-fibrin microthread extrusion can be found in Appendix B.

Table 2 Volumes of ECM solution and fibrinogen and thrombin to make ECM-Fibrin microthreads.

ECM Final Concentration by Volume	Fibrinogen Volume	Thrombin Volume	ECM Volume in F and T
10%	900µL	900µL	100µL
15%	850µL	850µL	150µL
20%	800µL	800µL	200µL
30%	700µL	700µL	300µL

Using the concentrations of the individual microthread components as well as their concentration within each microthread type, we were able to calculate an overall fibrinogen, thrombin and ECM concentration in each microthread type. For example, in order to make the 5% ECM microthreads, 50uL of the ECM solubilized solution was added to fibrinogen and 50uL of the ECM solubilized solution was added to the thrombin. In order to add this 50uL to the fibrinogen and thrombin, the initial volumes of fibrinogen and thrombin were reduced by 50uL, or an overall 5%. Therefore, the final concentrations of fibrinogen and thrombin changed from their initial concentrations. The initial concentration of fibrinogen is 70mg/mL. When decreasing this by 5%, the concentration of fibrinogen is 66.5mg/mL. The initial concentration of thrombin is 6U/mL. When decreasing this by 5%, the concentration of thrombin is 5.7U/mL. The initial concentration of ECM being added into the fibrinogen and thrombin is 10mg/mL. For the 5% ECM microthreads, a total of 100uL is used. Therefore, there is 1mg of ECM in the final 2000uL of fibrinogen and thrombin, or 0.5mg of ECM per 1000uL of fibrinogen and thrombin. Using the average number of threads produced per extrusion, we calculated the average amount of ECM within each thread. Table 3 below shows the values derived from the calculations to determine the final concentrations of fibrinogen, thrombin and ECM.

Table 3 The final concentrations of fibrinogen, thrombin and ECM calculated based on the final ECM solution volume for each thread type.

Microthread Type	Final Total Fibrinogen Concentration	Final Total Thrombin Concentration	Final Total ECM Concentration
Fibrin	70 mg/mL	6 U/mL	0 mg/mL
5% ECM	66.5 mg/mL	5.7 U/mL	0.5 mg/mL
10% ECM	63 mg/mL	5.4 U/mL	1 mg/mL
15% ECM	59.5 mg/mL	5.1 U/mL	1.5 mg/mL

4.2.5 Immunohistochemical Staining for Cardiac Extracellular Matrix Proteins

Once the microthreads were created, they were fluorescently stained for some of the major cardiac ECM proteins including Collagen I (Santa Cruz Biotechnologies, Dallas, TX), Fibronectin (Abcam, Cambridge, UK) and Laminin 111 (Abcam, Cambridge, UK) to confirm ECM incorporation. Similar to how samples for diameter measurements were prepared, a 2cm section of an individual microthread was secured to a glass slide using superglue. For each microthread type, 2 samples were prepared per stain so that one could be used for a negative control. Each stain was performed 4 times, making the total number of positive stained sampled per protein stain, 4.

The staining for proteins followed a general protocol to fix and stain for specific proteins. Briefly, the samples were rinsed in DPBS twice for approximately 5 minutes and then fixed in 4% paraformaldehyde (Fisher Scientific, Fair Lawn, NJ) in DPBS for 10 minutes. Samples were then washed two times again in DPBS and then treated with 0.25% Triton X-100 (Sigma Aldrich, St. Louis, MO) in DPBS for 10 minutes. Following two more DPBS washes, the samples were blocked in 1% bovine serum albumin (BSA) (Fisher Scientific) in DPBS for 45 minutes. Following blocking, the samples intended to show a positive signal were treated with the primary antibody for the protein of choice overnight. The samples intended for a negative signal were kept in 1% BSA in DPBS. The next day, all samples were washed in DPBS twice for 5 minutes each and treated with the secondary antibody of the protein of choice for 1

hour. Samples were then washed two final times in DPBS. Coverslip spacers were added and the sampled were sealed with Cytoseal™ 60 and then covered with glass coverslips. Table 4 lists the primary and secondary antibodies used for protein staining as well as the concentrations of each.

Table 4 Concentrations for IHC protein staining for major cardiac proteins.

Protein	Primary Antibody	Primary Concentration	Secondary Antibody	Secondary Concentration
Collagen I	Anti-Collagen I sc8783	1:200μL in BSA	Rabbit Anti-goat 488	1:400μL in BSA
Fibronectin	Anti-Fibronectin ab2413	1:200μL in BSA	Goat-Anti-Rabbit 546	1:500μL in BSA
Laminin 111	Anti-Laminin ab11575	1:100μL in BSA	Goat-Anti Rabbit 488	1:500μL in BSA

Stained thread samples were visualized and imaged on a Leica Upright DMLB2 fluorescent microscope at 20X magnification. Images were also taken on a Leica TCP SP5 confocal laser scanning microscope (Leica, Germany) for higher quality imaging and to assess the surface changes on the microthreads following ECM incorporation. Images were qualitatively assessed for protein fluorescent signal. A detailed procedure for the immunofluorescent protein staining can be found in Appendix C.

4.2.6 Structural Analysis of ECM-Fibrin Microthreads

Fibrinogen is a fairly viscous fluid and it can be hypothesized that when adding the solubilized ECM, a much less viscous fluid, the resulting microthreads will have different structural properties than normal fibrin microthreads. To determine how the ECM affects the structure of fibrin, diameter measurements of the microthreads were taken for each type of ECM-fibrin microthread. A 3cm section of an individual microthread was cut and secured to a glass slide using Gorilla Glue® super glue. An image at three different locations on the microthread were obtained on Leica SM LB2 inverted microscope at 20X magnification. In order to get a representative diameter over the 3cm section, the first image was taken within the first centimeter of the thread, the second image was taken within the middle centimeter of the thread and the third image was taken in the final centimeter of the thread. The microthread sections were then hydrated in DPBS for 20 minutes. Following hydration, two drops of DPBS were placed on each

www.manaraa.com

microthread and a glass coverslip was then laid across the microthread. Three images of each hydrated thread were taken again at 20X magnification in the same manner as the dry images. This was repeated so that each microthread type had 8 total representative microthread sections for diameter measurements.

Diameters were measured using the measuring feature in ImageJ software. Briefly, each image was loaded into the software for analysis. The image was scaled to ensure the measurements to be accurate: for 20X magnification: 376 pixels: 100µm. Once scaled, a line was drawn across the microthread from edge to edge to represent the true diameter of the thread. The length of the drawn line was then measured using the software. This was repeated so that 10 total measurements were taken per image. The measurements for each image were then combined with the measurements from the images of the rest of the microthread section. These 30 measurements were then compiled with the rest of the measurements for the microthread type so that all 240 measurements could be used for statistical analysis.

Diameter measurements were taken for all images of dry and wet microthreads. In the hydrated state, the microthreads were imaged in the same manner that the dry images were taken. This allowed us to have dry diameter measurements and wet diameter measurements that were taken for the same area on the microthread. Once all measurements were made, the swelling ratio between the wet and dry measurements was determined by dividing the individual wet diameter measurements by their corresponding dry diameter measurement. The swelling ratio of the threads is used to determine the potential that the threads will have to increase their surface area to attain maximum cell seeding in future experiments. For all measurements, standard deviations were determined as well using Excel.

4.2.7 Tensile Testing of ECM-Fibrin Microthread Mechanical Properties

Mechanical testing was performed on an Instron E1000, using a 1N load cell. The samples were pulled to failure at a rate of 10mm/min. For each microthread type; fibrin, 5% ECM, 10% ECM, and 15%

ECM, six samples were tested using a strain to failure method. Each round of testing was performed 6 times, making the total number of samples 36. Each sample consists of a four-centimeter section of a microthread that is attached to a mechanical testing construct made of vellum paper, cut into rectangles measuring 2cm x 4cm. In the middle of the construct, a 3cm long section has been cut out of the rectangle. The microthread sample was laid over this open space and secured on either end using medical grade silicone adhesive (Bluestar Silicones, Ventura, CA). The microthread construct can be seen in Figure 6.
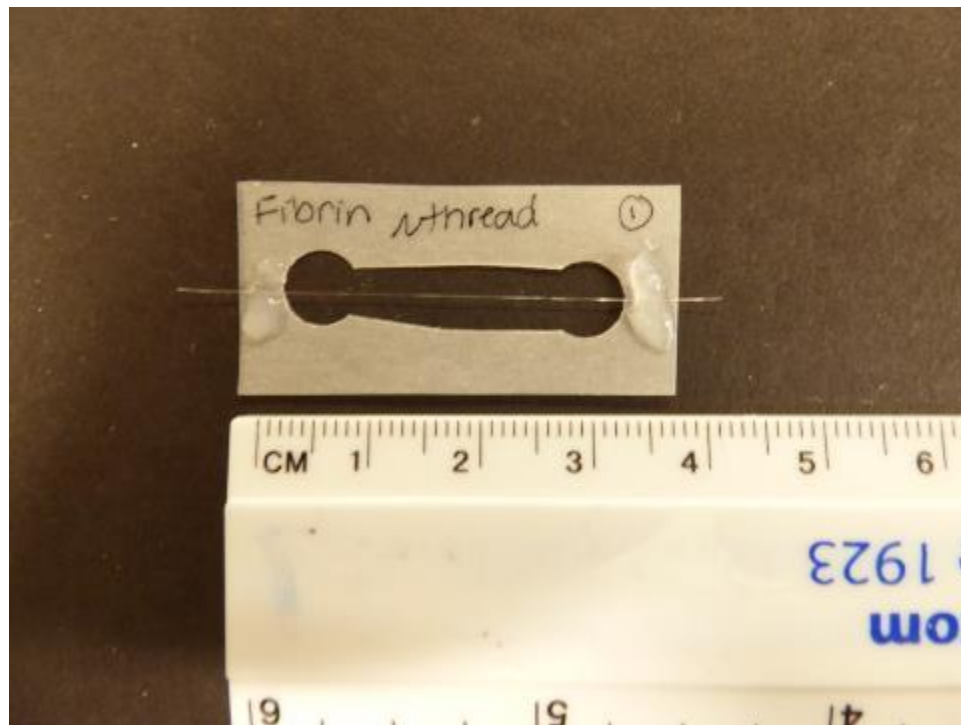
Figure 6 Microthread Mechanical Tensile Testing Constructs.

Each testing sample will be taken from one single microthread to ensure the data collected is an accurate representation of the microthread type. The testing constructs were left overnight to allow the silicone adhesive to fully cure.

In preparation for mechanical testing, each construct was hydrated in Dulbecco's phosphate buffered saline (DPBS) for 20 minutes. Each sample was imaged for hydrated diameter measurements as described previously in section 4.2.6. The average diameter for each thread will be used to calculate the

original cross sectional area to then accurately determine the ultimate tensile strength. The construct was then loaded on to the Instron and secured using custom modified steel alligator clips seen in Figure 7.

Figure 7 Modified Steel Alligator Clips for Microthread Tensile Testing.

The microthreads were continuously hydrated using DPBS from a dropper until the test began. Upon the start of the test, the vellum paper construct was cut to allow for tensile pulling and the microthread was pulled taught, in case the microthread was drooping slightly between the grips. Once the microthread was completely loaded, the length was measured in order for accurate calculations of the ultimate tensile stress and strain.

Using Bluehill software, a tensile test to failure was performed on each microthread. Microthread diameter and initial microthread length between the grips was input into the Bluehill software for calculations and the test was started. The data output by the Bluehill software was in Force (N)/ Displacement (mm). Using the measured diameter and length of the microthread, the Force-Displacement was converted to Stress-Strain and plotted. Finally using a MatLAB code, the stress-strain curve was used to determine the Ultimate Tensile Strength (UTS), Elastic Modulus (E), and Strain at Failure (SAF). Other

parameters calculated were Plastic Modulus and Yield Strength, however these parameters were not used for statistical analysis.

4.2.8 Statistical Analysis

All results are presented as mean ± standard deviation. Individual data points are represented graphically in a vertically aligned scatter plot. The diameter measurements and mechanical testing parameters were first analyzed to remove data point outliers. For diameter measurements, a computer calculation was used to determine outliers. For mechanical testing measurements, two round of data analysis was used to remove outliers. First, samples were removed from further data analysis if they experienced failure at the grips. Secondly, the data points for each mechanical parameter were analyzed using a computer calculation to remove further outliers. The results were then compared using an ordinary one-way ANOVA test. The statistical significance for the diameter comparisons was determined as $p<0.0001$. The mechanical statistical significance was determined as $p< 0.05$.

4.3 Aim 1 Results

4.3.1 Immunohistochemical Staining Results

Microthreads of varying ECM-fibrin concentrations were stained for major cardiac proteins including Collagen I, Fibronectin, and Laminin 111. Following the staining, the microthreads were imaged using a fluorescent microscope to qualitatively assess the incorporation of ECM into the fibrin as well as a confocal microscope to assess microthread surface changes with the inclusion of ECM. The figures below show the inverted microscope and confocal microscope images of the microthreads after being stained for the proteins collagen I (Figure 8), laminin 111 (Figure 9) and fibronectin (Figure 10). The fluorescent images taken using the inverted microscope (Figures 8 A, 9 A, and 10 A) show that when compared to normal fibrin microthreads, the ECM-fibrin microthreads exhibit the fluorescent signal when the major cardiac proteins are present. The control fibrin microthreads does not exhibit this signal, suggesting that

these proteins are not present in the fibrin microthreads but become present when the solubilized ECM is incorporated during the extrusion process. The images taken using a confocal microscope (Figures 8 B, 9 B, and 10 B) show the effect that ECM incorporation has on microthread surface topography. As seen, the surface topography of the microthreads visibly changes as the ECM incorporation concentration increases.
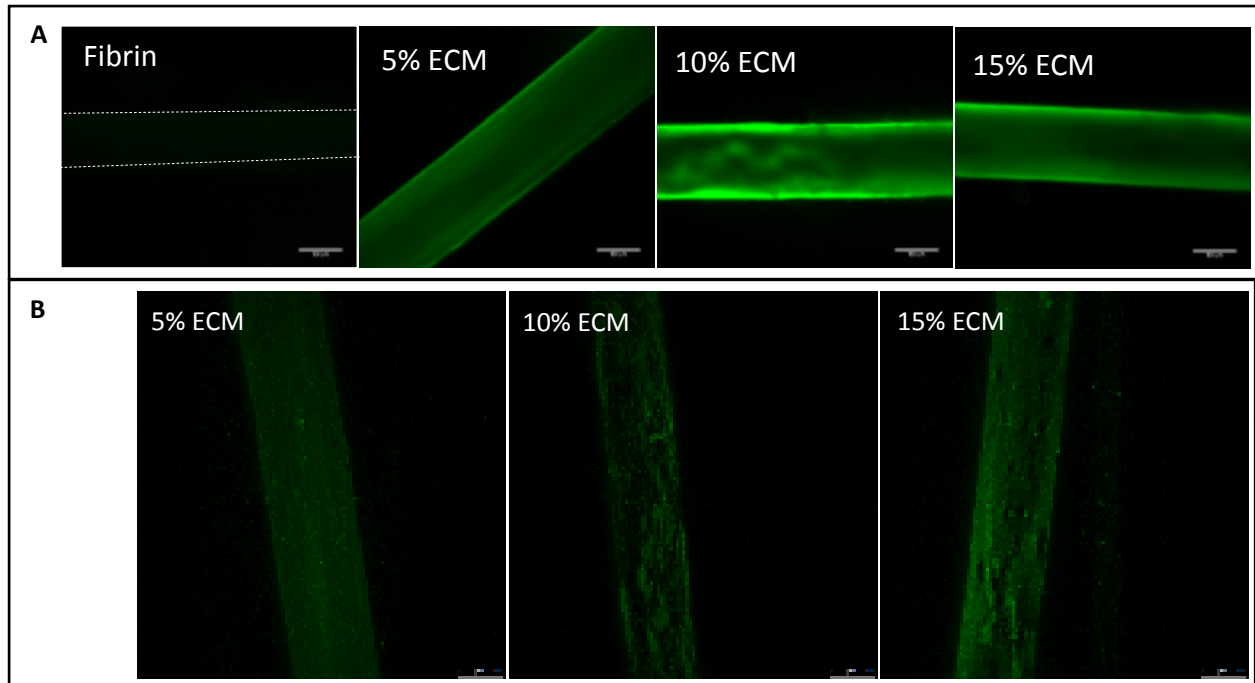
*Figure 8 Immunofluorescence of ECM-fibrin microthreads that had been stained for Collagen I. **A.** Inverted fluorescent microscope images of the microthreads. **B.** Confocal microscope images of the microthreads. Scale bar=100um*
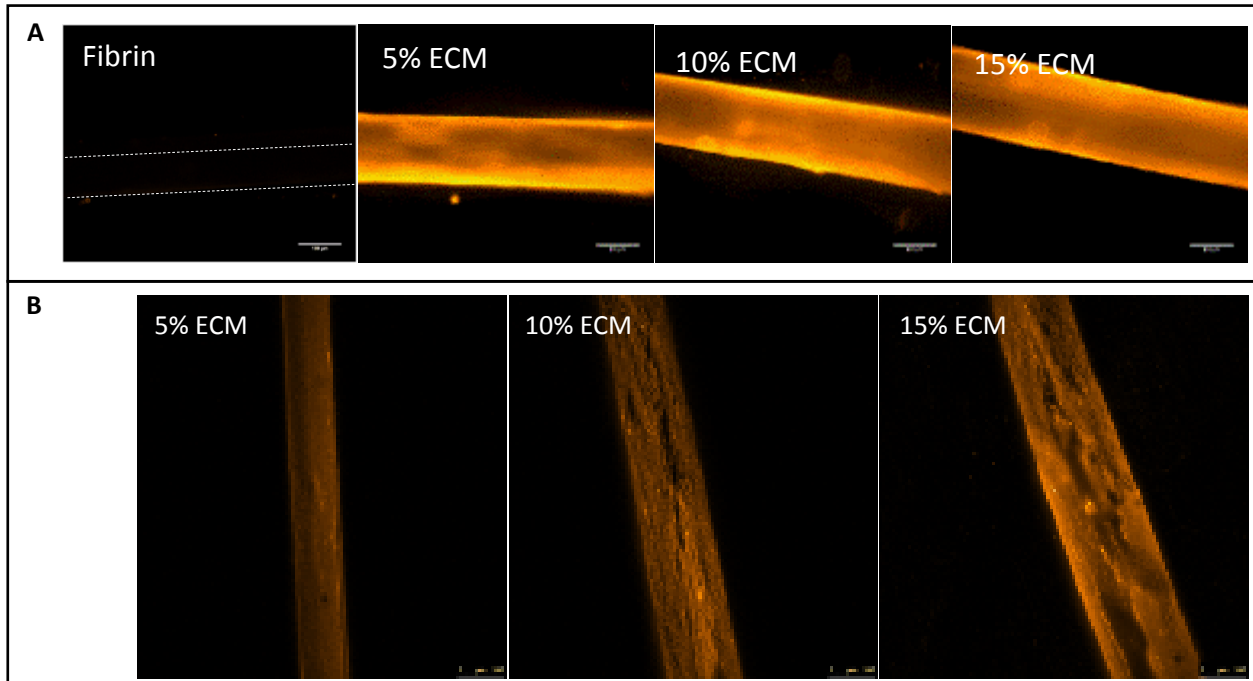
*Figure 9 Immunofluorescence of ECM-fibrin microthreads that have been stained for Laminin 111. **A.** Inverted fluorescent microscope images of the microthreads. **B.** Confocal microscope images of the microthreads. Scale bar=100um*
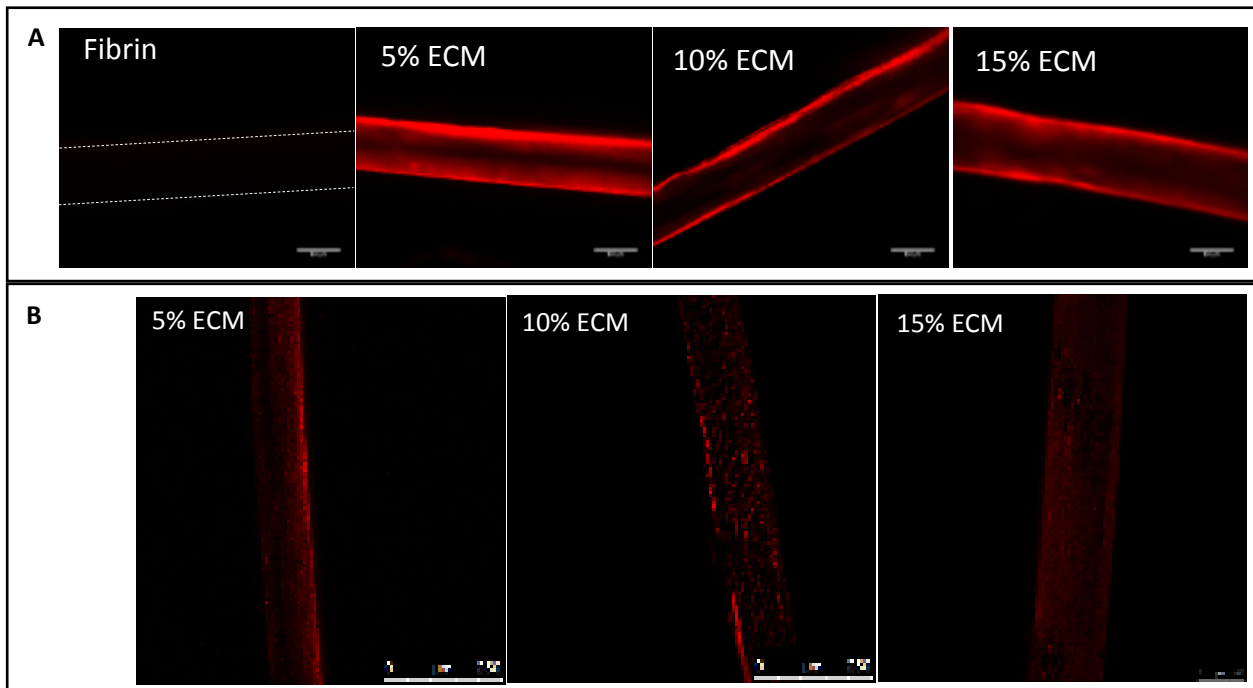
*Figure 10 Immunofluorescence of ECM-fibrin microthreads that have been stained for Fibronectin. **A.** Inverted fluorescent microscope images of the microthreads. **B.** Confocal microscope images of the microthreads. Scale bar=100um*

4.3.2 Microthread Diameter Results

Diameter measurements of the ECM-fibrin microthreads were used to determine the effect that ECM incorporation can have on structural properties of fibrin microthreads. Following microthread extrusion, the ECM-fibrin microthread types underwent measuring of their dry and wet diameters using microscope imaging and ImageJ software. The diameters determined from the dry and wet threads were also used to determine the swelling capability of the threads. Table 5 below shows the average diameters of the varying types of ECM-fibrin microthreads in their natural dry state as well as after being hydrated for 20 minutes. The average swelling percentage is also shown in the table.

*Table 5 Average dry and wet diameter measurements and swelling ratio of the microthread types. * $p<0.001$, ** $p<0.0001$, n=8 microthreads*

	5% ECM	10% ECM	15% ECM	FIBRIN
DRY DIAMETER (UM)	71.4±14.3*	51.9±15.1	65.6±25.9	88.8±18.8**
WET DIAMETER (UM)	157.2±38.1**	124.4±42.8	145.3±59.3	195.7±75.9**
SWELLING RATIO (%)	219.6±26.9	231.9±50.0	225.7±39.6	224.5±82.6

Figure 11 graphically shows the values in Table 5 as a comparison of the diameters of the ECM-fibrin microthreads when dry and wet. The dry diameters of the microthreads decrease with increasing ECM concentration with the exception of the 15% ECM microthreads when compared to the 10% ECM. However, overall the diameters of the microthreads that have ECM incorporated into them have diameters that are significantly less than that of the fibrin only microthreads. The wet diameters follow this same trend as well.
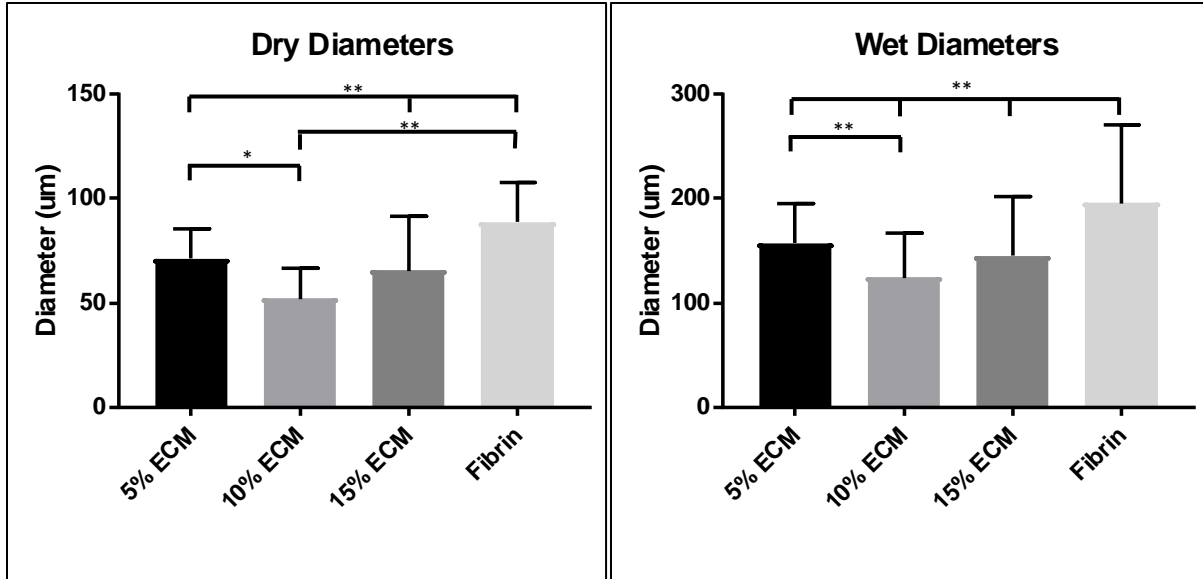
*Figure 11 Comparison of average Right: dry diameters and Left: wet diameters of the fibrin and ECM-fibrin microthreads. An asterisk (*) is used to indicate a statistical significance. * p<0.001, ** p<0.0001, n=8 microthreads*

Figure 12 shows the comparison of the swelling ratio values as percentages of the varying types of ECM-fibrin microthreads. Coupled with the data shown in Table 5 above, for every ECM-fibrin microthread concentration, the microthreads swell by nearly or more than 200%. This shows that while the incorporated ECM decreases both the dry and wet diameters of the microthreads, it does not significantly affect the microthread's ability to swell and increase its' surface area.
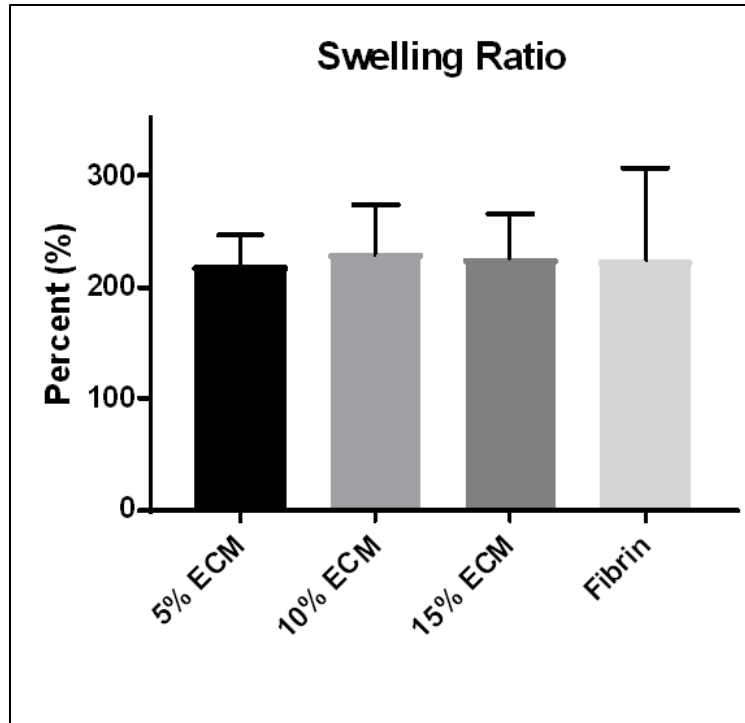
Figure 12 Comparison of the average swelling percentage for each ECM-fibrin microthread type.

4.3.3 Microthread Mechanical Testing Results

Uniaxial tensile testing was used to quantify the mechanical properties of the ECM-fibrin microthreads and to determine the effect that ECM incorporation has on microthread mechanical properties. The first microthread mechanical parameter that was analyzed was the ultimate tensile strength, UTS. Table 6 below shows the mean UTS for each of the ECM-fibrin microthread types. Figure 13 shows a graphical representation all the resultant data points from each microthread tested. The results are presented as individual data points in a vertically aligned scatter plot that shows the first, second (mean), and thirst quartiles for each data set.

Table 6 Mean ultimate tensile strengths of the ECM-fibrin microthread types. (n=32, n=33, n=33, n=25)

	5% ECM	10% ECM	15% ECM	FIBRIN
ULTIMATE TENSILE STRENGTH (MPa)	1.8 ± 1.2	2.1 ± 1.7	2.4 ± 1.7	1.9 ± 1.3
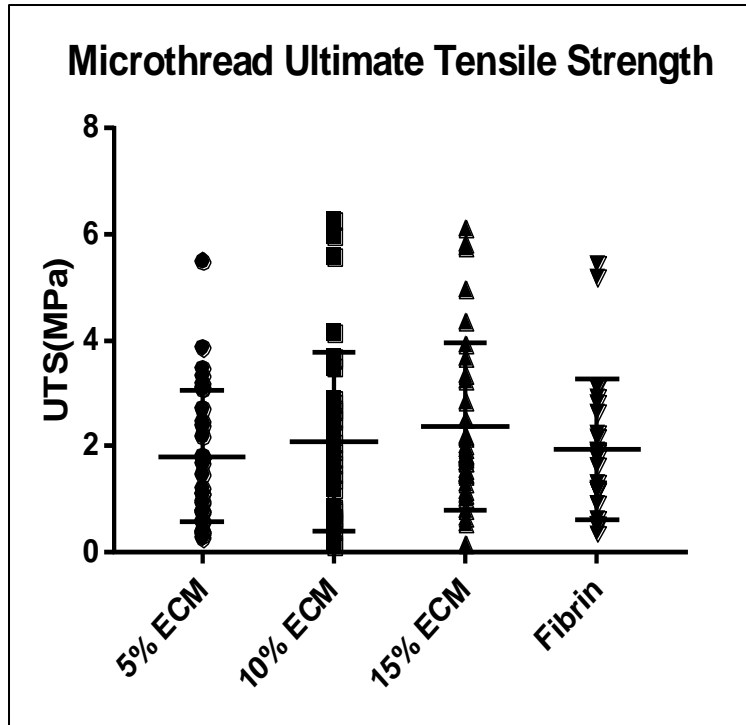
Figure 13 Ultimate tensile strength results for the varying ECM-fibrin microthread types. (n=32, n=33, n=33, n=25)

The mean UTS for each ECM-fibrin microthread type shown in Table 6 shows an increase in the UTS at 10% ECM and 15% ECM incorporation when compared to fibrin. The 5% ECM showed a decrease in mean ultimate tensile strength when compared to fibrin. After statistically analyzing these results it was found that the differences in mean ultimate tensile strengths were not statistically significant.

Another microthread mechanical parameter that was analyzed was the microthread strain at failure, SAF. Table 7 below outlines the mean SAF for each of the microthread types. The individual data points are represented graphically in Figure 14 as a vertically aligned scatter plot that shows the first, second (mean) and third quartile of each data set.

Table 7 Mean strain at failure (mm/mm) for the ECM-fibrin microthread types. (n=29, n=30, n=32, n=24)

	5% ECM	*10% ECM*	*15% ECM*	*FIBRIN*
STRAIN AT FAILURE (mm/mm)	0.422 ± 0.302	0.471 ± 0.308	0.488 ± 0.283	0.564 ± 0.353
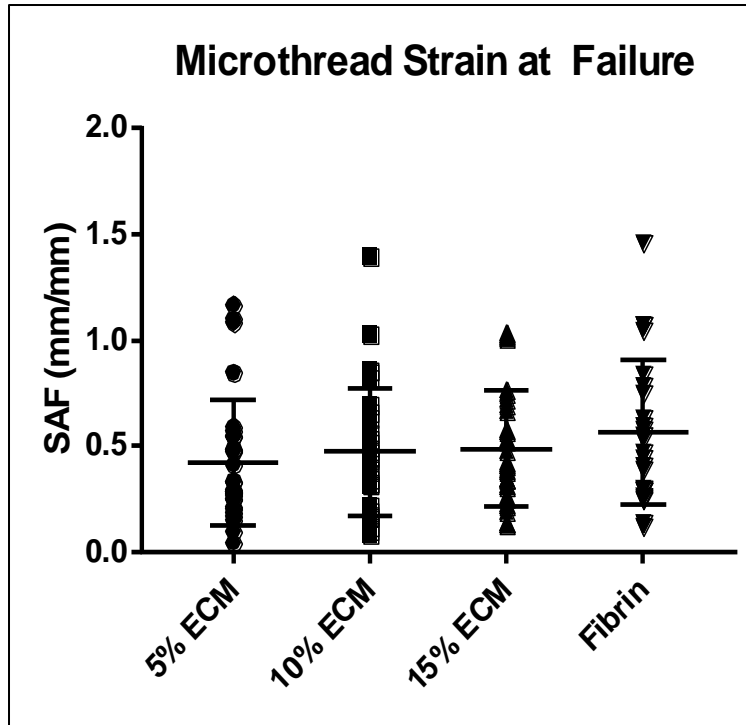
Figure 14 Strain at failure (mm/mm) results for the varying ECM-fibrin microthread types. (n=29, n=30, n=32, n=24)

When compared to the mean SAF for the fibrin microthread group, the ECM-fibrin microthreads all had a mean strain at failure that was less than the fibrin. Within the ECM incorporated microthread groups, a slight increase in mean SAF is seen as the ECM incorporation increases. The statistical analysis showed however, that the differences between the mean strains at failure were found to not be significant.

The final microthread mechanical parameter that was evaluated was the microthread elastic modulus, E. The elastic modulus is a measurement of the stiffness of a material. Table 8 below shows the mean modulus for each of the ECM-fibrin microthread types. Figure 15 represents the individual data points graphically as a vertically aligned scatter plot that shows the first, second (mean), and third quartile for each data set.

*Table 8 Mean elastic modulus (MPa) for each of the ECM-fibrin microthread types. *p<0.05, (n=29, n=33, n=32, n=21)*

	5% ECM	*10% ECM*	*15% ECM*	*FIBRIN*
ELASTIC MODULUS (MPa)	3.1 ± 3.2	5.9 ± 6.5*	4.7 ± 4.1	2.4 ± 2.3
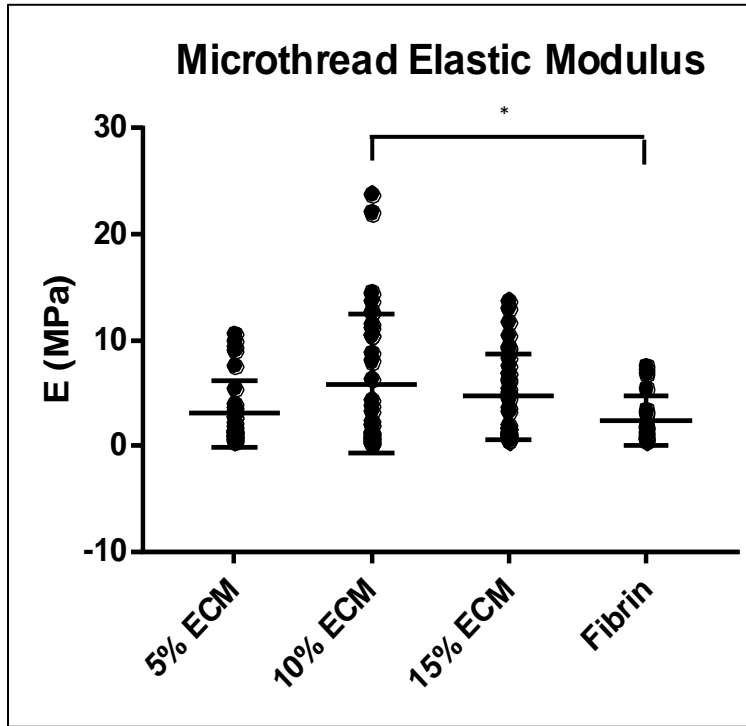
Figure 15 Elastic modulus results of the varying types of ECM-fibrin microthread types. (n=29, n=33, n=32, n=21). An asterisk (*) is used to indicate a statistical difference between the elastic moduli for the 10% ECM microthreads and the fibrin microthreads. *p<0.05

The mean modulus of fibrin was 2.36 ± 2.34 MPa. A comparison of this value to the three values for the 5% ECM (3.05 ± 3.18 MPa), 10% ECM (5.90 ± 6.51 MPa), and 15% ECM (4.65 ± 4.05 MPa), shows that ECM incorporation increases the elastic modulus of the microthreads. The statistical analysis showed significance (p<0.05) between the mean modulus of fibrin microthreads and the mean modulus of 10% ECM microthreads. The mean moduli of all ECM-fibrin microthread types are represented by the graph below in Figure 16.
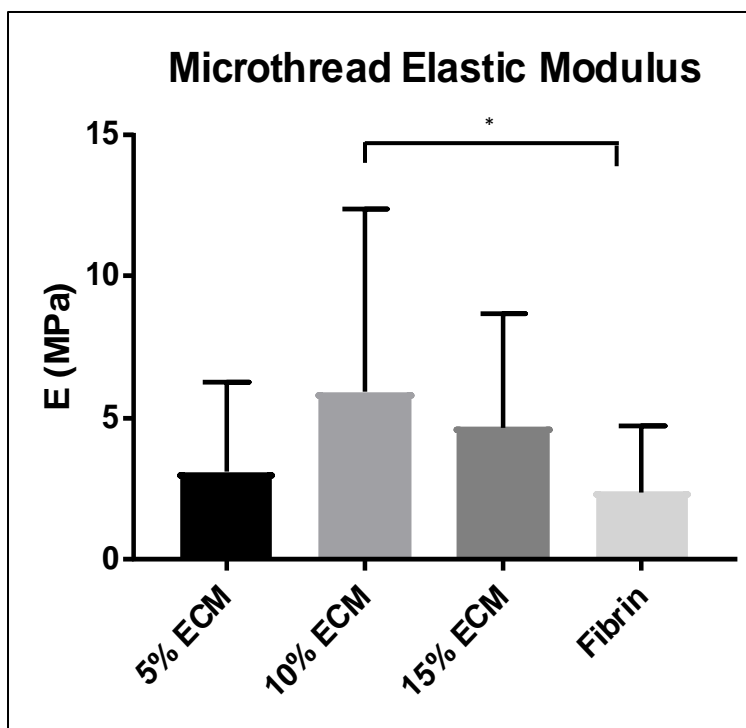
Figure 16 Mean elastic moduli (MPa) for the varying types of ECM-fibrin microthreads. (n=29, n=33, n=32, n=21). An asterisk (*) is used to indicate a statistical difference between the elastic modulus for the 10% ECM microthreads and the fibrin microthread modulus. *p<0.05

The results from this experiment indicate a few key findings relating the effect that ECM incorporation has on structural and mechanical properties of fibrin microthreads. First, the ECM can be successfully incorporated into the fibrin microthread extrusion process and the proteins present in cardiac ECM can be detected within the microthreads using immunohistochemistry. Secondly, the diameters of the microthreads significantly decreases with the addition of ECM into the fibrin. This was seen when comparing the diameter of the fibrin only microthreads to the diameters of the varying ECM-fibrin microthread concentrations. This decrease in diameter was seen in both dehydrated and hydrated microthreads. While the diameters did decrease, the swelling ratio of the microthreads was not affected by the ECM incorporation. The control fibrin microthreads showed to swell by a two-fold increase. This was also seen in the microthreads that had ECM incorporated into the fibrin. Lastly, we can conclude that the results from the uniaxial mechanical testing indicate that the incorporation of ECM into fibrin microthreads is neither statistically increasing nor decreasing the ultimate tensile strengths or strains at

failure of the microthreads. However, the ECM does increase the stiffness or elastic modulus of the microthreads, statistically when incorporated at 10% ECM.

4.4 Aim 1 Discussion

This aim sought to explore the effects that ECM incorporation has on fibrin microthread structural and mechanical properties. The following discussion seeks to support our results and conclusions gained from the first series of experiments.

4.4.1 Microthread Diameters

Our first experiment in this aim was to determine how ECM incorporation affects microthread diameter. We hypothesized, that when the ECM solution is mixed into thrombin and fibrinogen prior to microthread extrusion, the resulting microthreads will have a diameter that is less than pure fibrin microthreads. In a study by Nayak, et al., a group researched the effects that a material's viscosity has on electrospun fiber diameter. In the study, Nayak et al. fabricated polypropylene (PP) nanofibers and adjusted the PP viscosity prior to electrospinning using additives such as sodium oleate (SO), poly(ethylene glycol) (PEG), and poly(dimethyl siloxane) (PDMS). It was found that the shear viscosity of PP decreased with the addition of PEG and PDMS and increased with the addition of SO. The results of diameter measurements showed a decrease in fiber diameter with the solutions of lower viscosity [100].

The viscosity of fibrinogen solutions depends on the total protein concentration and the temperature of the solution. In a study by Jensen et al., the viscosity of a fibrinogen solution that was at 5.4g/L at 20°C was found to be about 1.1mPa.s [101]. Our fibrinogen solution that we use for microthread extrusion is 70mg/mL, or an equivalent 70g/L. While we did not measure the viscosity of our fibrinogen, we can assume that when we use it, at room temperature, the viscosity will be higher than 1.1mPa.s. The digested ECM solution was visibly less viscous following the solubilization. We hypothesized that when this less viscous solution was added to the more viscous fibrinogen, the resulting microthreads would be finer than those of pure fibrinogen. Due to the previously mentioned research, we can determine that the

viscosity of the ECM solution does affect fibrin microthread formation and the resulting microthread diameter. Our findings found that the microthread diameters significantly decreased following the addition of ECM into the fibrin microthreads. The decrease in diameter was seen when the microthread was both in a dehydrated and hydrated state. However, when we calculated the swelling ratio, we saw that all the types of fibrin-ECM microthreads increased their size by nearly 200%. This leads us to conclude that while the ECM incorporation does decrease the microthread diameter in both dehydrated and hydrated states, the ECM does not affect the microthread capability to swell. The swelling of the microthreads is an important factor during stem cell seeding. The microthread ability to increase its surface area allows for more potential binding are for stem cell adhesion.

4.4.2 Microthread Mechanics

The second experiment in this aim sought to determine the mechanical differences between the fibrin only microthreads and the ECM-fibrin microthreads. Our findings found that the mean values for strain at failure and ultimate tensile strength did not substantially differ between the different concentrations of ECM-fibrin microthreads and fibrin only microthreads. Our results for mean elastic modulus values found a significantly higher modulus in the microthreads that were 10% ECM when compared to fibrin only microthreads.

Previous studies have created fibrin and collagen matrices in the hopes of creating a scaffold with properties that are superior to fibrin only scaffolds and collagen only scaffolds. These studies have looked at both the mechanical properties of fibrin-collagen co-gels as well as their cell seeding abilities. In a study by Rowe and Stegemann, bovine collagen, bovine thrombin, and bovine fibrinogen were used to create fibrin-collagen mixed tubular constructs of varying protein concentration [99]. During formation, the gel constructs were seeded with rat aortic smooth muscle cells (RAMSCs) and cultured for a period of 7 days. Uniaxial mechanical testing was performed on the constructs at day 7. The constructs were sectioned into rings and subjected strain to failure test at 0.3 mm/s. The study found that in the mixed fibrin-collagen

52

constructs (35-55kPa), the material moduli were significantly increased when compared to pure collagen (11.2kPa) and pure fibrin (21.9kPa) constructs. The study also found that the ultimate tensile strength (UTS) for the pure collagen construct (4.6kPa) was significantly less than that of the pure fibrin construct (27.7kPa). However, the pure fibrin construct was nearly equivalent to the fibrin-collagen construct that was 50% fibrin and 50% collagen (28.4kPa). All other fibrin-collagen mixture constructs had UTS values of around 20kPa [98]. In a later study by the same group, fibrin-collagen constructs created using either bovine thrombin or an ancrod snake venom enzyme to polymerize the constructs. Uniaxial mechanical testing was performed on the constructs to compare mechanical properties. This study too found that the fibrin-collagen constructs polymerized with thrombin showed significantly increased modulus when compared to the control pure collagen scaffolds [103]. These studies concluded that the mechanical properties of biopolymer networks can be improved by varying the quantity and ratios of the component proteins. A structure-function relationship could be determined by a further study of how the protein component fibers interact with each other and with a cellular component [102, 103].

Our results aligned with the trend that these studies found. The material moduli for the fibrin-ECM microthreads were greater than that of the fibrin only microthread, significantly between the 10% ECM-fibrin and fibrin microthreads. Out study also found that the fibrin microthread UTS was not significantly different that the UTS values of all fibrin-ECM microthread types.

Chapter 5 Aim #2: Human Mesenchymal Stem Cell Seeding on Fibrin-ECM Sutures

5.1 Introduction

The purpose of the experiments in this aim is to determine if the ECM-fibrin microthreads promote a higher cell attachment density for human mesenchymal stem cells. In order to evaluate the effect that the ECM-fibrin microthreads have, sutures made from a bundle of microthreads will be seeded with a suspension of human mesenchymal stem cells for 24 hours. Following, the seeded sutures will undergo both qualitative analysis consisting of immunohistochemical staining for cell nuclei and the cytoskeletal protein f-actin as well as quantitative analysis consisting of a CyQuant cell proliferation assay.

We hypothesize that the ECM present in the fibrin-ECM microthreads will aid in the attachment of hMSCs to the sutures. Also, with increasing ECM concentration, we will see an increase in the density of cell attachment.

5.2 Methods

5.2.1 ECM-Fibrin Microthread Bundle Making

To increase the mechanical properties of the fibrin microthreads and increase the area for potential cellular attachment, Guyette et al. bundled several microthreads together to create a single large diameter microthread to form sutures [39]. ECM-fibrin sutures were created following this same manner. Briefly, twelve microthreads were lined up close together on a dark surface and secured using a small piece of laboratory tape. The microthreads were then hung by the tape using a clamp. The initial length of the bundle of threads was measured to ensure the bundle was not overstretched in the final step of the bundling process. The threads were grouped together by dragging a drop of DI water along the threads until the entirety of the bundle was hydrated. The bundle was then twisted in a clockwise

motion from the bottom of the bundle to entwine microthreads together. The unsecured end of the bundle was then clamped and pulled tightly so that the final length of the bundle should be close to that of the original length of the dry unbundled microthreads. This bundling process can be seen in Figure 17 below.
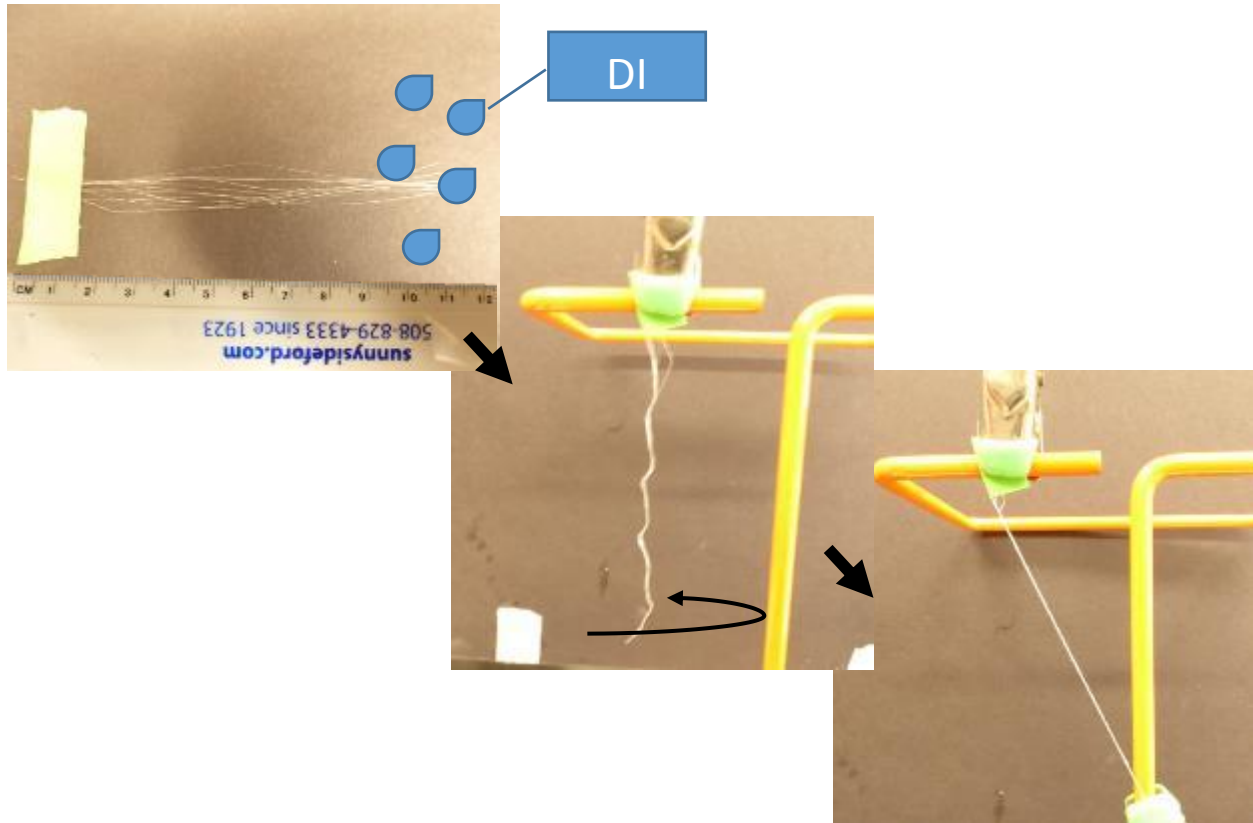
*Figure 17 Microthread bundling process. **Left**: 12 individual microthreads are bound together with lab tape. **Middle**: Microthread cluster is hung on a lab stand and hydrated with DI water and then twisted together. **Right**: The bundle is stretched taught to dry.*

5.2.2 ECM-Fibrin Suture Production

Microthread bundles were cut to 5 cm lengths and threaded through the eye of a size 26, 3/8 circle reverse cutting surgical suture needle (Havel's Inc., Cincinnati, OH). With the needle situated so that it is placed in the middle of the bundle, the bundle was hydrated in DPBS for twenty minutes. Following hydration, the needle was clamped in curved hemostats. The bundle ends were then folded over the needle and adjusted to be the same length on either side of the needle, in case the bundle moved during

handling. The ends were then twisted in a clockwise motion to entwine the bundle, then clamped using a

second hemostat and pulled taught and left to dry. After the suture was completely dry, it was removed

from the hemostats and cut to a final length of 2 cm. This process can be demonstrated in Figure 18 below.
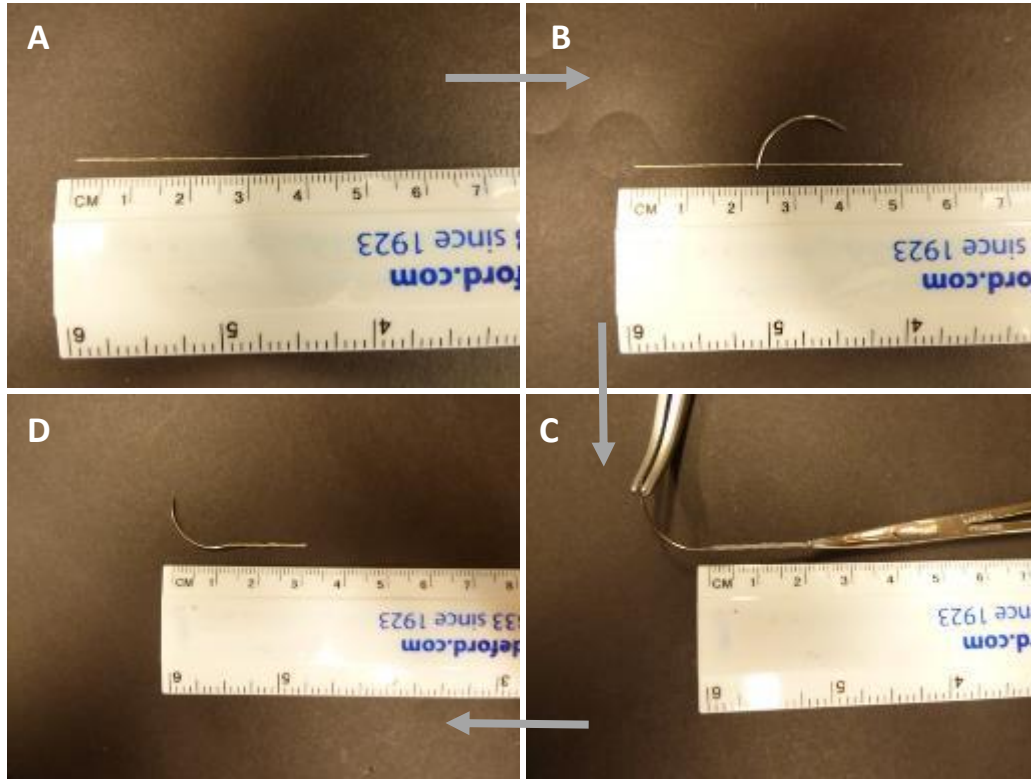
*Figure 18 **A.** A 5cm section of a bundle is cut. **B.** The bundle is threaded through the eye of a needle. The bundle will then be hydrated to 20 minutes in DPBS. **C.** The hydrated bundle is twisted together and stretched between two hemostats. **D.** A 2 cm fibrin suture.*

For future seeding experiments, the sutures were placed in a specially designed bioreactor. This

bioreactor consists of a section of gas-permeable Silastic silicone tubing (1.98 mm inner diameter, Dow

Corning, Midland, MI) cut to approximately 5 cm. A slide clamp is used to secure the suture needle in the

tube as well as a 27-gauge needle that will be used to deliver a cell suspension to the suture during

seeding. The bioreactor system as well as a second slide clamp was placed in an instant sealing pouch

(Chex-All II, Long Island City, NY). Sutures were sterilized via ethylene oxide sterilization for 14 hours and

were degassed for at least 24 hours before cell seeding. The seeding bioreactor can be seen in Figure 19

below. A detailed procedure of the bundling and suture making process can be found in Appendix D.
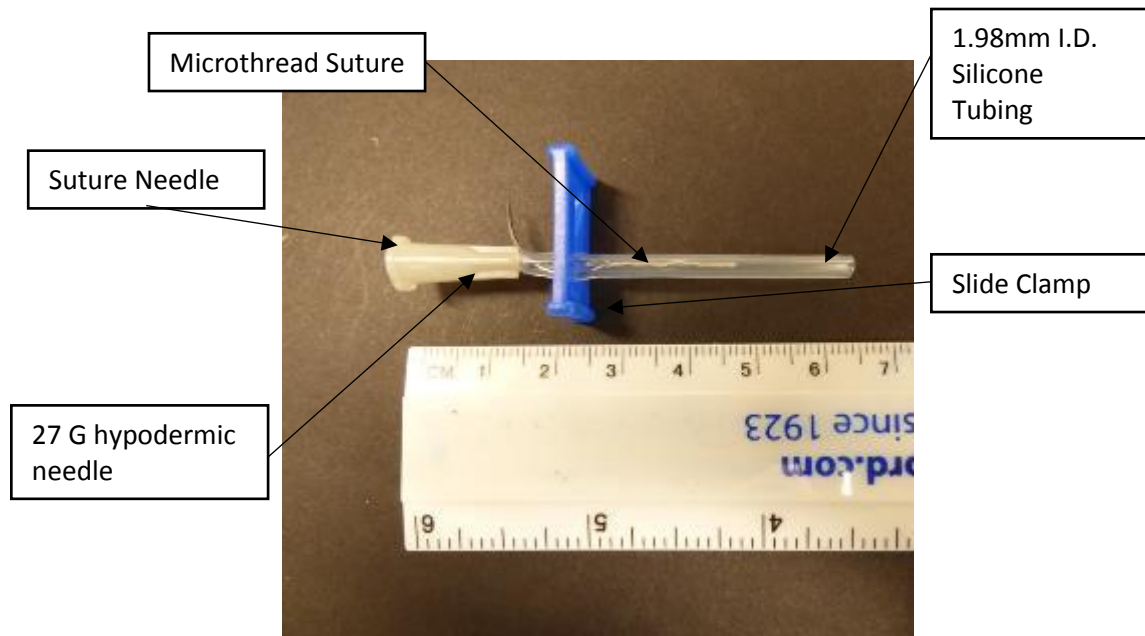
Figure 19 Suture housed inside a bioreactor. Gas permeable silicone tubing s used to allow ethylene oxide sterilization to occur as well as gas exchange for cell survival during seeding. A 27G needle will be used to deliver DPBS and the cell suspension. The slide clamps are used to create a seal and hold the cells within the bioreactor.

5.2.3 Cell Culture

Human mesenchymal stem cells (hMSCs; Lonza, Walkersville, MD) were cultured in Mesenchymal Stem Cell Growth Medium (MSCGM; Lonza PT-3001, Walkersville, MD) in compliance with the manufacturer's guidelines. Cells were grown until they reached between passages 5 and 7 before they were used for cell seeding experiments.

5.2.4 Suture Seeding

Sterile sutures, prepared according to section 5.2.2, were used in hMSC seeding experiments. For each seeding experiment, 8 sutures of each of the four types of microthreads were used. Within the group of 8 sutures, 6 sutures would be seeded with hMSCs and 2 sutures would be seeded with media only and would act as controls for further analysis. This cell seeding experiment was performed 5 separate times.

The procedure to seed the sutures with hMSCs followed a protocol previously developed by Guyette et al [39]. Briefly, in a biological safety hood, the sutures were first hydrated in sterile DPBS for at least twenty minutes. During the hydration, a cell suspension of hMSCs at a concentration of 1×10^6

57

cells/mL was created. After removing the DPBS, sutures were seeded with 100uL of the hMSC cellular suspension, delivering approximately 50,000 cells per 1 cm of suture. This was done by drawing 100uL of the cell suspension into a sterile 1mL syringe via a 20-gauge hypodermic needle. The syringe was then detached from the 20-gauge needle and re-attached to the 27-gauge needle included in the suture bioreactor. The cell suspension was injected into the tubing containing the suture. After removing the syringe and 27-gauge needle, the second slide clamp included with the bioreactor was placed onto the tube to seal the bioreactor. Bioreactors were placed into a vented 50mL conical tube and placed onto a Scilogex MX-T6-S rotator in a 37°C incubator (5% CO_2, atmospheric gas concentration). The samples were rotated for 24 hours. A more detailed procedure of hMSC cell seeding onto sutured can be found in Appendix E.

5.2.5 Cell Seeding Quantitative Analysis: CyQuant Cell Proliferation Assay

The CyQuant cell proliferation assay kit (Molecular Probes, Eugene, OR) uses a DNA stain to fluorescently label DNA and standard curve to correlate the fluoresced DNA to a number of cells. Of the original 6 sutures from each thread type that were seeded with cells, 4 were used in this CyQuant assay. One of the control sutures with media only was also used as the control for this assay.

Following the suture seeding protocol described in 5.2.4 previously, the sutures were removed from the bioreactors and removed from the suture needle. The sutures were then placed in 500μL of DPBS in 1.7mL microcentrifuge tubes. Sutures were then centrifuged for 5 minutes at 2000 RPM to remove any non-adherent cells. After centrifugation, 400μL of the DPBS was removed from each microcentrifuge tubes and the samples were placed in a -80°C freezer overnight. The DPBS lyses the cells in the freezer and releases the DNA in solution. After freezing the samples overnight, the samples were gradually brought to room temperature. Once fully thawed, the samples were frozen a second time at -80°C for at least 1 hour to ensure total cell lysis. The samples were then removed from the freezer and brought to room temperature a second time.

After reaching room temperature, 400μL of a cell lysis buffer was added to each sample microcentrifuge tube. The CyQuant cell lysis buffer consists of 1mL of the stock cell lysis buffer included in the kit, 50μL of CyQuant GR fluorescent dye and 19mL of DPBS. The microcentrifuge tubes were lightly agitated after the addition of the lysis buffer using a Vortex Genie to mix the lysis buffer and microthread sample.

In order to properly quantify the number of cells seeded onto the sutures, a standard curve of cells is used to correlate the amount of DNA detected by the assay to the number of cells. The standard curve consists of a starting cell suspension of 120,000 hMSCs in 100μL of DPBS. This cells suspension was created according to the following steps. First, a cell suspension of 120,000 cells per 1mL of media is created and placed into a 1.5mL microcentrifuge tube. The suspension is then centrifuged at 2000 RPM for 5 minutes. The media is then removed from the microcentrifuge tube and 500μL of sterile DPBS is added to the cells. The cells are then centrifuged again at 2000 RPM for 5 minutes. Finally, 400μL of DPBS is removed from the microcentrifuge tube, leaving a final cell suspension of 120,000 cells in 100μL of DPBS. This cell sample is then frozen overnight at -80˚C to lyse the cells in the cell suspension. After freezing, the cell suspension was brought to room temperature and 900μL of the cell lysis buffer was added to the microcentrifuge tube. This solution was then briefly vortexed.

Using a flat bottomed 96 well plate, 100uL of the CyQuant lysis buffer was added to wells in columns 1-4 and rows B-H. In row A, columns 1-4, 200μL of the DNA cell suspension for the standard curve, approximately 24,000 hMSCs, was added. Immediately afterwards, 100μL of the solution in well A1 was transferred to well B1 and mixed thoroughly with the 100μL of cell lysis buffer present in the well. This process was then repeated down the column to cell G1 and then repeated for columns 2, 3 and 4. An additional 100μL of cell lysis buffer was added to each well A1-H4 to bring the total volume in each well to 200μL. Row H contained no cells to serve as blanks for the standard curve. The standard curve is illustrated in Figure 20.

Figure 20 Schematic of a 96-well plate used for CyQuant cell proliferation assay. In Columns 1-4 and Rows A-H, a standard curve is created to correlate the amount of DNA detected on the sutures to a set number of cells.

Following the DNA standard curve preparation, the suture samples were each lightly vortexed before being removed from their individual microcentrifuge tubes and placed on microscope slides and hydrated in DPBS. Next, 100μL of the cell lysis buffer/cell solution for each sample was added into four wells of the 96 well plate. Once all samples had been added to the 96 well plate, the plate was placed in a Victor3 1420 Plate Reader to record the optical density at 480 nm. The standard curve was created using the values from A1-H4 and each sample reading was correlated to number of cells. The fluorescent reading for each of the four wells per suture were averaged to calculate the average number of cells per centimeter of suture. Figures 21 and 22 illustrate the orientation of the seeded and control samples in the 96-well plate. Two 96-well plates are used in order to accommodate for the standard curve as well as the number of samples seeded during each experiment performed.

	1	2	3	4	5	6	7	8	9	10	11	12
A					FIBRIN CONTROL SUTURE				5% ECM SEEDED SUTURE 3			
	12000	12000	12000	12000	1	2	3	4	1	2	3	4
B					FIBRIN SEEDED SUTURE 1				5% ECM SEEDED SUTURE 4			
	6000	6000	6000	6000	1	2	3	4	1	2	3	4
C					FIBRIN SEEDED SUTURE 2				10% ECM CONTROL SUTURE			
	3000	3000	3000	3000	1	2	3	4	1	2	3	4
D					FIBRIN SEEDED SUTURE 3				10% ECM SEEDED SUTURE 1			
	1500	1500	1500	1500	1	2	3	4	1	2	3	4
E					FIBRIN SEEDED SUTURE 4				10% ECM SEEDED SUTURE 2			
	750	750	750	750	1	2	3	4	1	2	3	4
F					5% ECM CONTROL SUTURE				10% ECM SEEDED SUTURE 3			
	375	375	375	375	1	2	3	4	1	2	3	4
G					5% ECM SEEDED SUTURE 1				10% ECM SEEDED SUTURE 4			
	187.5	187.5	187.5	187.5	1	2	3	4	1	2	3	4
H					5% ECM SEEDED SUTURE 2				15% ECM CONTROL SUTURE			
	0	0	0	0	1	2	3	4	1	2	3	4

Figure 21 Complete 96-well plate used for CyQuant. This first plate contains the standard curve as well as seeded and control suture samples for each suture type.

	1	2	3	4	5	6	7	8	9	10	11	12
A	15% ECM SEEDED SUTURE 1											
	1	2	3	4								
B	15% ECM SEEDED SUTURE 2											
	1	2	3	4								
C	15% ECM SEEDED SUTURE 3											
	1	2	3	4								
D	15% ECM SEEDED SUTURE 4											
	1	2	3	4								
E												
F												
G												
H												

Figure 22 The orientation of samples for the second 96-well plate used for CyQuant.

Following the CyQuant assay, the now lysed sutures were fixed and stained with Hoescht (1 in 6000μL of DPBS for 5 minutes). Following, they were viewed under a Leica Upright DMLB2 fluorescent microscope to confirm that all cells have been removed during the cell lysis process. A detailed version of this procedure can be found in Appendix F.

5.2.6 Cell Seeding Qualitative Analysis: Hoescht and Phalloidin Fluorescent Staining

The remaining 2 seeded sutures and one control suture were used to qualitatively assess the hMSC seeding with the use of fluorescent staining. Sutures were removed from their bioreactors following 24 hours of rotation with the cell suspension. They were then rinsed twice with DPBS for 5 minutes to remove any non-adherent cells. Sutures were then fixed in 4% paraformaldehyde in DPBS for 10 minutes. Following two more DPBS washes, the cells were permeabilized using 0.25% Triton X-100 (Sigma Aldrich) for 10 minutes. Then sutures were rinsed another two times with DPBS and blocked for 30 minutes using 1% BSA in DPBS. Cytoskeleton filament actin (f-actin) present in microtubules and microfilaments were stained with Phalloidin at 2.5% (conjugated to AlexaFluor 488, Invitrogen, Carlsbad, CA) or 50 in 1950uL in DPBS for 30 minutes. Sutures were then rinsed two times in DPBS. Cell nuclei were counter-stained with Hoechst 33342 dye (Invitrogen, Life Technologies, Eugene, OR) at 0.0167% or 1 in 6000μL in DPBS for 5 minutes. Sutures were rinsed two final times in DPBS.

Sutures and cells were visualized with a Leica Upright DMLB2 fluorescent microscope at 20X magnification. Images were also taken on a Leica TCP SP5 confocal laser scanning microscope at 20X magnification. Following confocal imaging, coverslip spacers were added and the sutures were sealed with Cytoseal™ 60 and covered with glass coverslips. Images were qualitatively assessed for cell coverage and morphology on the suture. A detailed protocol for Hoescht and Phalloidin staining can be found in Appendix G.

5.3.7 Statistical Analysis

All results are presented as mean ± standard deviation. The cell seeding data obtained from the CyQuant cell proliferation assays were first analyzed to remove data point outliers. The results were then compared using an ordinary one-way ANOVA test.

5.3 Aim 2 Results

5.3.1 CyQuant Cell Proliferation Assay

Sutures created from the varying ECM-fibrin microthread types were seeded with 100,000 human mesenchymal stem cells for 24 hours. Following, a quantitative CyQuant cell proliferation assay was performed in order to determine the exact number of cells seeded onto each suture. Table 9 below shows the average number of cells that successfully attached to each microthread type. Figure 23 below represents these values graphically.

Table 9 Average number of cells seeded on each ECM-fibrin suture type as determined through a CyQuant cell proliferation assay. (n=15 sutures)

	5% ECM	10% ECM	15% ECM	FIBRIN
AVERAGE NUMBER OF CELLS SEEDED	9555±3000	12485±8000	10658±5000	9710±3000
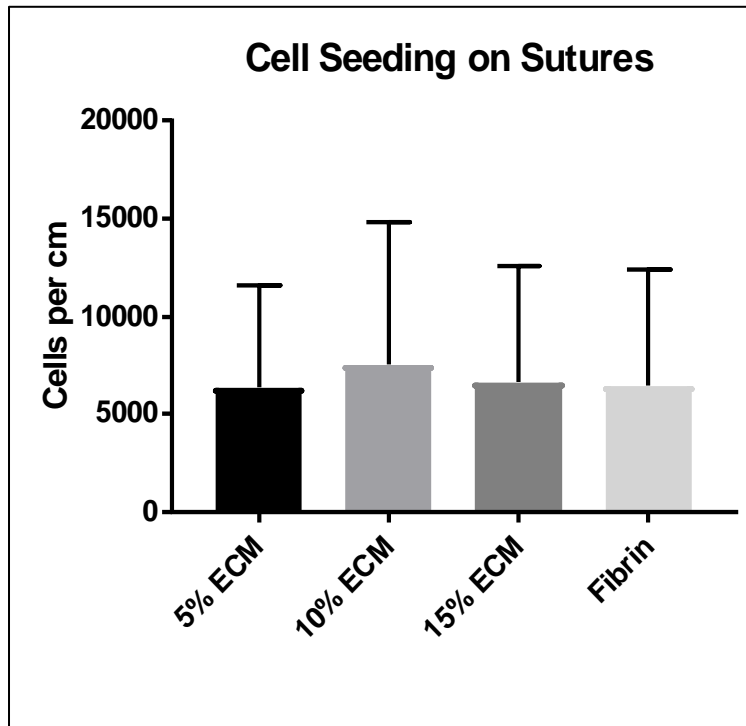
Figure 23 Cell Seeding of the varying types of fibrin-ECM microthreads quantified using a CyQuant DNA Assay, n=15

A one-way ANOVA revealed that the mean number of hMSCs seeded onto the fibrin sutures was not statistically different from the mean number of cells seeded onto the ECM-fibrin based sutures.

5.3.2 Hoescht and Phalloidin Immunohistochemistry

Along with the quantitative CyQuant cell proliferation assay, seeded sutures also underwent a qualitative analysis consisting of immunohistochemical staining for Hoescht 33342 for cell nuclei and Fluor 488 conjugated Phalloidin for the cytoskeletal protein, f-actin. The stained sutures were viewed and imaged under a fluorescent inverted microscope as well as a fluorescent confocal microscope. Figure 24 below shows the images gained from imaged the seeded sutures under an inverted fluorescent microscope. The column on the left consists of the images taken for the Hoescht channel where cell nuclei were visible. The middle column consists of the images taken for the Fluor 488 channel, where the Phalloidin stain was visible showing us the f-actin that had been laid down by attached cells. The final column on the right is an overlay image of the two channels brought together.

64
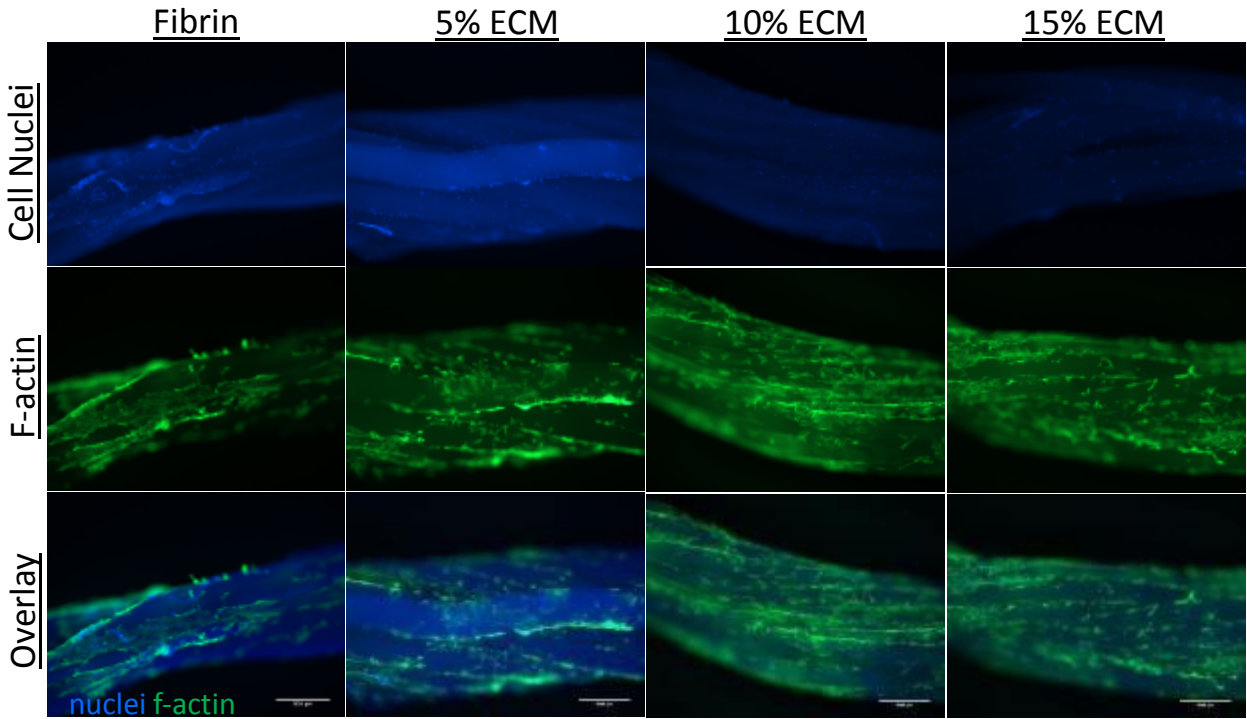
*Figure 24 Fluorescent inverted microscope images of seeded sutures after being stained for hoescht (cell nuclei) and phalloidin (f-actin) taken at 10X magnification. **Left**: Images of the sutures taken using the Hoescht objective **Middle**: Images of the sutures taken using the Fluor 488 (Phalloidin) objective **Right:** An overlay of the two channels. Scale bar=100um*

Figure 25 below shows the confocal imaging of the stained seeded sutures at 20X magnification.

These images were taken along with the inverted fluorescent microscope images above in order to obtain

higher quality and higher magnification images of different areas on the sutures. Because each suture is

made from 24 individual microthreads, obtaining in-focus images on either an upright or inverted

microscope proved to be difficult. A confocal microscope provided us with clear images that showed us a

clearer view of the cell nuclei and the f-actin cytoskeleton that was created by the cells attached to the

sutures.
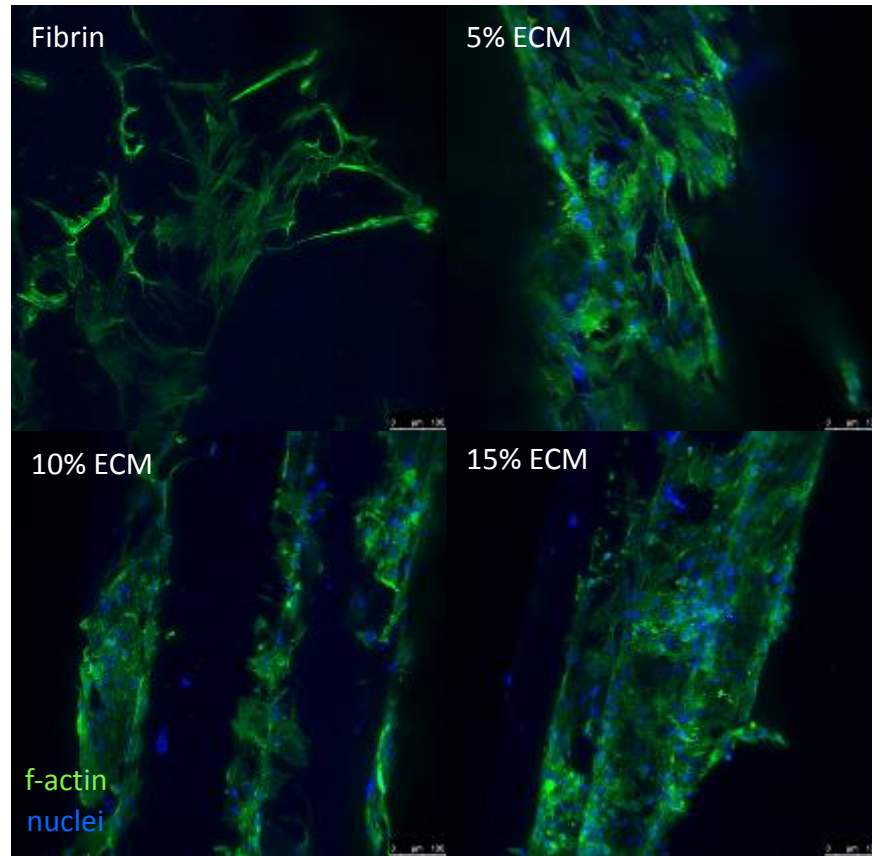
Figure 25 Confocal fluorescent microscope images of seeded sutures after being stained for hoescht (cell nuclei) and phalloidin (f-actin).

5.4 Aim 2 Discussion

This aim sought to determine the effect that ECM incorporation into fibrin microthreads has on the cell seeding capability when the microthreads are used in the form of a suture. The following discussion seeks to support our findings and conclusions gained from our 24-hour seeding experiment.

A study by Park et al investigated the effects of five hydrogels on the differentiation of human adipose stem cells (ASCs). The five hydrogels were collagen, fibrin and hyaluronic acid, collagen and hyaluronic acid and fibrin and collagen. The co-gels were created in a 1:1 ratio. During gelation, a suspension of 200,000 ASCs was mixed with the hydrogel and cultured for 7 days. The ASCs were transfected with lentivirus-expressing green fluorescent protein (GFP) prior to gelation. Following culture, the total DNA content was measured using a PicoGreen cell proliferation assay. The cells in the hydrogels

were also viewed for cell elongation and shape at day 7. This study found that the cells grown in the fibrin based hydrogels (fibrin only, fibrin-collagen, and fibrin-HA) had significantly higher levels of DNA when compared to the collagen based gels (collagen only and collagen-HA). However, it was found that there was no significant difference between the fibrin based hydrogels, whether they were single component (fibrin only) or dual component (fibrin-collagen and fibrin-HA). The study also found that cells appeared to be more elongated after 7 days of culture in the fibrin-collagen and fibrin-HA hydrogels when compared to the fibrin only, collagen only, and collagen-HA hydrogels [104]. This conclusion was also seen in a separate study by Rowe and Stegemann [102].

The results from the 24-hours hMSC seeding experiment on the varying fibrin-ECM microthread type sutures revealed that there was no statistical difference between the number of cells that successfully attached to the fibrin sutures and the fibrin-ECM sutures. This conclusion aligns with the aforementioned studies that found no statistical difference in adipose stem cell attachment between fibrin only and fibrin-collagen hydrogels.

Chapter 6: Aim #3: Evaluate Endothelial Progenitor Outgrowth Cell Outgrowth

6.1 Introduction

The purpose of this aim is to determine if the ECM-fibrin microthreads promote a greater endothelial cell outgrowth. In order to evaluate the effect the ECM-fibrin microthreads will have, we have modified a standard scratch assay. In brief, human endothelial progenitor outgrowth cells (hEPOCs) will be subjected to a scratch assay by scratching the cells with a 200uL micropipette tip. Within the scratch, microthreads, either a 15% ECM-fibrin microthread or a fibrin microthread, will be placed and secured. The outgrowth of the cells toward the microthreads will be evaluated at 0, 6, 12, 18, and 24 hours by imaging the cell movement and calculating the total distance the cells move.

We hypothesize that the ECM incorporated into the microthreads will provide signaling cues to promote cells to migrate toward the microthread faster than the cells subjected to a fibrin only microthread or no microthread.

6.2 Methods

6.2.1 Cell Culture

Prior to cell plating, a sterile 6-well plate was marked with 2 parallel dotted lines down the center of each well as illustrated in Figure 26. These two lines will be used as a guide to scratch the wells for outgrowth. The dotted lines will also be used as reference points to image the outgrowth assay at the same locations over time.
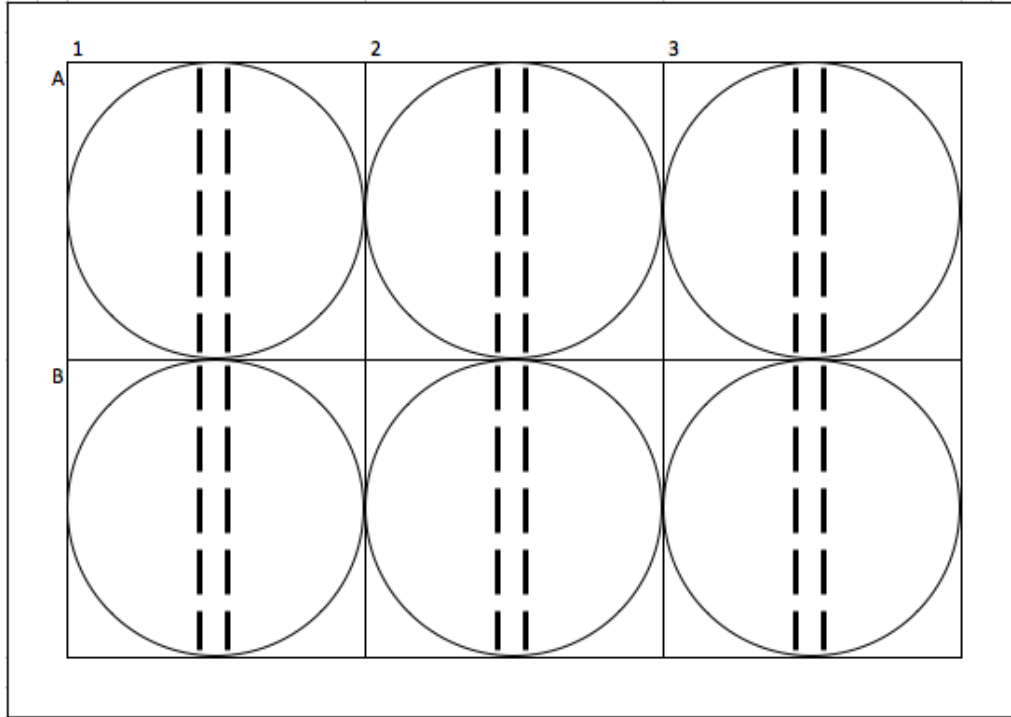
Figure 26 Schematic of the 6-well plate used for the outgrowth assay. Each plate was marked with 2 parallel dotted lines prior to cell culture.

Human endothelial progenitor outgrowth cells (hEPOCs; Biochain Z7030001, Newark, CA) were cultured in human endothelial progenitor outgrowth cell growth medium (Biochain Z7030003) in compliance with the manufacturer's guidelines. Upon arrival from Biochain, the cells were immediately plated into 6-well plates at 10,000 cells/ cm^2 at passage 4 in preparation for a scratch assay. Cells were grown until they reached full confluency. The cells were used at either passage 4 or 5 as later passages of cells failed to continue growing. A detailed protocol to the preparation of the 6-well plates can be found in Appendix H.1.

6.2.2 Microthread Sample Preparation for Outgrowth

For this experiment, in one 6-well plate, 2 wells will be subjected to a fibrin microthread within the scratch, 2 wells will have a 15% ECM-fibrin microthread within the scratch and 2 wells will serve as controls and will have no microthreads within the scratch. Constructs were created in order to secure the microthread within the scratch in place to avoid microthread movement.

69

Each construct consists of a 1.5 cm section of 50 mL polypropylene conical tube. The conical tube section was cut from the original conical tube by heating a scalpel over a bunsen burner and cutting through the tube. Each conical tube section used for the experiments were then sanded to have even edges. The conical tube section was then attached to a stainless-steel washer using medical grade silicone adhesive from Bluestar Silicones.

Microthreads were then adhered to the conical tube and washer constructs. A 3cm section of either a fibrin or 15% ECM microthread was cut and laid across the bottom side of the washer, opposite side of the conical tube section. The microthread section was then oriented so that it lay across the approximate middle of the washer. Using the silicone adhesive, the microthread was secured to the construct and left overnight to allow the adhesive to cure. The control wells for this experiment would have a blank construct place within the well. These constructs consisted of only the conical tube section and washer. A schematic of the washer and conical tube construct is seen below in Figure 27. A detailed procedure for the production of the microthread constructs can be found in Appendix H.2.
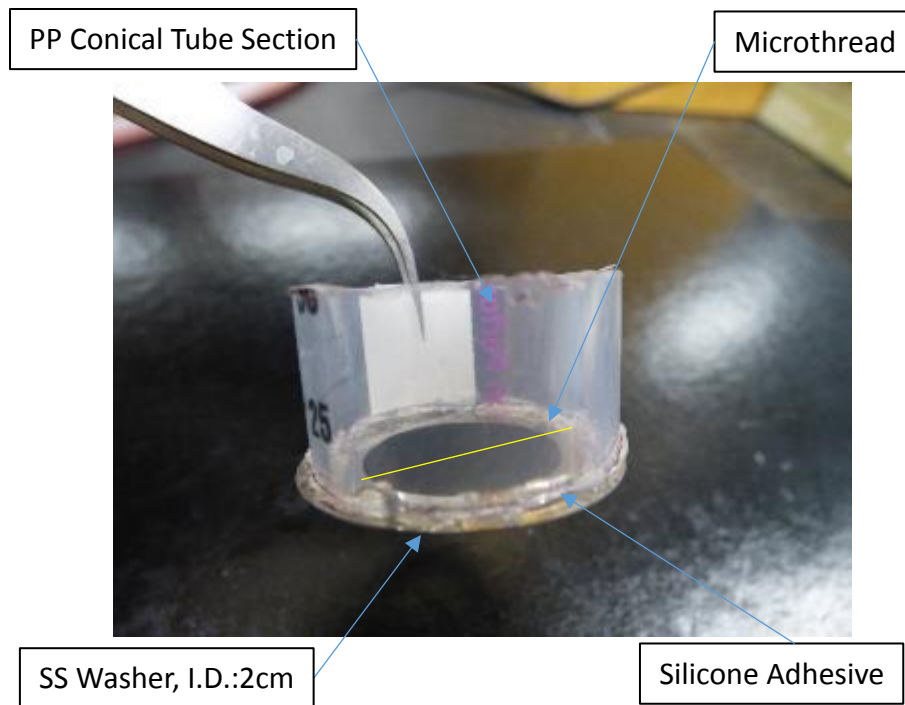
Figure 27 Microthread construct consisting a stainless-steel washer and a section of a polypropylene 50 mL conical tube These two components are brought together using silicone adhesive. Finally, the microthread is placed in the middle of the construct.

6.2.3 Endothelial Progenitor Outgrowth Cell Outgrowth

Once the hEPOCs had reached full confluency in each well of the 6-well plate, the outgrowth assay could begin. First, the hEPOC growth media was removed from each well. Then, using a 200uL micropipette tip, a scratch was drawn down the middle of each well between the dotted lines. Following the scratch, each well was gently washed with 2000uL of sterile DPBS two times to remove cells that were detached due to the scratch.

Following, the microthread constructs were placed in their designated wells so that the microthread would lie within the scratch. With the constructs placed within the well, 2000uL of hEPOC growth medium was added to each well. Plates were viewed under a Nikon Inverted Light Microscope to confirm the microthread was within its respective scratch. Adjustments of the construct were made until each microthread was within each scratch. Figure 28 below is a schematic of the final setup of the constructs within the 6-well plate.
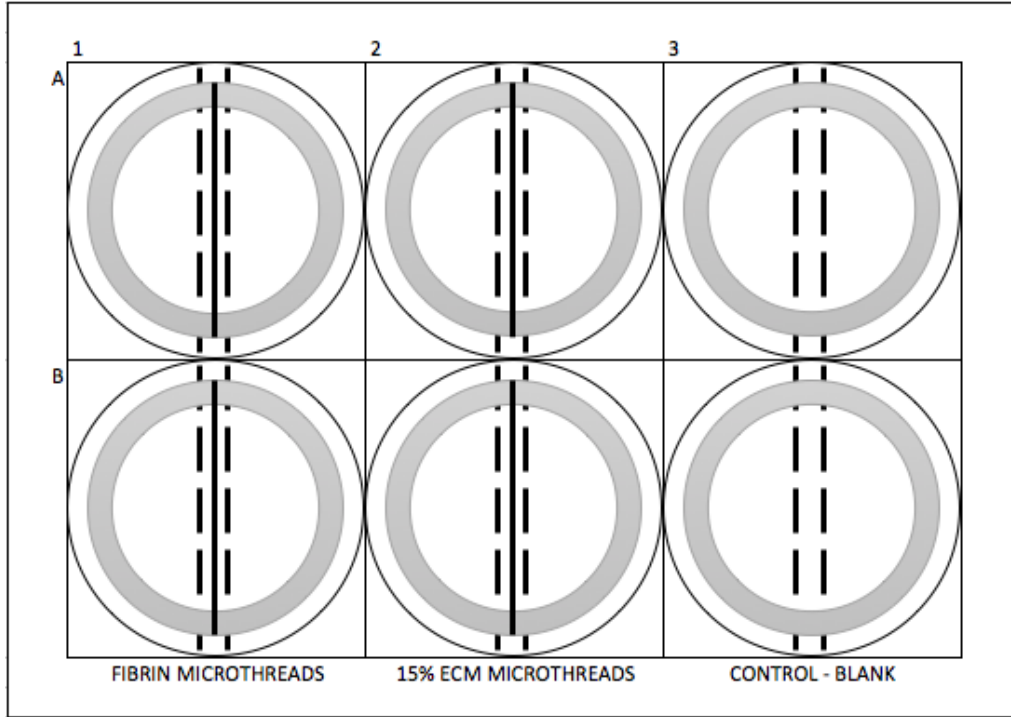
Figure 28 Schematic of a 6-well plate that has been prepared for the EPOC Outgrowth assay. The scratch has been made and the microthread constructs have been placed within the scratch.

Once the constructs were in place, the wells were imaged on a Leica DMIL LED inverted microscope at 20X for the 0-hour time point. Each well was imaged at the specific points were the dotted lines were visible within the washer. Depending on how many sets of dots fell within the boundary of the construct, this was between 4 and 5 locations for imaging. Imaging was repeated for all locations at 6, 12, 18, and 24 hours. A detailed procedure of the 24-hour EPOC outgrowth assay can be found in Appendix H.3.

6.2.4 DAPI Staining

Following the final outgrowth images being taken at 24 hours, the microthreads present within the wells of the 6-well plates were removed from the wells and subjected to a DAPI stain to evaluate any cell attachment onto the microthreads from the outgrowth. Briefly, the microthread constructs were removed from their respective wells. The microthread was cut from the construct and placed onto a microscope slide. Each microthread was rinsed in DPBS twice for 5 minutes each. Next the microthreads

were fixed in 4% paraformaldehyde in PBS for 10 minutes and then washed in DPBS for 5 minutes three times. Any cells on the microthreads were then permeabilized with a 0.25% Triton-X 100 for 10 minutes. Following three more washes in DPBS, microthreads were then stained with DAPI (Invitrogen, Life Technologies Corporation, Eugene, OR) for 5 minutes. DAPI was obtained from the manufacturer and immediately put into solution at 10mg in 2mL of deionized water and kept at -30˚C. For staining, the DAPI stock solution was diluted to a concentration of 1ug in 1mL of PBS, or 0.2uL of stock solution in 1000uL DPBS. Following the DAPI stain, microthreads were washed in DPBS. This protocol can be found in more detail in Appendix I. The microthreads were then analyzed on a Leica SM LB2 inverted microscope. Using a handheld tally counter, cells that had migrated onto and attached to the microthreads were counted across each microthread.

6.2.5 Cell Outgrowth Evaluation

The images taken for each well at each time point were used to measure the percent change in the distance between the two sides of the endothelial cell scratch. Using the software ImageJ, each image taken for each time point was scaled so that the measurements would be accurate. Once scaled, the scratch distance on each image was measured at 10 locations within the scratch. This is done by using the line function in ImageJ to draw a horizontal line across the scratch and then using the measuring feature to determine the length of the drawn line. Figure 29 below demonstrates the 10 horizontal lines that are drawn in parallel down the scratch. Figure 30 shows an image that has been uploaded into ImageJ and has had the ten measurements made between the scratch. These 10 measured lengths were then imported into Microsoft Excel in order to perform necessary measurements.

73
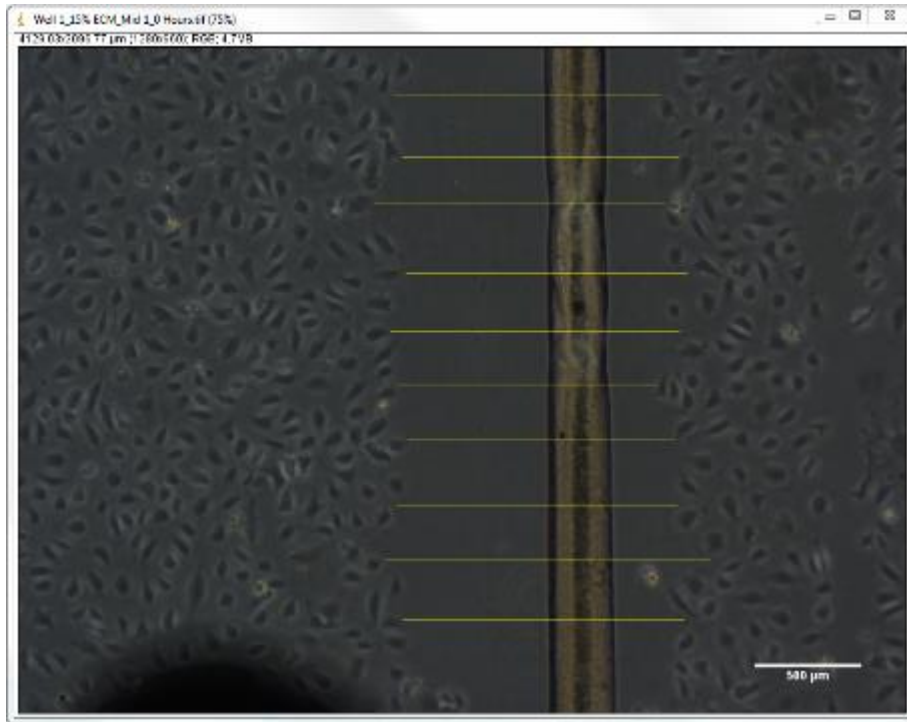
Figure 29 Ten horizontal lines are drawn in parallel across the scratch and then measured using the measuring function in ImageJ.
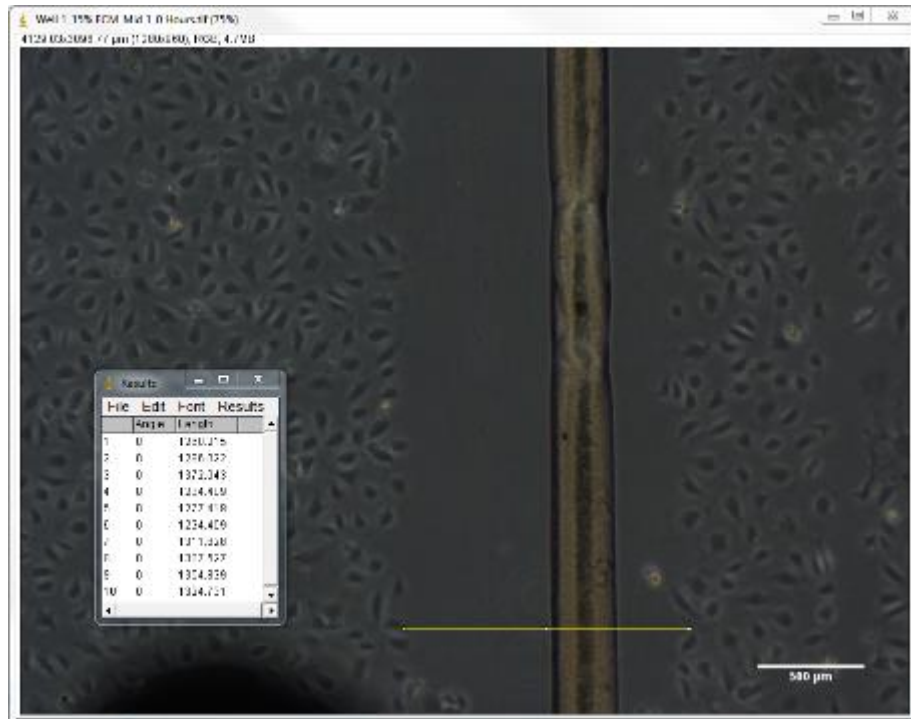
Figure 30 Ten measurements are made for a single image in ImageJ to calculate the average distance between the scratch for this image.

A number of calculations were performed to determine the overall percent change in distance

between 0 and 24 hours for each outgrowth condition. Prior to calculations, every measurement made

for each well at each time point was imported into excel. As mentioned previously, ten measurements were taken for each location in each well. These measurements were taken in the same area each time. The first calculation made was to subtract the final distance from the initial distance for each measurement at each location in each well. This calculation provides us with a data set of the differences in the distances between the scratch. Next these measurements were used to determine the percent change in distance by dividing the change in distance over the initial distance and multiplying by 100.

Other calculations were made in order to determine the distance travelled between each time point as well as an average change in distance for each well. These calculations were not used in the final analysis of the outgrowth assay, however, they can be found in Appendix J. In order to compare the three well conditions, fibrin microthread, 15% ECM microthread and blank, the overall average percent change in distances were compared.

6.2.6 Microthread Media Control

A control is required to compare the DAPI staining to, so we chose to run a control media-only experiment. This experiment consisted of incubating a fibrin microthread and a 15% ECM microthread in media for 24 hours. The experiment was set up in the same manor of the initial outgrowth assay. Microthreads were cut into sections measuring approximately 3cm and attached to the constructs described previously. Once sterilized, the microthread constructs were placed in a 6-well plate and incubated in 2mL of complete EPOC growth media for 24 hours. The 6-well plate consisted on 3 fibrin constructs and 3 15% ECM constructs. Following the 24-hour incubation, each construct was removed from the 6-well plate and the microthreads were cut from the contract and placed on a glass slide. The microthreads then underwent the DAPI stain protocol mentioned previously. Following the stain, the microthreads were viewed and imaged on a Leica Upright DMLB2 fluorescent microscope at 10X magnification. The images taken were then compared to the microthreads that were used in the EPOC outgrowth.

6.2.7 Statistical Analysis

All results are presented as mean ± standard deviation. The individual initial and final distance measurements were used to determine the change in distance between the scratch for each measurement. The individual changes in distance were then analyzed to remove outliers from the dataset. Also analyzed were the comparisons of all the initial and final distances separately in order to show that the initial distances for each migration condition did not significantly vary. The results were then compared using an ordinary one-way ANOVA test. Statistical significance was determined as $p < 0.0001$. The number of cells counted on the microthreads following the outgowth assay were also analyzed using a t-test.

6.3 Aim 3 Results

6.3.1 Endothelial Progenitor Outgrowth Cell Migration

A modified scratch assay was used to determine the effect that the ECM in the ECM-fibrin microthreads has on endothelial cell outgrowth. As described previously, endothelial progenitor outgrowth cells (EPOCs) were cultured in a 6-well plate and then subjected to a 24-hour scratch assay. When the scratch in the culture was created, either a fibrin microthread or a 15% ECM microthread was placed within the scratch. Wells with no microthread within the scratch were used as controls. The outgrowth of the EPOCS was evaluated over 24 hours by imaging each well at specified locations every six hours. From these images, measurements of the distances between the scratch were taken using ImageJ software. Figure 31 below shows a time progression of the EPOC outgrowth under each condition: 15% ECM microthread, fibrin microthread, and control. From these images, we can see that wells containing a 15% ECM microthread fully closes at the 24-hour time point while the wells containing the fibrin microthread or no microthread do not full close. This initial result suggests that the ECM incorporated into the 15% ECM microthread does play a role in rate of the EPOC outgrowth.
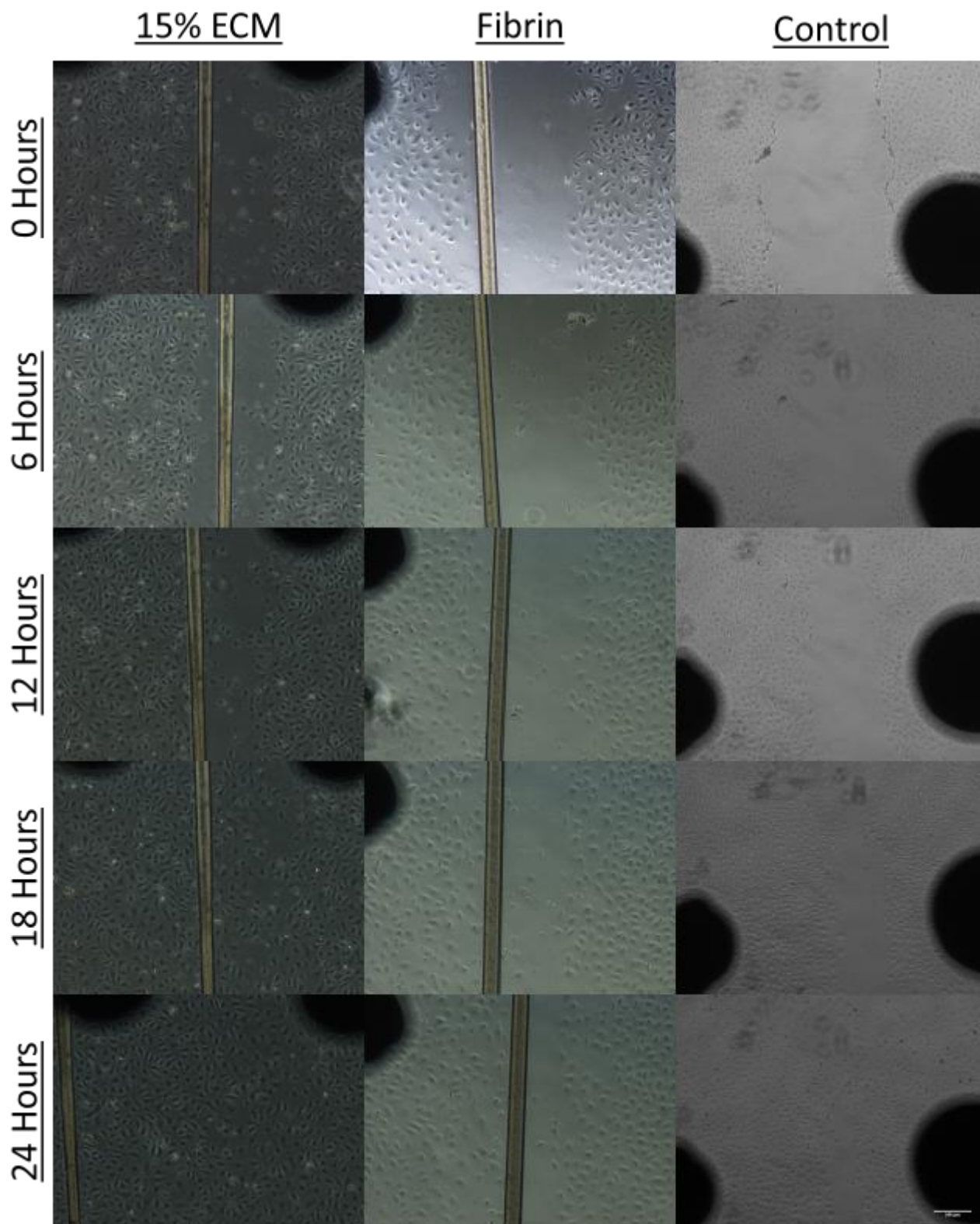
Figure 31 EPOC outgrowth progression over 24 hours under the conditions of a control (no microthreads), a fibrin microthread and a 15% ECM microthread.

6.3.2 Evaluation of Endothelial Progenitor Outgrowth Cell Outgrowth

In order to quantify the effect that ECM has on EPOC outgrowth, the images taken for each well at each time point were used. For each well in the 6-well plate, four or five images were taken at specific locations for each time point. Each of these images were used to measure the distances between the sides of the scratch at the specific location every 6 hours. These measurements were then used in a series of calculations to determine the overall percent change in the distance between the sides of the scratch for each condition. Figure 32 below shows the distance between the scratch over time for each of the three conditions. By fitting a linear line to the trends, we were able to determine the slopes of the lines. As it can be seen on the graph, the 15% ECM microthread condition for outgrowth had a steeper slope (m=-287) than the slopes for the fibrin microthread (m=-237.25) and control (m=-221.49) conditions.
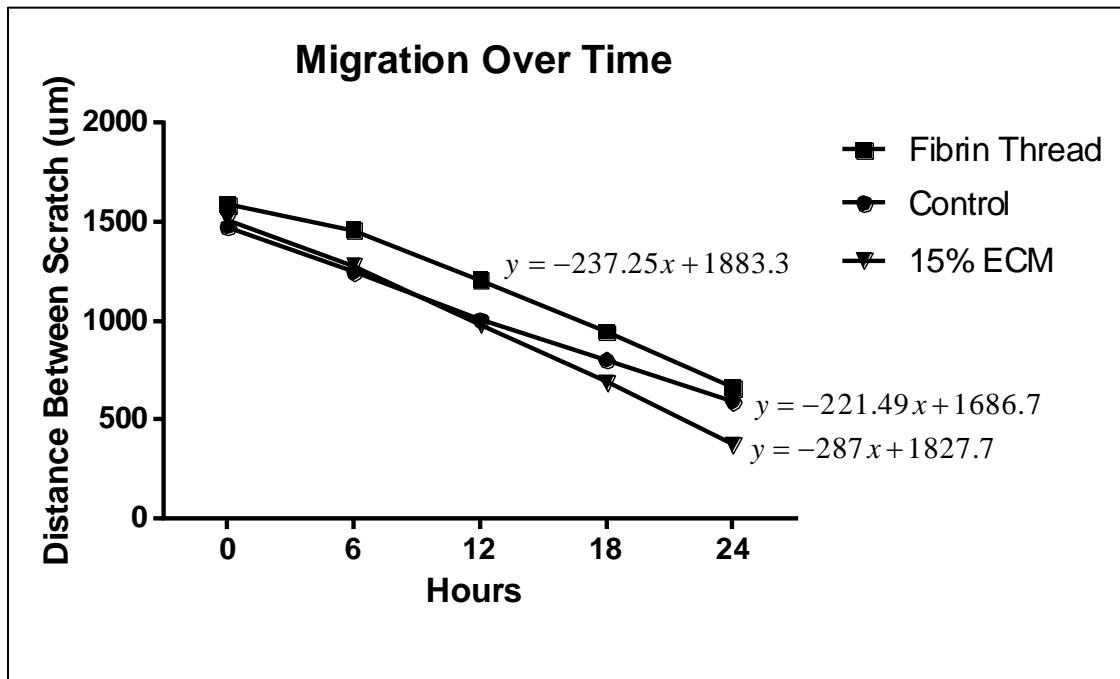
Figure 32 Outgrowth of EPOCs over time.

Figure 33 below shows the final values for the average percent change in distance for the EPOC scratch for wells with a 15% ECM microthread, a fibrin microthread or no microthread. On average, the wells that contained a 15% ECM microthread within the scratch closed $77 \pm 21\%$ of

their initial distance. Respectively, the average percent distance closed for wells containing a fibrin microthread within the scratch and the control wells were 61 ± 33% and 59 ± 34%. A one-way ANOVA determined that the percent change in distance at 24 hours was significantly higher in the 15% ECM microthread wells when compared to the fibrin microthread and control wells.
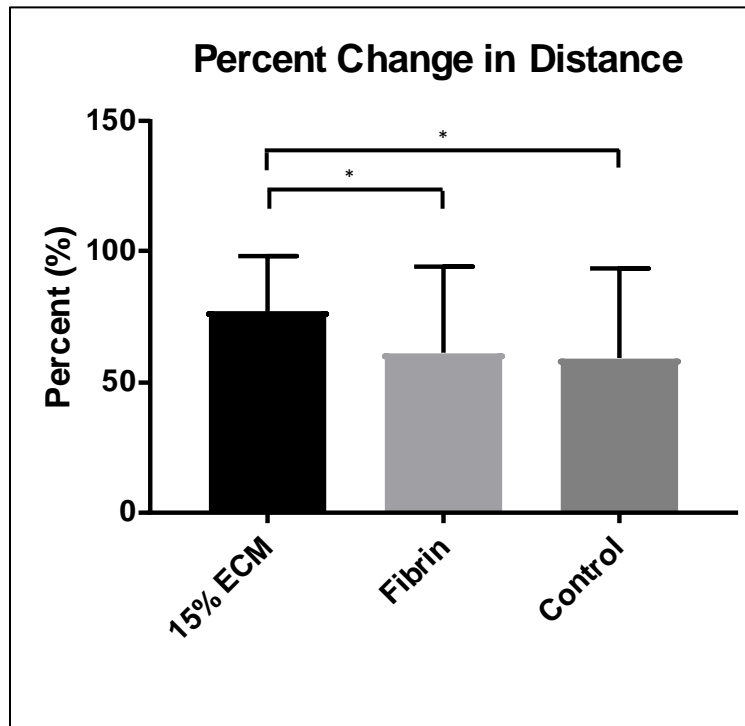
*Figure 33 Mean percent change in distance between the edges of the scratch for each outgrowth condition. An asterisk (*) is used to indicate a statistical difference between outgrowth conditions. *p<0.0001. n=6*

In order to demonstrate that each well in the 6-well plate was starting at the same distance, the measurements of the average initial distances for each condition are presented below in Figure 34. As it is shown in the graph, the distance between the scratch for each condition at 24 hours if nearly the same. For 15% ECM microthread wells, the average initial distance was 1528 ± 248 um. For fibrin microthread wells, the average initial distance was 1590 ± 44 um. For control wells, the average initial distance was 1542 ± 379 um.
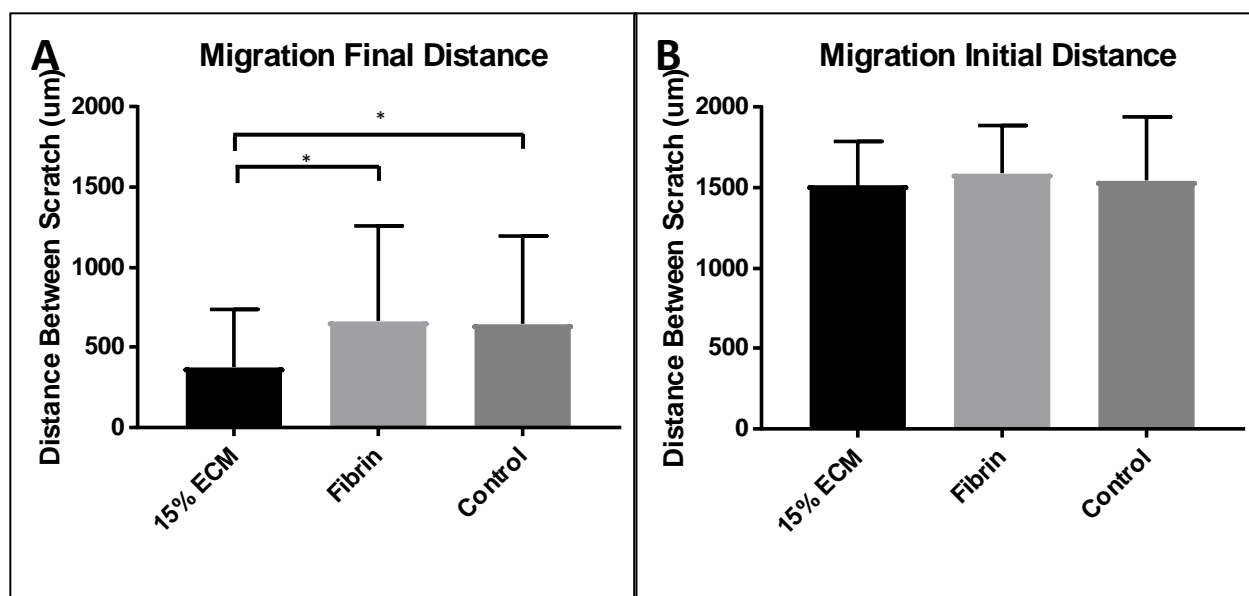
Figure 34 A comparison of the initial and final distances for each outgrowth condition. An asterisk (*) is used to indicate significance between the final distances between the scratch. *p<0.0001

6.3.3 Endothelial Progenitor Outgrowth Cell DAPI Stain

Following the 24-hours EPOC outgrowth, the microthreads that were present within the scratch for 24 hours were removed from their respective wells and stained for DAPI (cell nuclei) to evaluate potential EPOC outgrowth onto the microthreads. The control group for this staining experiment consisted of 15% ECM and fibrin microthreads that were incubated in EPOC growth medium for 2 hours. This control was used in order to rule out any autofluorescence. In Figure 35 below, 15% ECM microthreads have been stained for DAPI following a 24-hour EPOC outgrowth and 24-hour EPOC growth medium incubation. The 15% ECM microthread that underwent the EPOC outgrowth assay shows an abundance of cell nuclei that have been stained with DAPI, indicating EPOCs have migrated and attached to the microthread. The control 15% ECM microthread does not show any indications of false cell staining.
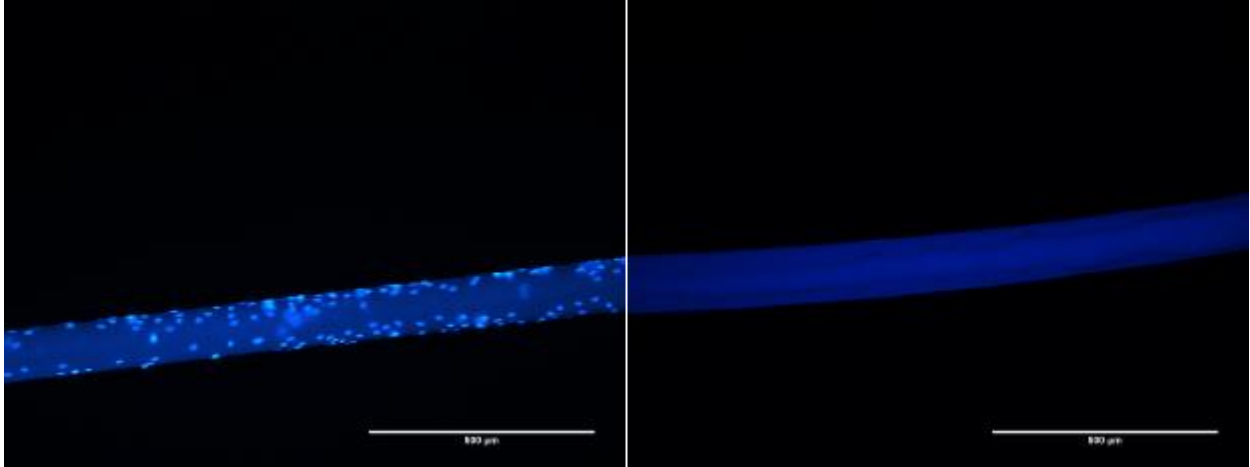
*Figure 35 15% ECM microthreads stained for DAPI (cell nuclei) following **Left**: a 24-hour EPOC outgrowth assay **Right**: a 24-hour EPOC media control incubation*

Similarly, Figure 36 below shows fibrin microthreads that have been stained following the 24-hours EPOC outgrowth assay as well as the control EPOC growth medium incubation. The fibrin microthread that underwent the 24-hour EPOC outgrowth assay shows some stained cell nuclei indicating that EPOCs did attach to the fibrin microthread. The control fibrin microthread does not show any false cell staining.
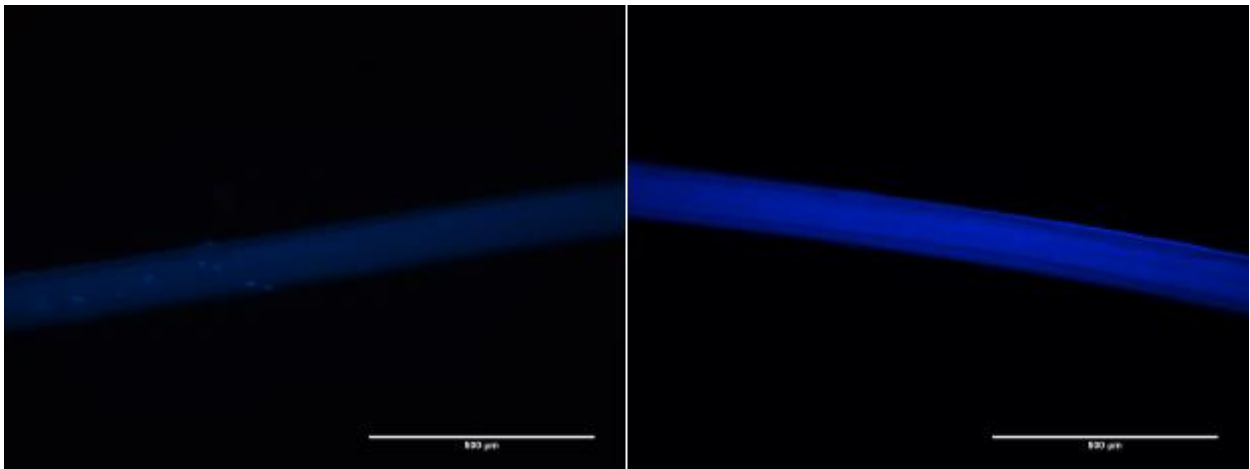
*Figure 36 Fibrin microthread stained for DAPI (cell nuclei) following **Left**: a 24-hour EPOC outgrowth assay **Right**: a 24-hour EPOC media control incubation*

When comparing the images taken for the 15% ECM microthread and the fibrin microthread that underwent the EPOC outgrowth, the 15% ECM microthread shows a much higher number of stained cell nuclei of cells that have attached to the microthread. The fibrin microthread does show some cell nuclei

that have attached to the microthread suggesting that fibrin does play a minor role in endothelial progenitor cell outgrowth.

In order to quantify the results of the EPOC outgrowth onto the microthreads, the DAPI stained cell nuclei were counted by hand using a tally counter. Figure 37 below shows the average number of DAPI stained cells counted on the microthreads. For each condition, 15% ECM and fibrin, there were a total of six microthreads from all the outgrowth assays that were stained for DAPI and evaluated. Out of the six 15% ECM microthreads, stained EPOCs were seen on three. As seen in the graph, on average there were 114 ± 162 cells on the 15% ECM microthreads. For the fibrin microthreads, cells were only seen on one of the six microthreads that underwent the outgrowth assay. The average of the cells counted on fibrin microthreads was 6.67 ± 16.2 cells. A t-test revealed that there was no statistical significance between the mean numbers of cells that adhered onto the microthreads.
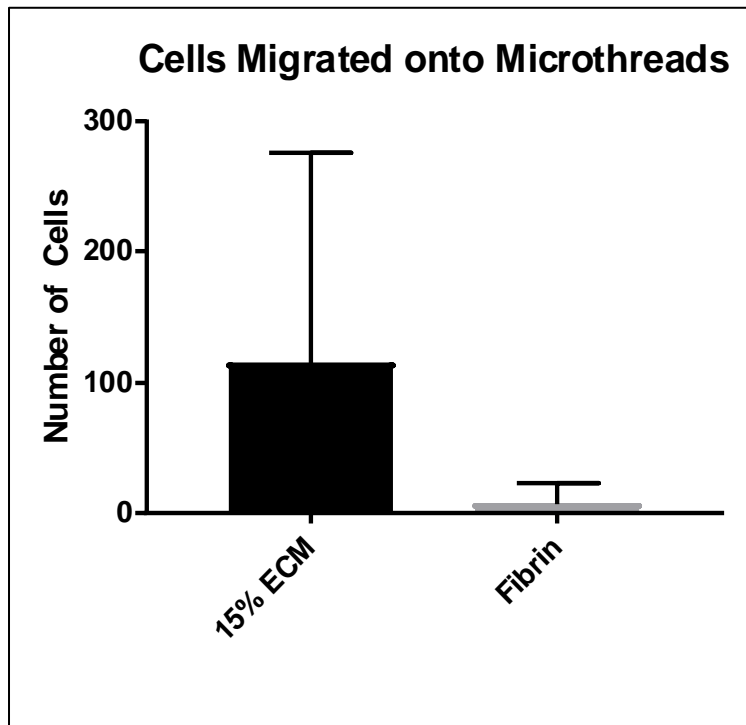
Figure 37 Mean number of EPOCs counted on microthreads following a 24-hour outgrowth assay.

6.4 Aim 3 Discussion

This experiment sought to explore the angiogenic potential that the ECM-fibrin microthreads may have through an endothelial progenitor cell outgrowth assay. The extracellular matrix plays a key role in regulating angiogenesis. In the event of injury or ischemia, the matrix is modulated to recruit endothelial progenitor cells to injury site. This causes the number of circulating endothelial progenitor cells to increase and promote blood vessel formation and tissue regeneration [105].

Many extracellular matrix molecules, including collagens, laminins, and fibronectins, play specific key roles in endothelial cell survival, growth, migration, and tube formation. Collagen I specifically promotes endothelial cell tube formation [103]. Other collagens are known to promote cell adhesion and migration (Collagen IV) as well as stabilizes endothelial cell tubes (Collagen XVIII) [106]. Collagen matrices have been shown to support endothelial progenitor cell differentiation into endothelial cells [107]. According to a study by Crister et al., endothelial progenitor cells vascularize collagen-based matrices *in vivo* [108]. Collagen has also been shown to protect endothelial progenitor cells against apoptosis [107].

Laminins are a group of proteins that are also known to encourage angiogenic events. Specific laminins play key roles such as laminin 1 specifically promoting endothelial cell tube formation and laminin 8 promoting endothelial cell morphogenesis [106, 107]. Finally, fibronectin too encourages endothelial cell adhesion, growth migration and survival [106, 107]. These findings thus show that the extracellular matrix and its proteins have pro-angiogenic properties.

Fibrin has also been shown to be involved in the regulation of endothelial progenitor cell biology. In a study by Barsotti et al., endothelial progenitor cells in a fibrin matrix showed the ability to differentiate into endothelial cells and migrate and integrate into newly formed blood vessels *in vivo* [109].

A study by Singelyn et al. developed an injectable cardiac extracellular matrix based hydrogel to promote angiogenesis *in vivo*. In the study, they performed an *in vitro* migration assay of vascular cells. Using a Chemotaxis 96-well Cell Migration Assay Kit, the group evaluated the migration of human coronary

artery endothelial cells (HCAECs) and rat aortic smooth muscle cells (RASMCs) toward a cardiac ECM, collagen, fetal bovine serum, and pepsin. The results of the migration assay revealed that the cardiac ECM increased the migration of the RASMCs significantly ($p<0.001$). The results also showed that while it was not significant, the HCAECs followed the same trend of increased migration toward the cardiac ECM matrix. The study concluded that the cardiac ECM hydrogel promoted migration of both cell types *in vitro*. The study further evaluated the injectable hydrogel *in vivo*. The hydrogel was injected into the hearts of rats. The hearts were analyzed at a short term 4-hour time point as well as a long term 11-day time point. Following immunohistochemical staining, the study revealed that after 11 days, endothelial and smooth muscle cells had significant infiltration into the matrix region [97].

The *in vitro* results of this study coincided with the outgrowth assay results we obtained from our experiment. Our study showed a significant increase in endothelial progenitor cell outgrowth toward the 15% ECM-fibrin microthreads. Our results also showed that endothelial progenitor cells migrate toward the microthreads and adhere to the surface of the microthreads. From the known roles that extracellular matrix molecules play in angiogenesis as well as the role that fibrin plays in endothelial progenitor cell outgrowth, our ECM-fibrin microthreads exhibit a high level of angiogenic potential.

Chapter 7: Future Work and Recommendations

The use of fibrin microthreads in the form of a bundled suture has been shown as a novel method for the delivery of hMSCs into the infarcted region of a heart used by the Gaudette lab. Fibrin based sutures have improved cell engraftment and localization when compared to the tradition intramyocardial (IM) cell injections [39]. The Gaudette lab has also shown new methods for improving the sutures potential as a stem cell delivery mechanism by prolonging the degradation of fibrin sutures in order to increase cell seeding time and ultimately increasing the number of cells that adhere to the sutures for delivery [54]. We demonstrated that native cardiac extracellular matrix can be incorporated into the fibrin microthreads and then used as a bundled suture. These ECM-fibrin sutures have showed the ability to increase endothelial progenitor cell outgrowth and attachment to the microthreads when compared to cell outgrowth toward fibrin only microthreads and no microthread. The ECM-fibrin microthreads also showed increased elastic modulus. These results implicate the potential for the ECM-fibrin microthreads to be used as a stem cell delivery mechanism.

While this study was able to draw conclusions about the use of native cardiac ECM to improve the properties of fibrin based sutures, additional research and future studies could provide more understanding of the effects that ECM incorporation has on the properties of fibrin microthreads. This experiment investigated the effects of ECM incorporation at 5%, 10% and 15% v/v. Performing these same experiments on microthreads that are 1% ECM could provide information on how the ECM can affect the fibrin microthread properties at the smallest incorporation. These experiments could also give an understanding of how important a higher ECM incorporation percentage is.

Similarly, our study performed the endothelial progenitor outgrowth cell outgrowth using on fibrin microthreads and 15% ECM microthreads. We used our highest concentration of ECM in order to determine if the EPOC outgrwoth was affected in any way by the ECM. Because we now know that the outgrowth of the EPOCs is increased by the ECM incorporation, performing a replicate study using the 5%

ECM and 10% ECM microthreads would provide an understanding on how the lower ECM concentrated microthreads can affect the EPOC outgrowth. Also, our study found that there was no significant difference in the number of endothelial progenitor cells that adhered to the microthreads. In a sample size of six, three 15% ECM microthreads had cells while three had zero cells. This resulted in high standard deviations. Similarly, with the fibrin microthreads, one out of the six had visible cells that adhered onto the microthreads. When comparing the results from the cell counts, the means were found to not be statistically different. A higher sample size of microthreads could provide for more data in order to make significant conclusions.

Fibrin degrades by fibrinolysis which is increased during hMSC seeding due to the cells releasing fibrinolytic enzymes. Aprotinin, a protease inhibitor, has been shown to decrease the degradation of fibrin in cell culture environments [54]. When the ECM is incorporated into the fibrin microthreads, the total fibrin concentration is reduced. This reduction in fibrin content could potentially affect the degradation of the microthreads. An investigation into the degradation of ECM-fibrin microthreads could determine the stability of the microthreads and all us to understand is the ECM incorporation increases or decreased the degradation of the microthreads.

While our hMSC seeding experiments determined that there was no statistical significance in the number of cells seeded to the ECM-fibrin based sutures and the fibrin only sutures, further experimentation may provide an understanding of the effect that ECM has on the molecular level. Performing experiments that determine the cell and matrix interactions would provide an inclination of the adhesion of strength of the cells to the microthreads. It is possible that the ECM could create a stronger bond between the cells and the microthread. Additionally, the staining of our seeded sutures appeared to show a trend of increasing f-actin with increasing ECM concentration. Further experimentation could provide an understanding on how the ECM is affecting the cells on a molecular level.

Therapies using hMSCs have shown that the cells aid in the healing process by reducing the inflammation caused by a myocardial infarction. The ultimate goal of using stem cell therapies is to regenerate tissue function. For the heart, this means regenerating and restoring total heart function and contraction. Induced pluripotent stem cell derived cardiomyocytes are cells that have had genes altered in order to become contractile cardiac cells. Efforts have been made to seed these contractile cells on fibrin sutures and implant them into healthy rat hearts to evaluate cell delivery and viability. Cardiac derived ECM is known to guide cardiac cell migration, proliferation and differentiation. It is possible that the cardiac ECM could aid in cardiac cell attachment and viability.

Finally, while our study was purely *in vitro*, seeded fibrin sutures have been delivered into healthy and infarcted hearts using a rat model. Many studies have been performed on the fibrin only sutures. Because the ECM-fibrin based sutures have behaved differently in the *in vitro* studies, *in vivo* studies must be performed in order to fully determine how the ECM-fibrin sutures compare to fibrin only sutures. Our *in vitro* endothelial progenitor cell outgrowth assay concluded that the ECM-fibrin microthreads are pro-angiogenic. This conclusion could be confirmed with *in vivo* studies.

Chapter 8: Conclusion

The goal of the project was to successfully incorporate cardiac extracellular matrix into fibrin microthreads and to explore the effects that the ECM incorporation has on structural and mechanical properties as well as hMSC adhesion and EPOC outgrwoth. The ECM incorporation caused an increase in the elastic modulus of the microthreads when comparing the ECM-fibrin microthreads to the fibrin only microthreads. This increase was especially significant in the 10% ECM microthread group. When evaluating the different types of microthread when used as a bundled suture in hMSC cell seeding. The sutures that were ECM-fibrin based did not exhibit any significant differences in the cell attachment when compared to the fibrin only based sutures. Lastly, when used in a 24-hour EPOC outgrwoth assay, the ECM-fibrin microthreads increased the rate of cell outgrowth as well as increased the number of cells that adhered to the microthreads when compared to fibrin only microthreads as well as a control with no microthread. EPOC outgrwoth toward a 15% ECM-fibrin microthread showed a 16% increase in distance travelled by the cells in 24 hours when compared to the outgrowth of cells toward the fibrin only microthread and an 18% increase when compared to a blank control. The incorporation of native cardiac ECM into fibrin microthreads increases the microthread elastic modulus and is able to increase EPOC outgrowth distance and attachment to the microthread.

References

1. Murphy, M.K., *Fibrin Microthreads Promote Stem Cell Growth for Localized Delivery in Regenerative Therapy*, in *Biomedical Engineering, Worcester Polytechnic Institute.* 2008, WPI:Worcester.
2. Humphrey, J., *Cardiovascular Soild Mechanics: Cells, Tissues, and Organs*. 2001, New York, New York: Springer-Verlag.
3. Marieb, E.N.K., K., *Human Anatomy and Physiology*, ed. Pearson. 2011.
4. Sherwood, L., *Human Physiology: from cells to systems*. 4th ed. Brooks/Cole. 2001, Pacific Grove, CA.
5. Bers, D.M., *Cardiac excitation-contraction coupling.* Nature, 2002. **415**(6868): p. 198-205.
6. Ferrero Jr, J., *Wiley Encyclopedia of Biomedical Engineering.* 2006: John Wiley and Sons Inc.
7. Kloner, R.A., R.B. Jennings, *Consequences of brief ischemia: stunning, preconditioning, and their clinical implications: part 1*. Circulation, 2001. **104**(24): p. 2981-9.
8. Sutton, M.S.N., *Left Ventricle Remodeling After Myocardial Infarction: Pathophysiology and Therapy*. Circulation, 2000(101): p. 2981-2988.
9. American Heart Association. *Heart disease and stroke statistics – 2015 update: A report from the American Heart Association.* 2015
10. The Heart Foundation. *Heart Disease: Scope and Impact.* 2015
11. Laflamme, M.A., Murry, C.E., *Regenerating the heart*. Nat Biotechnol, 2005. **23**(7): p. 845-56.
12. *Heart and Stroke Statistics*. 2015.
13. US Department of Health and Human Services. *Timeline of Historical Event Significant Milestones in organ Donation and Transplantation.* 2015.
14. Pfeffer M.A., Braunwald, E., *Ventricular remodeling after myocardial infarction. Experimental observations and clinical implications*. Circulation, 1990. **81**(4): p. 1161-72.
15. Athanasuleas, C.L., Buckberg, G.D., Stanley, A.W., Siler, W., Dor, V., DiDonato, M., Menicanti, L., Almeida de Oliveira, S., Beyersdorf, F., Kron, I.L., Suma, H., Kouchoukos, N.T., et al., *Surgical ventricular restoration in the treatment of congestive heart failure due to post-infarction ventricular dilation*. J Am Coll Cardiol, 2004. **44**(7): p. 1439-45.
16. Buckberg, G., *Ventricular structure and surgical history*. Heart Fail Rev, 2004. **9**(4): p. 255-68; discussion 347-51.
17. Tonnessen, T., Knudsen, C.W., *Surgical left ventricular remodeling in heart failure*. Eur J Heart Fail, 2005. **7**(5): p. 704-9.
18. Fang J.C.G., *Surgical Management of Congestive Heart Failure*. 2005, Totowa, NJ: Humana Press Inc.
19. Kochupura, P.V., Azeloglu, E.U., Kelly, D.J., Doronin, S.V., Badylak, S.F., Krukenkamp, I.B., Cohen, I.S., Gaudette, G.R., *Tissue-engineered myocardial patch derived from extracellular matrix provides regional mechanical function*. Circulation, 2005. **112**(9 Suppl): p. 144-9.
20. Taylor, D.A., Atkins, B.Z., Hungspreugs, P., Jones, T.R., Reedy, M.C., Hutchenson, K.A., Glower, D.D., Kraus, W.E., *Regenerating functional myocardium: improved performance after skeletal myoblast transplantation*. Nat Med, 1998. **4**(8): p. 929-33.
21. Kolossov, E., Bostani, T., Roell, W., Breitbach, M., Pillekamp, F., Nygren, J.M., Sasse, P.,Rubenchik, O., Fries, J.W., et al., *Engraftment of engineered ES cell-derived cardiomyocytes but not BM cells restores contractile function to the infarcted myocardium*. J Exp Med, 2006. **203**(10): p. 2315-27.
22. Beltrami, A.P., Barlucchi, L., Torella, D., Baker, M., Limana, F., Chimenti, S., Kasahara, H., Rota, M., Musso, E., Urbanek, K., Leri, A., Kajstura, J., Nadal-Ginard, B., Anversa, P., *Adult cardiac stem cells are multipotent and support myocardial regeneration.* Cell, 2003. **114**(6): p. 763-76.

23. Schuldt, A.J., Rosen, M.R., Gaudette, G.R., Cohen, I.S., *Repairing damaged myocardium: evaluating cells used for cardiac regeneration.* Curr Treat Options Cardiovasc Med, 2008. **10**(1): p. 59-72.

24. Reffelmann, T., Kloner, R.A., *Cellular cardiomyoplasty--cardiomyocytes, skeletal myoblasts, or stem cells for regenerating myocardium and treatment of heart failure?* Cardiovasc Res, 2003. **58**(2): p. 358-68.

25. Christman, K.L., Lee, R.A., *Biomaterials for the treatment of myocardial infarction*. J Am Coll Cardiol, 2006. **48**(5): p. 907-13.

26. Rane, A.A., Christman, K.L., *Biomaterials for the treatment of myocardial infarction: a 5-year update*. J Am Coll Cardiol, 2011. **58**(25): p. 2615-29.

27. Pittenger, M.F., Martin, B.J., *Mesenchymal stem cells and their potential as cardiac therapeutics*. Circ Res, 2004. **95**(1): p. 9-20.

28. Barry, F.P., Murphy, J.M., *Mesenchymal stem cells: clinical applications and biological characterization*. Int J Biochem Cell Biol, 2004. **36**(4): p. 568-84.

29. Tae, S.K., Lee, S.H., Park, J.S., Im, G.I., *Mesenchymal stem cells for tissue engineering and regenerative medicine*. Biomed Mater, 2006. **1**(2): p. 63-71.

30. Toma, C., Pittenger, M.F., Cahill, K.S., Byrne, B.J., Kessler, P.D., *Human mesenchymal stem cells differentiate to a cardiomyocyte phenotype in the adult murine heart*. Circulation, 2002. **105**(1): p. 93-8.

31. Hou, M., Yang, K.M., Xhang, H., Xhu, W.Q., Duan, F.J., Wang, H., Song, Y.H., Wei, Y.J., Hu, S.S, *Transplantation of mesenchymal stem cells from human bone marrow improves damaged heart function in rats*. Int J Cardiol, 2007. **115**(2): p. 220-8.

32. Orlic, D., Kajstura, J., Chimenti, S., Limana, F., Jakoniuk, I., Quaini, F., Nadal-Ginard, B., Bodine, D.M., Leri, A., Anversa, P., *Mobilized bone marrow cells repair the infarcted heart, improving function and survival*. Proc Natl Acad Sci U S A, 2001. **98**(18): p. 10344-9.

33. Behfar, A., Yamada, S., Crespo-Diaz, R., Nesbitt, J.J., Rowe, L.A., Perez-Terzic, C., Gaussin, V., Homsy, C., Bartunek, J., Terzic, A., *Guided cardiopoiesis enhances therapeutic benefit of bone marrow human mesenchymal stem cells in chronic myocardial infarction*. J Am Coll Cardiol, 2010. **56**(9): p. 721- 34.

34. Potapova, I.A., Doronin, S.V., Kelly, D.J., Rosen, A.B., Schuldt, A.J., Lu, Z., Kochupura, P.V., Robinson, R.B., Rosen, M.R., Brink, P.R., Gaudette, G.R., Cohen, I.S., *Enhanced recovery of mechanical function in the canine heart by seeding an extracellular matrix patch with mesenchymal stem cells committed to a cardiac lineage.* Am J Physiol Heart Circ Physiol, 2008. **295**(6): p. H2257-63.

35. Mauritz, C., Schwanke, K., Reppel, M., Neef, S., Katsirntaki, K., Maier, L.S., Nquemo, F., Menke, S., Haustein, M., Hescheler, J., Hasenfuss, G., Matin, U., *Generation of functional murine cardiac myocytes from induced pluripotent stem cells.* Circulation, 2008. **118**(5): p. 507-17.

36. Kreutziger, K.L., Murry, C.E., *Engineered human cardiac tissue*. Pediatr Cardiol, 2011. **32**(3): p. 334-41.

37. Muller-Ehmsen, J., Whittaker, P., Kloner, R.A., Dow, J.S., Sakoda, T., Long, T.I., Laird, P.W., Kedes, L., *Survival and development of neonatal rat cardiomyocytes transplanted into adult myocardium*. J Mol Cell Cardiol, 2002. **34**(2): p. 107-16.

38. Hou, D., Youssef, E.A., Brinton, T.J., Zhang, P., Rogers, P., Price, E.T., Yeung, A.C., Johnstone, B.H., Yock, P.G., March, K.L., *Radiolabeled cell distribution after intramyocardial, intracoronary, and interstitial retrograde coronary venous delivery: implications for current clinical trials*. Circulation, 2005. **112**(9 Suppl): p. I150-6.

39. Guyette, J.P., Fakharzadeh, M., Burford, E.J., Tao, Z.W., Pins, G.D., Rolle, M.W., Gaudette, G.R., *A novel suture-based method for efficient transplantation of stem cells*. J Biomed Mater Res A, 2013. **101**(3): p. 809-18.

40. Zhang, M., Methot, D., Poppa, V., Fujio, Y., Walsh, K., Murry, C.E., *Cardiomyocyte grafting for cardiac repair: graft cell death and anti-death strategies*. J Mol Cell Cardiol, 2001. **33**(5): p. 907-21.

41. Clark, R.A., *Fibrin and wound healing*. Ann N Y Acad Sci, 2001. **936**: p. 355-67.

42. Kofidis, T., de Bruin, J.L., Hoyt, G., Lebl, D.R., Tanaka, M., Yamane, T., Chang, C.P., Robbins, R.C., *Injectable bioartificial myocardial tissue for large-scale intramural cell transfer and functional recovery of injured heart muscle*. J Thorac Cardiovasc Surg, 2004. **128**(4): p. 571-8.

43. Ryu, J.H., Kim, I.K., Cho, S.W., Cho, M.C., Hwang, K.K., Piao, H., Piao, S., Lim, S.H., Hong, Y.S., Choi, C.Y., Yoo, K.J., Kim, B.S., *Implantation of bone marrow mononuclear cells using injectable fibrin matrix enhances neovascularization in infarcted myocardium*. Biomaterials, 2005. **26**(3): p. 319-26.

44. Mol, A., van Lieshout, M.I., Dam-de Veen, C.G., Neuenschwander, S. Hoerstrup, S.P., Baaijens, F.P., Bouten, C.V., *Fibrin as a cell carrier in cardiovascular tissue engineering applications*. Biomaterials, 2005. **26**(16): p. 3113-21.

45. Ahmed, T.A., Dare, E.V., Hincke, M., *Fibrin: a versatile scaffold for tissue engineering applications*. Tissue Eng Part B Rev, 2008. **14**(2): p. 199-215.

46. Buchta, C., Hedrich, H.C., Macher, M., Hocker, P., Redl, H., *Biochemical characterization of autologous fibrin sealants produced by CryoSeal and Vivostat in comparison to the homologous fibrin sealant product Tissucol/Tisseel.* Biomaterials, 2005. **26**(31): p. 6233-41

47. Leo, A.J., Grande, D.A., *Mesenchymal stem cells in tissue engineering*. Cells Tissues Organs, 2006. **183**(3): p. 112-22.

48. Gruber, H.E., Leslie, K., Ingram, J., Norton, H.J., Hanley, E.N., *Cell-based tissue engineering for the intervertebral disc: in vitro studies of human disc cell gene expression and matrix production within selected cell carriers*. Spine J, 2004. **4**(1): p. 44-55.

49. Ringe, J., Kaps, C., Burmester, G.R., Sittinger, M., *Stem cells for regenerative medicine: advances in the engineering of tissues and organs*. Naturwissenschaften, 2002. **89**(8): p. 338-51.

50. Schense, J.C., Hubbell, J.A., *Cross-linking exogenous bifunctional peptides into fibrin gels with factor XIIIa*. Bioconjug Chem, 1999. **10**(1): p. 75-81.

51. Cornwell, K.G., Pins, G.D., *Discrete crosslinked fibrin microthread scaffolds for tissue regeneration.* J Biomed Mater Res A, 2007. **82**(1): p. 104-12.

52. Kowaleski, M., *Increasing Cell Attachment and Adhesion on Fibrin Microthread Sutures for Cell Delivery, in Biomedical Engineering*. 2012, Worcester Polytechnic Institute: Worcester, MA.

53. Neuss, S., Schneider, R.K., Tietze, L., Knuchel, R., Jahnen-Dechent, W., *Secretion of fibrinolytic enzymes facilitates human mesenchymal stem cell invasion into fibrin clots*. Cells Tissues Organs, 2010. **191**(1): p. 36-46.

54. Coffin, S.T., Gaudette, G.R., *Aprotinin extends mechanical integrity time of cell-seeded fibrin sutures.* J Biomed Mater Res. 2016. **104**(9). p. 2271-79

55. Borg, T.K., Gay, R.E., Johnson, L.D., *Changes in the distribution of fibronectin and collagen during development of the neonatal rat heart*. Coll. Relat. Res. 1982. **2**(3): p. 211–8

56. Alberts, B., Johnson, A., Lewis, J., Raff, M., *Molecular biology of the cell*. New York: Garland .... 2008.

57. Pruitt, N.L., Karp, G., *Cell and Molecular Biology Concepts and Experiments.* A Wiley Company 6 ed. 2009

58. Di Lullo, G.A., Sweeney, S.M., Körkkö, J., Ala-Kokko L., *Mapping the ligand-binding sites and disease-associated mutations on the most abundant protein in the human, type I collagen*. J. Biol. Chem. American Society for Biochemistry and Molecular Biology. 2002. **277**(6): p. 4223–31.
59. MD, S., RT, R., *Collagen structure and stability*. Annu Rev Biochem. NIH Public Access. 2009. **78**(1): p. 929–58.
60. Jackson, D.S., *Collagens*. Journal of Clinical Pathology. 1978.
61. Brinckmann, J., *Collagens at a Glance*. Springer Berlin Heidelberg; 2005. p. 1–6.
62. Heino, J., *The collagen family members as cell adhesion proteins*. BioEssays. Wiley Subscription Services, Inc., A Wiley Company. 2007. **29**(10): p. 1001–10.
63. Aumailley, M., Bruckner-Tuderman, L., Carter, W.G., *A simplified laminin nomenclature.* Matrix Biology. 2005.
64. Haralson, M.A., Hassell, J.R., *Extracellular matrix: a practical approach*. IRL Press. 1995.
65. Colognato, H., Yurchenco, P.D., *Form and function: the laminin family of heterotrimers*. Developmental Dynamics. 2000.
66. Pankov, R., Yamada, K.M., *Fibronectin at a glance*. Journal of Cell Science. 2002.
67. Maheshwari, G., Brown, G., Lauffenburger, D.A. *Cell adhesion and motility depend on nanoscale RGD clustering.* Journal of Cell . 2000.
68. Alberts, B., Johnson, A., Lewis, J., Raff, M., Roberts, K., Walter, P., *Integrins*. Molecular Biology of the Cell. 2002. **4**.
69. Campbell, I.D., Humphries, M.J., *Integrin Structure, Activation, and Interactions*. Cold Spring Harb Perspect Biol. 2011. **3**(3).
70. Hynes, R.O., *Integrins: bidirectional, allosteric signaling machines*. Cell. 2002.
71. Krieger, M., Scott, M.P., Matsudaira, P.T., Lodish, H., Molecular Cell Biology. Macmillan. 2008.
72. Calderwood, D.A., *Talin Controls Integrin Activation*. Biochemical Society Transactions. 2008.
73. Duffy, A.M., Bouchier-Hayes, D.J., Harmey, J.H. *Vascular Endothelial Growth Factor (VEGF) and Its Role in Non-Endothelial Cells: Autocrine Signalling by VEGF.* Madame Curie Bioscience Database. 2000-2013, Austin, TX.
74. Detillieux K.A., Sheikh F., Kardami E., Cattini P.A. *Biological activities of fibroblast growth factor-2 in the adult myocardium*. Cardiovasc. Res*.* 2003. **57**: p. 8–19.
75. Crapo P.M., Medberry C.J., Reing J.E., Stephen T., Yolandi V.D.M., Jones K.E., Badylak S.F. *Biologic scaffolds composed of central nervous system extracellular matrix*. Biomaterials. 2012. **33**: p. 3539–3547.
76. Chen, R.N., Ho, H.O., Tsai, Y.T., Cheu, M.T., *Process development of an acellular dermal matrix (ADM) for biomedical applications*. Biomaterials. 2004. **25**. p. 2679-86.
77. Bader, A., Schilling, T., Teebken, O.E., Brandes, G., Herden, T., Steinhoff, G., *Tissue engineering of heart valves – human endothelial cell seeding of detergent acellularized porcine valves.* Eur J Cardiothorac Surg. 1998. **14**. p. 279-84.
78. Booth, C., Korosis, S.A., Wilcox, H.E., Watterson, K.G., Kearney, J.N., Fisher, J., *Tissue engineering of cardiac valve prostheses I: development and histological characterization of an acellular porcine scaffold.* J heart Valve Dis. 2002. **11**. p. 457-62.
79. Grauss, R.W., Hazekamp, M.G., Oppenhuizen, F., van Munsteren, C.J., Gittenberger-de-Groot, A.C., DeRuiter, M.C., *Histological evaluation of decellularised porcine aortic valves: matrix changes due to different decellularisation methods.* Eur J Cardiothorac Surg. 2005. **27.** p. 566-71.
80. Kasimir, M.T., Rieder, E., Seebachler, G., Silberhumer, G., Wolner, E., Weigel, G., *Comparison of different decellularzation procedure on porcine heart valves.* Int J Artif Organs. 2003. **26**. p. 421-27.

81. Korossis, S.A., Booth, C., Wilcox, H.E., Watterson, K.G., Kearney, J.N., Fisher, J., *Tissue engineering of cardiac valve prostheses II: biomechanical characterization of decellularized porcine aortic heart valves.* J Heart Valve Dis. 2002. **11**. p. 463-71.

82. Rieder, E., Kasimir, M.T., Silberhumer, G., Seebacher, G., Wolner, E., Simon, P., *Decellularization protocols of porcine heart valves differ importantly in efficiency of cell removal and susceptibility of the matrix to recellularization with human vascular cells.* J Thorac Cardiovasc Surg. 2004. **127**. p. 399-405.

83. Schenke-Layland, K., Vasilevski, O., Opitz, F., Konig, K., Riemann, I., Halbhuber, K.J., et al. *Impact of decellularization of xenogeneic tissue on extracellular matrix integrity for tissue engineering of heart valves.* J Struct Biol. 2003. **143**(3). p. 201-08.

84. Hudson, T.W., Liu, S.Y., Schmidt, C.E., *Engineering an improved acellular nerve graft via optimized chemical processing.* Tissue Eng. 2004. **10**. p. 1346-58.

85. Kim, B.S., Yoo, J.J., Atala, A., *Peripheral nerve regeneration using acellular nerve grafts.* J Biomed Mater Res. 2004. **68A**(2). p. 201-09.

86. Conklin, B.S., Richter, E.R., Kreutziger, K.L., Zhong, D.S., Chen, C., *Development and evaluation of a novel decellularized vascular xenograft*. Med Eng Phys. 2002. **24**. p. 173-83.

87. Dahl, E.L., Koh, J., Prabhakar, V., Niklason, L.E., *Decellularized native and engineering arterial scaffolds for transplantation.* Cell Transplant. 2003. **12**. p. 659-66.

88. Schmidt, C.E., Baier, J.M., *Acellular vascular tissues: natural biomaterial for tissue repair and tissue engineering.* Biomaterials. 2000. **21**(22). p. 2215-31.

89. Uchimura, E., Sawa, Y., Taketani, S., Yamanaka, Y., Hara, M., Matsuda, H., *Novel method of preparing acellular cardiovascular grafts by decellularization with poly(ethylene glycol).* J Biomed Mater Red A. 2003. **67**. p. 834-37.

90. Badylak, S.F., Lantz, G.C., Coffey, A., Geddes, L.A., *Small Intestinal submucosa as a large diameter vascular graft in the dog*. J Surg Res. 1989. **47**(1). p. 74-80.

91. Badylak, S.F., Tullius, R., Kokini, K., Shelbourne, K.D., Klootwyk, T., Voytik, S.L., et al. *The use of xenogeneic small intestinal submucosa as a biomaterial for Achilles tendon repair in a dog model.* J Biomed Mater Res. 1995. **29**(8). p. 977-85.

92. Kropp, B.P., Eppley, B.L., Prevel, C.D., Rippy, M.K., Harruff, R.C., Badylak, S.F., et al. *Experimental assessment of small intestinal submucosa as a bladder wall substitute.* Urology. 1995. **43**(3). p. 396-400.

93. Cartmell, J.S., Dunn, M.G., *Effect of chemical treatment on tendon cellularity and mechanical properties*. J Biomed Mater Res. 2000. **49**. p. 134-40.

94. Woods, T., Gratzer, P.F., *Effectiveness of three extraction techniques in the development of a decellularized bone-anterior cruciate ligament-bone graft.* Biomaterials. 2005. **26**(35). p. 7339-49.

95. Borschel, G.H., Dennis, R.G., Kuzon, J.W.M., *Contractile skeletal muscle tissue-engineered on an acellular scaffold.* Plast Reconstr Surg. 2004. **113**. p. 595-602.

96. Sullivan, K.E., Quinn, K.P., Tang, K.M., Georgakoudi, I., Black, L.D., *Extracellular matrix remodeling following myocardial infarction influences the therapeutic potential of mesenchymal stem cells.* Stem Cell Research & Therapy. 2014. **5**(14).

97. Singelyn, J.M., DeQuach, J.A., Seif-Naraghi, S.B., Littlefield, R.B., Schup-Magoffin, P.J., Christman, K.L., *Naturally derived myocardial matrix as an injectable scaffold for cardiac tissue engineering*. Biomaterials. 2009. **30**(29). p. 5409-16.

98. French, K.M., Boopathy, A.V., DeQuach, J.A., Chingozha, L., Lu, H., Christman, K.L., David, M.E., *A naturally-derived cardiac extracellular matrix enhances cardiac progenitor cell behavior in vitro.* Acta Biomater. 2012. **8**(12). p. 4357-64.

99. Oberwallner, B., *Preparation of Cardiac Extracellular Matrix Scaffolds by Decellularization of Human Myocardium.* J Biomed Mater Res A. 2014. **102**(9). p. 3263-72

100. Nayak, R., Padhye, R., Kyratzis, I.L., Truong, Y.B., Arnold, L., *Effect of viscosity and electrical conductivity on the morphology and fiber diameter in melt electrospinning of polypropylene.* Textile Research Journal. 2013. **83**(6). p. 606-17.

101. Jensen, T., Halvorsen, S., Godal, H.C., Sandset, P.M., Skjonsberg, O.H., *The viscosity of fibrinogen subfractions and of EDTA denatured fibrinogen do not differ from that of native fibrinogen.* Thrombosis Research. 2004. **113**. p. 51-56.

102. Rowe, S.L., Stegemann, J.P., *Interpenetrating collagen-fibrin composite matrices with varying protein contents and ratios*. Biomacromolecules. 2006. **7**(11). p. 2942-48.

103. Rowe, S.L., Stegemann, J.P., *Microstructure and mechanics of collagen-fibrin matrices polymerized using ancrod snake venom enzyme.* J Biomech Eng. 2009. **131**(6).

104. Park, H., Karajanagi, S., Wolak, K., Aanested, J., Daheron, L., Kobler, J.B., Lopez-Guerra, G., Heaton, J.T., Langer, R.S., Zeitels, S.M., *Three-dimensional hydrogel model using adipose-derived stem cells for vocal fold augmentation.* Tissue Engineering: Part A. 2010. **16**(2). p. 535-43.

105. Williams, P.A., Silva, E.A., *The role of synthetic extracellular matrices in endothelial progenitor cell homing for treatment of vascular disease.* Annals of Biomedical Engineering. 2015. **43**(10). p. 2301-13.

106. Sottile, J., *regulation of angiogenesis by extracellular matrix.* Biochimica et Biophysica Acta. 2004. **1654**. p. 13-22.

107. Ciaiado, F., Dias, S., *Endothelial progenitor cells and integrins: adhesive needs.* Fibrogenesis & Tissue Repair. 2012, **5**(4).

108. Crister, P.J., Kreger, S.T., Voytic-Harbin, S.L., Yoder, M.C., *Collagen matrix physical properties modulate endothelial colony forming cell-derived vessels in vivo.* Microvas Res. 2010. **80**. p. 23-30.

109. Bleiziffer, O., Hammon, M., Naschberger, E., Lipnik, K., Arkudas, A., Rath, S., Pryymachuk, G., Beier, J.P., Sturzl, M., Horch, R.E., Kneser, U., *Endothelial projecnitor cells are integrated in newly formed capillaries and alter adjacent fibrovascular tissue after subcutaneous implantation in a fibrin matrix.* J Cell Mol Med. 2011. **15**. p. 2452-61.

Appendix A: Cardiac ECM Preparation

A.1. Decellularization of Cardiac Tissue

Materials:
- 50 mL conical tube
- Large petri dish
- Iris scissors
- Fine tooth forceps
- 1% Sodium Dodecyl Sulfate
- 1% Triton-X 100
- Dulbeccos Phosphate Buffered Saline
- Scilogex Tube Rotator
- Hearts obtained from rats

Procedure:
1. Obtain hearts from rats after following animal euthanization and heart extraction. Store hearts in DPBS at -30°C
2. In a large petri dish, place about 10 mL of PBS in the dish
3. Place heart in the dish and using the fine tooth forceps and the iris scissors, cut up the heart into small pieces
   a. Approximately 3mmx3mmx3mm
4. Once the heart is fully minced, place all heart pieces into a 50 mL conical tube
5. Add about 25 mL of 1% SDS into the conical tube
6. Place the conical tube on the tube rotator and rotate overnight
7. Replace the SDS every 12 hours until the heart tissue pieces are fully transparent
8. Once the hearts are fully transparent, replace the 1% SDS solution with approximately 25 mL of 1% Triton-X 100 solution
9. Replace the Triton-X solution every 12 hours for 24 hours
10. Following 24 hours of Triton-X immersion, replace the solution with deionized water
11. Replace the DI water every 12 hours for 24 hours
12. Once decellularization is complete, place the tissue sections in about 10 mL of DI water for storage at -30°C

A.2. Lyophilization of Decellularized Cardiac ECM

Materials:
- Decellularized cardiac ECM (frozen in 10 mL of DI water)
- Kim wipe
- Lab Tape
- Lyophilizer

Procedure:
1. Remove the decellularized ECM from the -30°C freezer
2. Remove the cap of the conical tube and tape a KimWipe over the opening of the tube

3. Keep the tube on ice until placed into the lyophilizer
4. Ensure that the lyophilizer is turned on and has reached the proper conditions
    a. Temperature = -104.3 °C
    b. Pressure = 14 millitorr
5. Place the conical tube into lyophilizer jars and attach the jar to the machine
    a. To do this place a vacuum seal over the jar and attach the jar to an open site
    b. Turn the white knob 180 degrees so that it is oriented in the up-down direction
6. Allow the process to lyophilize the tissue until the ECM is visibly dry and all ice crystal are gone
    a. This can take between 24 and 48 hours
7. Once process is complete, turn the white knob again 180 degrees to release the pressure inside the jar
8. Remove the jar from attachment site and remove sample
9. Replace the cap on the conical tube and store in a dry area

A.3. Solubilization of Cardiac ECM

Materials:
- Lyophilized cardiac ECM
- 0.1 M Hydrochloric Acid
- Pepsin from Gastric Mucosa
- 1 M Sodium Hydroxide
- Weigh boat
- Disposable Scintillation Vial
- Scale
- Stir Plate
- Stir bar
- Ceramic Mortar and Pestle

Procedure:
1. Obtain lyophilized cardiac ECM
2. Grind ECM using the mortar and pestle until it is a fine powder
    a. Larger ECM pieces may need to be additionally cut using iris scissors to be successfully ground
3. Once ECM is ground, weight out 100 mg
    a. This is easiest if it is weighed inside the vial in order to ensure no ECM is lost
4. Weigh 10 mg of pepsin from gastric mucosa and add it to the vial
    a. This is easiest if it is weighed inside a 1.7 mL microcentrifuge tube. Then using 1000 uL of 0.1M HCl, mix the pepsin into the HCl and add it to ECM.
5. Add 0.1 M HCl to the vial. There should be a total of 10 mL of HCL in the vial.
6. Place a small stir bar in the vial and stir the solution
7. Stir the solution until all ECM is visibly solubilized. This can take between 3 and 7 days depending on the size of the ECM particles within the solution.
8. Once the ECM is fully solubilized, neutralize the solution with 1M NaOH to a pH of 7.4
9. Store the solution in the refrigerator for up to 1 week.

Appendix B: ECM-Fibrin Microthread Production

Materials:

- Extrusion baking pan
- Syringe pump
- 1 aliquot fibrinogen - 70mg/ml
- 1 aliquot thrombin – 8U/200µl
- 10mM HEPES solution
- 2 - 1mL syringes
- 1 – 3ml syringe
- 1000mL graduated cylinder
- Clear cup of room temperature water
- 40mM $CaCl_2$
- 1000µl Micropipetter
- 2 sets of fine toothed forceps
- Cardboard drying box
- Kimwipes
- Extruding tube
- Blending connector
- Polyethylene Tubing
- Solubilized ECM solution (10mg/mL)

Procedure:

Preparation:

1. Rinse graduated cylinder with DI water
2. Fill Graduated cylinder with 500mL of 10mM HEPES solution. Transfer HEPES into silver baking pan
3. Obtain 1 aliquot of Fibrinogen and 1 aliquot of Thrombin from -30C freezer
4. Obtain 40mM $CaCl_2$ from fridge.
5. Defrost frozen aliquots by placing them into room temperature water
6. Once completely defrosted, add 850µL of 40mM $CaCl_2$ into the thrombin, mix thoroughly
7. Label two 1ml syringes, one as T and one as F

ECM Preparation:

1. Obtain the ECM solubilized solution from the refrigerator
2. The ECM solution must be filtered prior to solution mixing to remove any large sized particles that may clog the polyethylene tubing and 27-gauge needle used in extrusion (ID:0.38 mm, OD:1.09mm)
3. Transfer 1000 uL of the ECM solution to a 1.7 mL microcentrifuge tube
4. Using a 20-gauge needle attached to a 1mL syringe, draw up the whole solution into the syringe

5. Transfer the filtered solution to a new 1.7 mL microcentrifuge tube
6. Repeat step 4 using a 22 gauge-needle
7. Transfer the filtered solution to a new 1.7 mL microcentrifuge tube
8. Repeat step 4 again using a 27-gauge needle
9. Transfer the filtered solution to a new 1.7 mL microcentrifuge tube

Solution Preparation:

1. For a 5% ECM microthread solution:
   a. Transfer 950ul of Thrombin and Fibrinogen into new 1.7 mL microcentrifuge tubes
   b. Add 50ul of filtered ECM solution into microcentrifuge tube (Total V=1000 ul) and mix thoroughly

Percentage	Volume of Thrombin	Volume of Fibrinogen	Volume of ECM in T and F
5%	950 ul	950 ul	50 ul
10%	900 ul	900 ul	100 ul
15%	850 ul	850 ul	150 ul
20%	800 ul	800 ul	200 ul

2. Using 20 G syringe appropriate withdraw thrombin and fibrinogen into separate labeled syringes
3. Remove all air bubbles from syringe
4. Balance the two syringes so that they contain the same volume of solution

Setting up Machine:
1. Plug in syringe pump and turn the power on (Power switch is in the back of the machine)
2. Make sure **DIAMETER** is set to 4.699mm and the **RATE** is set to 0.23 mL/min.
3. Plug the Fibrinogen and Thrombin syringes into the blending connector. The Fibrinogen syringe should ALWAYS be placed into the side with the small circle
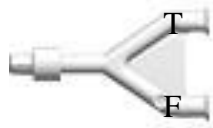
4. Place syringes into syringe pump.
   ➢ Lift black knob and slide the ends of the syringes under black bar, splitting the two syringes with the knob. Make sure syringe body flanges are inserted in to clamp. Release black knob.
   ➢ Tighten syringe clamp using the silver nuts.
5. Make syringe pump block flush with the syringe connector

> ➢ Push down black button and pinch white piece
6. Attach polyethylene tubing to the free side of the blending connector

<u>Thread Extrusion:</u>
1. Press start on the machine.
2. Wait for <u>ALL</u> the air bubbles to pass through the PE tubing. Use a Kimwipe to collect anything that comes out while air bubbles are passing through.
3. Once there is a constant flow, start making the threads.
   Hold extruding tube ≈ 4 inches from the end. Drag end of tube horizontally along the bottom of the silver pan filled with 10mM HEPES. Move the tube from the left side of the pan to right side at a constant rate. At the end of one thread move quickly bring the end of the tube back to the left side of the pan, move ≈ 1 inch down and begin a new thread. Repeat until you cannot make anymore. *Make sure the end of the tube is clean and free of fibrin debris, wipe clean if needed
4. Turn off machine once you are done.

<u>Clean Up Part 1:</u>
1. Immediately clean tube. Fill a 3ml syringes with water and flush extruding tube with water. Remove syringe from extruding tube, withdraw syringe with just air and blow air through extruding tube with syringe. Repeat with white co-extruder.
2. Throw away any used materials into the proper trash receptacle.

<u>Transferring Threads:</u>
1. Use the two sets of forceps to take the threads out of the pan.
   - ➢ Grab each end of the thread with the forceps
   - ➢ Move right hand counterclockwise and left hand clockwise so you can pick up the thread.
   - ➢ Make sure not to pull too fast and to keep threads in the HEPES as long as possible.
2. Transfer the threads to the cardboard box. Secure one side to the box and stretch the thread. Secure the middle of the stretched out thread to the box. Cut the thread in half then stretch the remaining half over the box. One extruded thread should produce two threads
3. Repeat this for all threads. Leave threads out to dry overnight.

<u>Clean Up Part 2:</u>
1. Pour HEPES down the drain and rinse off pan. Dry the pan with paper towel.
2. Put all items away.
3. Dispose of any other used items in the appropriate receptacle.

Appendix C: ECM Protein Staining Protocols

Materials:

- Phosphate Buffered Saline
- 4% Paraformaldehyde (Only needed for tissues/cells that have not been fixed);
- 0.25% Triton-X
  - 0.25% V/V Triton-X in PBS
  - 10 μL Triton-X in 3990 μL PBS
- 1% BSA
  - 1% V (W)/V BSA in PBS
  - 40 μL in 3960 μL
- Primary for protein of choice- 1:200 in blocking agent, 1% BSA
  - Fibronectin (anti-fibronectin antibody ab2413)
- Secondary antibody – goat anti rabbit IgG AF 546 1:500 in BSA
- Glass slides with microthread sections
- Hydrophobic marker
- Slide staining box

Procedure:

1. Rinse in PBS 2x
2. Fix in 4% para for 10 min
3. Wash PBS 3x, 5 min each
4. 0.25% Triton-X 100, 10 min
5. Wash PBS 3x, 5 min each
6. Block with 1% BSA, 45 min
7. Leave BSA on negative, aspirate off positive
8. Primary: 1:200 anti-fibronectin in 1% BSA at 4°C overnight
9. Wash PBS 3x, 5 min each
10. Secondary: 1:500 goat anti-rabbit AF 488, 1 hour @ room temp in the dark
11. Wash PBS 3x, 5 min each
12. Coverslip, image, store @ -20°C

The table below shows the concentrations that should be use for the staining of Collagen I and Laminin 111.

Protein	Primary Antibody	Primary Concentration	Secondary Antibody	Secondary Concentration	Stain Color
Collagen I	Anti-Collagen I	1:200μL in BSA	Rabbit Anti-goat 488	1:400μL in BSA	Green
Fibronectin	Anti-Fibronectin ab2413	1:200μL in BSA	Goat-Anti-Rabbit 546	1:500μL in BSA	Red
Laminin 111	Anti-Laminin ab11575	1:100μL in BSA	Goat-Anti Rabbit 488	1:500μL in BSA	Green

Appendix D: Suture Production

Materials:

- ECM-fibrin microthreads of all concentrations
- DI H2O
- Laboratory Tape
- Ruler
- Iris scissors
- Fine toothed forceps
- Havel's regular eye suture needles
- 27 gauge hypodermic needles
- Blue slide clamps
- Silastic Silicone tubing (ID: 1.98 mm, OD: 3.18 mm)
- DPBS
- SIMCO Air blower (optional)
- Chex-All sterilization pouches

Procedure:

1. On a clean dark surface, gather 12 microthread of the same type together. Align the ends of the microthreads so that they are even. Secure all 12 microthreads together with a piece of laboratory tape.
2. Fold the tape in half and secure the cluster of threads to a lab bench-top stand.
3. Using a disposable pipet, drop water down the microthreads to hydrate them and form them together.
4. Once fully hydrated, twist the microthreads together by twisting from the bottom of the bundle.
5. After twisting the microthreads together, secure the end of the bundle to the middle bar on the lab benchtop stand.
6. Allow the bundle to dry.
7. Once dry, remove the bundle from the stand cur off the two ends (the tape and the opposite end of the bundle where it was clamped to the stand).
8. Cut a 5cm section of bundle and thread the section through the eye of a suture needle.
9. Hydrate the bundle in DPBS for 10 minutes.
10. Remove the bundle and needle from DPBS.
11. Fold the bundle in half over the needle and align the two ends.
12. Using a surgical clamp, secure the two ends of the suture together.
13. Twist the needle about 4 times to bundle the two sides of the suture together.
14. Secure the needle with a second surgical clamp. Pull the clamps so that they are at least 2cm apart.
15. Allow the suture to dry. Use the SIMCO Air blower if the sutures are taking a long time to air dry.
16. Once dry, remove the suture from the clamps and small bit of suture that was clamped off.
17. Place the suture inside a 4cm section of silicone tubing so that the whole suture is within the tubing and the curved portion of the needle is not.
18. Slide a blue slide clamp over portion of the needle that is within the tubing to secure the tubing and suture together.
19. Insert a 27G hypodermic needle next to the suture in the tubing.

20. Place the whole bioreactor inside a Chex-All sterilization pouch along with an extra blue slide clamp.
21. Sterilize the sutures using ethylene oxide gas sterilization.

Appendix E: hMSC Seeding Protocol

<u>Materials</u>**:**
- Sterile sutures in seeding bioreactor
- Sterile DPBS
- Sterile 20-Gauge hypodermic needles (25X)
- Sterile 1 mL syringes (approximately 30)
- Sterile 3 mL syringe
- hMSCs in culture (passages 5-7)
- Vented 50 mL conical tube
- Scilogex Rotator

<u>Procedure</u>**:**
1. Use a sterile 3 mL syringe attached to a sterile 20G needle, draw up approximately 3 mL of sterile DPBS
2. Remove the needle from the syringe and inject approximately 100 uL of sterile PBS into each bioreactor by attaching the syringe to the already inserted 27G needle
3. Ensure all bubbles are eliminated from the bioreactor.
4. Remove the syringe from the needle. Keep 27G needle in the bioreactor.
5. Allow 20 min for suture hydration.
6. While bundle hydrates prepare cell suspension according to cell passaging protocol
    a. Trypsinize cells and perform a cell count
    b. Create a cell suspension of 100,000 cells/100 uL
    c. Alliquot 100 uL of the cell suspension into 0.65 mL microcentrifuge tubes. The number of tubes with the cell suspension should be the number of samples that are being seeded with cells.
    d. Add 100 uL of fresh media into 0.65 mL microcentrifuge tubes. The number of tubes with media only should be the number of control sutures being used.
7. Use new syringe to remove all sterile PBS from the bioreactor before seeding by drawing the DPBS back into the syringe.
8. Use a sterile 1 mL syringe attached to a sterile 20G needle, draw up the cell suspension or the media into the syringe. First pull the syringe plunger back about 0.1 mL to place some air into the syringe. Next slowly draw up the cell suspension into the syringe. If the cell suspension has been sitting long, tritrate the solution to mix the cells back into suspension. Then slowly inject cell suspension (100,000 cells / 100 µL) into the bioreactor. For this, hold the bioreactor leveled horizontally. Slowly push the plunger to introduce the cell suspension into the bioreactor. Watch the needle in order to know when to stop the plunger. If the air in the syringe is pushed into the bioreactor, the cell suspension will exit the tubing of the bioreactor through the open end.
9. Place the extra slide clamp on the open end of the bioreactor. Situate it so that there is no air left after the cell suspension.
10. After injecting the cell suspension and adding the slide clamp, remove the 27G needle from the bioreactor.

11. Place the bioreactor into a vented 50 mL conical tube. About 4 sutures can fit in 1 50 mL tube.
12. Place the bioreactor into the 3D printed conical tube holder.
13. Place the holder on the Scilogex rotator that is inside the cell incubator. Turn the knob to the designated place (this speed equals 4 RPM) and rotate in the incubator for 24 hours.

Appendix F: CyQuant Cell Proliferation Assay Protocol

<u>Materials:</u>
- Complete MSCGM, Lonza
- Micropipette 1000µL
- Micropipette tips for 1000µL micropipette
- Micropipette 200µL
- Micropipette tips for 200µL micropipette
- Drummond® Pipette Aid
- VWR™ Serological Pipettes 10mL
- Molecular Probes/Invitrogen #C7026
- Lysis buffer Invitrogen #C7027
- Costar® 3599 96 Well Culture Cluster (96 well plate)
- DPBS (Dulbecco's Phosphate buffered saline)
- 1.7 mL microcentrifuge tubes
- Microcentrifuge tube rack
- Daigger Vortex Genie 2® A. Daigger & Co., INC.
- VWR Microcentrifuge

<u>Dilutions:</u>
1. Using a micropipette, add 1 mL Lysis buffer to 19mL DPBS
2. Using a micropipette, add 50 µL GR (fluorescent) to 20 mL 1x Lysis buffer

<u>Procedure:</u>

<u>Standard Curve Preparation:</u>
1. Obtain a culture of hMSCs
2. Aspirate off media, using a Pasteur pipette.
3. Using a micropipette, add 10 mL of DPBS.
4. Using a Pasteur pipette, aspirate off DPBS.
5. Using a micropipette, add 5 mL of trypsin.
6. Perform a cell count.
7. Using a micropipette, add as much media as necessary to create a cell suspension of 12,000 cells/100uL.
    Note: Can change cell concentrations if using/counting larger number of cells.
8. Add 1000 uL of cell suspension to a 1.7 mL microcentrifuge tube.
9. Centrifuge cell suspension down at 2,000 rpm for 5 minutes using the microcentrifuge.
10. Without disrupting the pellet, remove as much media as possible.
11. Add 1000 µL DPBS.
12. Centrifuge at 2,000 rpm for 5 min using the centrifuge.
13. Remove 900 µL.
14. Freeze at -80°C overnight.
    Note: The sample can be store up to 4 weeks in a -80°C freezer.

15. Remove the micrcentrifuge tube from the freezer and allow it to come to room temperature. Once thawed place it back in the freezer for at least 1 hour.
16. In a 96 well plate, place 100 µL of CyQUANT dye/lysis buffer into each well in Columns 1-4, Rows B-H.
17. Add additional 100 µL of CyQUANT buffer to each well of H1-H4.
18. Remove microcentrifuge tube from freezer. Allow the cell suspension to come to room temperature.
19. Vortex lightly using Vortex Genie 2.
20. When thawing is complete, add 900 µL of CyQUANT buffer to Standard Curve microcentrifuge tube.

    Note: The total volume in the Standard Curve should be 1000 µL.

21. Lightly vortex using the Vortex Genie 2®.
22. Using a micropipette, take up the Standard Curve solution and dispense 200 µL into each of the wells A1-A4.
23. Using a 1000 µL micropipette, take up 100 µL of CyQUANT buffer from the topmost well in a Column and dispense it into the well directly beneath it. Mix the solution in each well 6 times. Repeat this step through Row G.

    Note: Row H wells have NO standard curve (this is blank).

24. Using a micropipette, add 100 µL of CyQUANT buffer to each well from A1 to G4.

    Note: This will return the full amount to 200 µL.

 Preparation of Samples:
1. After seeding cells on microthreads and incubating, remove materials from bioreactor and place each sample into a 1.7 mL microcentrifuge tube.

    Note: At this point, the cells on the microthreads should be ready to be counted.
    Note: Make sure you have seeded a control thread with just media – this will give you a baseline fluorescent reading that your calculations depend on.

2. Using a micropipette, add 500 µL of DPBS.
3. Centrifuge microcentrifuge tube at 2,000 rpm for 5 minutes.
4. Using a micropipette, remove 400 µL of DPBS.
5. Place microcentrifuge tube in microcentrifuge tube rack.
6. Place rack in -80°C freezer overnight.

    Note: The sample can be store up to 4 weeks in a -80°C freezer. The sample will include the thread. Once in freezer, the de-ionized water will lyse the cell membrane leaving the DNA behind. This means no trypsinization is required to remove cells from thread.

7. Remove rack from freezer.

    Note: Allow microcentrifuge tube and contents to reach room temperature. Do NOT place in water bath. Once thawed, place the samples back in the freezer for at least 1 hour.

8. Remove rack from freezer following re-freeze and allow samples to come to room temperature.
9. Using a micropipette, add 400 µL of CyQUANT lysis buffer.
10. Vortex lightly using the Vortex Genie 2®.
11. Using a micropipette, remove material from sample.
12. Place materials on a slide for staining.

Note: This will confirm cell removal.

13. Using a pipette, take up of solution with cells and dispense 100 µL solutions into each of 4 wells. Start at the wells directly adjacent to the standard curve.
14. Once all intended wells are complete,
15. For de-gassing, place in vacuum. This will remove bubbles.
16. Place 96 well plate on plate reader.
17. Run plate reader. (480nm excitation, 520nm absorption)

> **Note:** Samples will saturate after 5 minutes of light exposure; work fast.
> Should be 200 µL in all wells of standard curve, if not add CyQUANT buffer until 200 µL is reached.

18. Dispose of waste properly.

<u>Calculations:</u>

1. Copy obtained data into an empty Excel document. Calculate average, correlation coefficient, slope, and x-intercept of standard curve.

> **Note**: To calculate the correlation coefficient type in desired cell (the cell locations should correspond to cells for calculation)
> Ex: =CORREL(A3:A10,F3:F10)
> To calculate the average type in desired cell (the cell locations should correspond to cells for calculation)
> Ex: =AVERAGE(B3:BE3)
> To calculate the intercept type in the desired cell (the cell locations should correspond to cells for calculation)
> Ex: =INETERCEPT(F3:F10,A3,A10)
> To calculate the slope type in the desired cell (the cell locations should correspond to cells for calculation)
> Ex: =SLOPE(F3:F10,A3,A10)

2. Using average, multiple the average by 5 for 500µL.
3. Cell value for sample = (Average – y-intercept)/slope.

Appendix G: Hoescht and Phalloidin Staining Protocol

Materials**:**
- Phosphate Buffered Saline
- 4% Paraformaldehyde (Only needed for tissues/cells that have not been fixed);
- 0.25% Triton-X
  - 0.25% V/V Triton-X in PBS
  - 10 μL Triton-X in 3990 μL PBS
- 1% BSA
  - 1% V (W)/V BSA in PBS
  - 40 μL in 3960 μL PBS
- Phalloidin (AF 488 Phalloidin A12379, Invitrogen)
  - 2.5% V/V Phalloidin in PBS
  - 50 μL in 1950 μL
- Hoechst
  - 0.0167% Hoechst dye in PBS
  - 0.5 μL in 3000 μL PBS

Procedure:

For unfixed sections/cells:
1. Rinse in PBS x2
2. Fix in 4% Paraformaldehyde for 10 minutes
3. Follow directions for fixed sections

For fixed sections/cells:
1. Rinse with PBS x2
2. Triton-X solution for 10 minutes
3. Rinse with PBS x2
4. Block with BSA solution for 30 minutes
5. Phalloidin solution for 30 minutes
6. Rinse with PBS x2
7. Hoechst solution for 3-5 minutes (typically 3)
8. Rinse with PBS x2
9. Cytoseal and coverslip
10. Store frozen at -20 degrees C.

Results**:**
- F-actin is stained green
- Nucleus is stained Blue

Appendix H: EPOC Outgrowth Assay Protocol

H.1. Microthread Construct Preparation

Materials:
- 50 mL conical tubes
- Scalple handle and blade
- Bunsen burner (and lighter)
- Stainless steel washers
- Medical grade silicone adhesive
- 15% ECM-fibrin microthreads
- Fibrin microthreads
- 6-well plate

Procedure:
1. Obtain 50 mL conical tubes
2. Using an ignited Bunsen burner, heat the edge of a scalpel blade in the flame.
3. "cut" the 50 mL conical tube into 1.5 cm sections using the heated blade.
   a. The tube will melt from the heated blade.
4. Once the sections are cut, place them in a 6-well plate to ensure that they are the proper height. The conical tube should NOT touch the surface of the 6-well plate cover. If it is too tall, use the scalpel blade to melt down the section or use course sand paper to shorten it.
5. For one type of microthread, cut 6 3cm sections of the microthread. Glue each section of microthread to an individual stainless steel washer using the silicone adhesive. Ensure to use a minimal amount of adhesive.
6. Once dry, glue the microthread-washer combo to one end of the conical tube section using the silicone adhesive. Glue the tube so that it is on the same side of the microthread on the washer.
7. Allow the glue to dry overnight. Place the constructs inside 6-well plates to keep them secure and sterilize them using ethylene oxide gas sterilization.
8. Control constructs should contain a stainless steel washer with a conical tube section and no microthread.

H.2. Plate Preparation and Cell Culture

Materials:
- 6-well tissue culture plate
- Complete EPOC media (Biochain)
- 1 vial Endothelial Progenitor Outgrowth Cells (Biochain)
- sterile ruler
- sterile laboratory marker
- 1000 uL micropipette
- 1000 uL micropipette tips

Procedure:
1. Prior to any cell culture, the 6-well culture plates must be prepared for the outgrowth.

2. In order to assess the outgrowth properly, parallel dotted lines must be drawn for imaging.
3. Obtain a sterile 6-well plate.
4. Place the plate upside-down, keep the cover on the plate to maintain sterility.
5. Using the ruler, locate the middle of the well and draw one vertical dotted line down the well approximately 1 mm to the left of the middle.
6. Move the ruler approximately 2 mm to the right and draw another dotted line. Make sure that the second line of dots are parallel to the dots in the left side line. These two lines create an approximate 2mm channel down the middle of the well.
7. Repeat for all wells.
8. Once the lines are drawn, thaw the EPOC vial from the manufacturer.
9. Perform a cell count and plate between 10,000 and 12,500 cells per cm^2 or approximately 95,000 to 118,750 cells per well.
10. Allow the cells to reach full confluency before continuing with outgrwoth experiment.

H.3. EPOC Outgrowth Assay

Materials:
- Complete EPOC Media (BioChain)
- Endothelial Progenitor Outgrowth Cells (Biochain)
- Sterile DPBS
- 6-well plate
- 1000 uL micropipette
- 1000 uL micropipette tips
- 200 uL micropipette tips
- Sterile microthread constructs.

Procedure:
1. Obtain a 6-well plate with confluent EPOCs.
2. Aspirate the media from each well.
3. Using a 200 uL micropipette tip, scratch the surface of each well in between the two dotted lines. Use a new micropipette tip for each well.
4. Rinse each well with 2000uL of DPBS twice. Swirl the plate in between washes.
5. Place a sterile microthread construct within the well so that the microthread lies within the scratch.
6. Add 2000uL of complete EPOC media to each well. Add the media to the edge of the well and not the middle as to not disturb any cells that lie within the construct.
7. Confirm that each microthread is within their designated scratch.
8. For each 6-well plate, there should be 2 fibrin microthread constructs, 2 15% ECM constructs, and 2 control constructs.
9. Evaluate the outgrowth by imaging each well at the individual pairs of dots that lie within the construct. Image each well at 0 Hours, 6 Hours, 12 Hours, 18 Hours and 24 Hours.
10. Following outgrowth, perform a DAPI stain on the microthreads as well as each well.

Appendix I: DAPI Staining Protocol

Materials:

- DPBS
- 4% Paraformaldehyde
- 0.25% Triton-X
    - 0.25% V/V Triton-X in PBS
    - 10 µL Triton-X in 3990 µL PBS
- DAPI
    - STOCK SOLUTION: 10 mg in 2 mL of DiH2O, or 5000 ug/mL
    - Dilute to: 1ug/mL
- 6-well plate from outgrowth assay
- microthread constructs

Procedure:

1. Remove each microthread construct from their respective wells.
2. Cut the microthread from the construct and place it on a glass slide.
3. Fix the microthreads and each well in the 6-well plate with 4% paraformaldehyde for 10 minutes.
4. Wash the microthreads and wells in DPBS 3 times for 5 minutes each.
5. Permeabilize with 0.25% Triton-X 100.
6. Wash in DPBS 3 times for 5 minutes each.
7. Stain with DAPI for 5 minutes.
8. Wash in DPBS.
9. View and analyze under a fluorescent microscope.

Appendix J: EPOC Outgrowth Calculations

The table below shows representative calculations for one well of the EPOC outgrowth assay. These calculations were performed for each well in each 6-well plate.

Well 2_ 15% ECM 2	12.12.16				
Top	**0 Hours**	**6 Hours**	**12 Hours**	**18 Hours**	**24 Hours**
	1144.086	1062.366	911.828	322.581	0
Scratch mostly complete	1101.075	1152.688	903.226	296.774	0
At 18 hours. Top and	1174.194	963.441	369.892	0	0
Bottom still slightly open	1354.839	950.538	529.032	0	0
	1182.796	881.72	387.097	0	0
Scratch Complete at 24	1208.602	791.398	417.204	0	0
hours	1122.581	1148.387	559.14	0	0
	1148.387	924.731	318.28	0	0
	1169.892	1092.473	606.452	421.505	0
	1126.882	1040.86	421.505	486.022	0
AVERAGE DISTANCE	**1173.3334**	**1000.8602**	**542.3656**	**152.6882**	**0**
	0--6 Hours	6--12 hours	12--18 hours	18--24 hours	**0--24 Hours**
Distance Change	**172.4732**	**458.4946**	**389.6774**	**152.6882**	**1173.3334**
Percent Change	15%	39%	33%	13%	100%
Mid 1					
	1243.011	959.14	623.656	455.914	0
Scratch mostly complete	1083.871	903.226	606.452	593.548	0
at 18 hours	1427.957	1156.989	769.892	576.344	0
	1212.903	1092.473	636.559	541.935	0
Scratch Complete at 24	1406.452	954.839	262.366	554.839	0
hours	1062.366	817.204	619.355	382.796	0
	1144.086	1109.677	941.935	0	0
	1182.796	1079.57	795.699	0	0
	1208.602	941.935	959.14	0	0
	1135.484	959.14	761.29	0	0
AVERAGE DISTANCE	1210.7528	997.4193	697.6344	310.5376	0
	0--6 Hours	6--12 hours	12--18 hours	18--24 hours	**0--24 Hours**
Distance Change	213.3335	299.7849	387.0968	310.5376	1210.7528
Percent Change	18%	25%	32%	26%	100%
Mid 2					
	1195.699	929.032	800	541.935	503.226
Scratch partially	1182.796	903.226	645.161	455.914	400
Complete at 24 hours	1333.333	984.946	847.312	404.301	481.72
	1290.323	1079.57	490.323	391.398	391.398
	1320.43	980.645	713.978	335.484	430.108
	1277.419	950.538	1002.151	752.688	387.097

	0--6 Hours	6--12 hours	12--18 hours	18--24 hours	0--24 Hours
	1281.72	1092.473	877.419	838.71	0
	1088.172	1208.602	920.43	701.075	0
	1148.387	1015.054	821.505	593.548	0
AVERAGE DISTANCE	1235.6989	1023.2258	804.7311	572.0429	259.3549
	0--6 Hours	6--12 hours	12--18 hours	18--24 hours	**0--24 Hours**
Distance Change	212.4731	218.4947	232.6882	312.688	976.344
Percent Change	17%	18%	19%	25%	79%
Bottom					
	1458.065	1113.978	739.785	838.71	533.333
Scratch partially closed	1359.14	1040.86	967.742	718.28	589.247
At 24 hours	1221.505	1238.71	1092.473	774.194	0
	1273.118	1092.473	1040.86	447.312	0
	1470.968	1212.903	937.634	412.903	0
	1307.527	1040.86	984.946	692.473	0
	1522.581	1191.398	890.323	726.882	0
	1518.28	1294.624	1002.151	860.215	0
	1470.968	1247.312	1148.387	632.258	0
	1436.559	1243.011	972.043	434.409	0
AVERAGE DISTANCE	1403.8711	1171.6129	977.6344	653.7636	112.258
	0--6 Hours	6--12 hours	12--18 hours	18--24 hours	**0--24 Hours**
Distance Change	232.2582	193.9785	323.8708	541.5056	1291.6131
Percent Change	17%	14%	23%	39%	92%
TOTAL AVERAGE	1255.91405	898.152717	755.591375	444.675709	92.903225
STD DEVIATION	129.300400	347.278449	231.594123	291.198337	190.796957
TOTAL CHANGE AVG	207.6345	292.688175	333.3333	329.35485	1163.01082
STD DEVIATION	25.1564058	119.4297642	73.6752934	160.053031	133.876685
Total % Change at 24hrs					93%